ABSTRACT OF THESIS

Name of Candidate ANTHONY REGINALD BLYTHE,

Address

Degree Ph.D. *Date* 15th May, 1962.

Title of Thesis The ultrasonic measurement of relaxation times.

With a view to studying translational-vibrational relaxation times in gaseous systems such as CO_2/Ar mixtures, an accurate ultrasonic interferometer was built. With this apparatus sound velocities may be determined at 83 kc./sec. in the ranges 0 - 2 atm. and 20-200°C. The wavelength is measured with the aid of an optical Moiré fringe device accurate to 10^{-5} cm.

Preliminary experiments with CO_2-free, dry air indicated that diffraction and wave-guide effects would have to be taken into account. These effects were examined using pure inert gases (He, Ne, Ar, Kr) whose free-space, plane-wave velocities were calculated from available thermodynamic and virial data. A straight line was obtained when the relative increase of observed wavelength above the calculated free-space, plane-wave wavelength, $(\lambda_{exp} - \lambda_{calc}) / \lambda_{calc}$, was plotted against λ^2_{calc}. Using this as a calibration curve for the interferometer, absolute velocities may be estimated reliably to 1 part in 2,000, or better, in gases with molecular weights greater than 30. Further investi-:gations were made in two gases with very low velocities: $CClF_3$ and $\underline{n}$ - C_4H_{10}.

A simple model of the interferometer has been treated theoretically using the method of normal modes of a tubular wave-guide. Numerical results, calculated on a computer (Deuce), give good agreement with experiment only when it is assumed that the appropriate boundary conditions at the sides of the interferometer tube are of the "free-wall" rather than "rigid-wall" type.

Additional theoretical work was done on the temperature dependence of the translational-vibrational energy transfer. Previous calculations have in general given unsatisfactory agreement with experiment; in these calculations the authors have only introduced the effect of attractive forces between the molecules in an indirect way. In low-energy encounters of polar molecules the attractive forces may be important and it was therefore decided to investigate the effect of including them directly. Numerical results have been calculated for methyl chloride; the temperature dependence of the relaxation time and second virial coefficient are well established for this gas. It was found that both the semi-classical and fully quantum mechanical methods gave the same result, which agrees well with experiment in both absolute magnitude and temperature dependence.

EX BIBL UNIV EDINBURGEN

Use other side if necessary.

THE ULTRASONIC MEASUREMENT OF RELAXATION TIMES.

Thesis submitted for the degree of Doctor of Philosophy by

A.R. Blythe, B.A., B.Sc. (Oxon.)

Edinburgh University Chemistry Department, June 1962.

EX BIBL UNIV EDINBURGEN

ACKNOWLEDGEMENTS.

I should like to thank Prof. T.L. Cottrell for his help and advice throughout this work, and for his stimulating discussions.

Thanks are due to the technical staff of the laboratory; without their skill and assistance I should not have been able to build the apparatus.

I should also like to thank the Department of Scientific and Industrial Research for the award of a Research Studentship.

CONTENTS.

FIGURES.

27./

INTRODUCTION.

A gas is a medium which, by virtue of its isotropy, homogenity, and compressibility, is ideally suited to the propagation of longitudinal wave motion. Thus sound is transmitted through air as a series of alternating compressions and rarefactions. The velocity, v, of a sound wave of infinitessimally small amplitude is related to the thermodynamic properties of the gas through the relation:

$$v = \sqrt{\frac{dp}{d\rho}}$$

where p and ρ are the pressure and density of the gas respectively. It has been established experimentally that the propagation of sound is an adiabatic process, so that:

$$\frac{dp}{d\rho} = \left(\frac{\partial p}{\partial \rho}\right)_s$$

For an ideal gas the relation may be transformed into:

$$v^2 = \frac{\gamma RT}{M} = \frac{RT}{M}\left(1 + \frac{R}{C_v}\right)$$

Where γ is the ratio of the specific heats of the gas, Cv is the molar heat capacity at constant volume, and M the molecular weight; R is the gas constant and T the absolute temperature. From this it follows that the measurement of the velocity of sound in a gas may be used to determine the heat capacity of the gas.

Another characteristic of wave motion is its periodicity. Now the derivation of the above equation for velocity of sound assumes/

assumes that thermodynamic equilibrium is maintained all the time, i.e. that the wave motion is reversible. Should the cyclic changes in the gas from one thermodynamic state to another, involve a process which takes a finite time, then at short periodic times, the changes will become irreversible. This irreversibility will effectively change the thermodynamic quantities governing the velocity of sound which will therefore also change.

To understand these changes it is necessary to go to the molecular model of the kinetic theory of gases. The immediate effect of an adiabatic compression in a gas is to raise the translational energy of the gas molecules. In the simple case of a monatomic gas this means that the temperature of the gas is raised. Besides translational energy, polyatomic gas molecules possess energy of vibration (the atoms oscillate about equilibrium positions within the molecule) and energy of rotation; the heat capacity is obtained by summing the contributions from translational, vibrational and rotational degrees of freedom:

$$C_v = C_{trans.} + C_{vib.} + C_{rot.}$$

Therefore an adiabatic compression of a polyatomic gas raises immediately only the "translational temperature". Equilibrium is eventually restored by a redistribution of the excess translational energy amongst the vibrational and rotational modes. The reverse process takes place on adiabatic rarefaction. Transfer of energy between translation and the other degrees of freedom takes place in molecular collisions when the molecules are strongly interacting with each other, (the effect of radiation is negligible).

The efficiency of the energy transfer process depends on two factors:

a) The number of collisions per second. Under ordinary experimental/

experimental conditions only binary collisions are important, so that the efficiency depends directly on pressure, p .

b) The probability that a quantum of vibrational or rotational energy will be transferred during a collision.

A quantity τ , called the relaxation time, is used to characterize the time dependence of an energy transfer process. If the temperature of a particular degree of freedom is perturbed from equilibrium by an amount ΔT then its temperature reverts to the equilibrium value at a rate given by:

$$\frac{d(\Delta T)}{dt} = - \frac{\Delta T}{\tau}$$

There is time for complete redistribution of energy in the adiabatic changes of a sound wave of low frequency and all degrees of freedom contribute to the heat capacity:

$$C_o = C_{trans.} + C_{vib.} + C_{rot.}$$

At high sound frequencies there is insufficient time for energy transfer to vibrational modes. The heat capacity is effectively reduced to:

$$C_\infty = C_{trans.} + C_{rot.},$$

i.e. the vibrational degrees of freedom do not participate in the acoustic cycle. A plot of v^2 vs. $\log f/p$ where f is the sound frequency, shows an inflexion point at a particular frequency, which is simply related to the translation-vibration relaxation time:

$$2\pi f \tau = \frac{C_o}{C_\infty} \qquad \text{(at the inflexion point)}$$

At very high sound frequencies the rotational heat capacity also relaxes.

Thus the measurement of sound velocity over a range of frequency yields information on the efficiency of intermolecular energy transfer.

The relaxation time of translational-vibrational energy transfer for simple polyatomic molecules is usually of the order of 1 μs., which means that ultrasound of 100 kc./s. is required for its study. If the sound is produced electrically the frequency may be measured very accurately by comparing it with broadcast standards (e.g. B.B.C. Light programme: 200 kc./sec.)

The wavelength of ultrasound may be measured in a Pierce interferometer, using a quartz crystal as a source of sound.

The aim of the present research was to develop a very accurate interferometer in order to investigate the translational-vibrational relaxation of systems such as CO_2/Ar.

It became necessary to take into account diffraction and wave-guide effects. These effects have been examined using air and inert gas, whose theoretical free-space, plane-wave velocities may be calculated for comparison from available data, and in gases of very low velocities ($CClF_3$ and $\underline{n}$ - C_4H_{10}).

Whilst the interferometer was being built, some calculations of translational-vibrational energy transfer probabilities in methyl chloride gas were made. This work is reported at the end of the thesis.

GENERAL ULTRASONIC THEORY.

Velocity of a sound wave.

An expression for the phase velocity of a compressional wave propagated in a gas may be derived by applying the equations of motion in the direction normal to the wave-front (an equi-phase surface). Plane waves and spherical waves are special cases where the wave-front retains its shape: both have the same velocity.

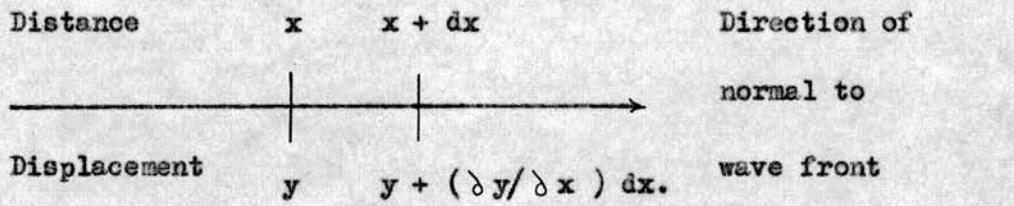

The above diagram represents an element of gas which resides between x and (x + dx) at equilibrium. Due to the displacement of the sound wave, at time t its boundaries change to (x + y) and (x + dx + y + $\frac{\partial y}{\partial x}$. dx). Equating masses in the two states, the equilibrium density ρ_0 is related to the density ρ in the disturbed state at time t by:

$$\rho_0 \, dx = \rho \left(1 + \frac{\partial y}{\partial x} \right) dx.$$

If the amplitude of the displacements is small compared with the wavelength:

$$\frac{\partial y}{\partial x} \ll 1$$

so

$$\rho = \rho_0 \left(1 - \partial y / \partial x \right)$$

and

$$\frac{\partial \rho}{\partial x} = - \rho_0 \frac{\partial^2 y}{\partial x^2}$$

Now/

Now applying Newton's second law to the element of Gas:

$$(\rho_0 \, dx) \cdot \frac{\partial^2 y}{\partial t^2} = - \frac{\partial p}{\partial x} \cdot dx$$

where p is the pressure. Writing

$$\frac{\partial p}{\partial x} = \frac{\partial p}{\partial \rho} \frac{\partial \rho}{\partial x} ,$$

$$\frac{\partial^2 y}{\partial t^2} = \frac{\partial p}{\partial \rho} \cdot \frac{\partial^2 y}{\partial x^2} .$$

Thus y satisfies the familiar equation of wave motion:

$$\frac{\partial^2 y}{\partial x^2} = \frac{1}{v^2} \frac{\partial^2 y}{\partial t^2}$$

when

$$v^2 = \frac{\partial p}{\partial \rho}$$

v is the phase velocity, related to the frequency f and wavelength λ by:

$$v = f \lambda . \qquad (1)$$

The adiabatic hypothesis.

There is conclusive experimental evidence that sound waves propagate adiabatically (viz:- Richards, 1939). Therefore:

$$\frac{\partial p}{\partial \rho} = \left(\frac{\partial p}{\partial \rho} \right)_S = - \left(\frac{\partial p}{\partial V} \right)_S \cdot \frac{V^2}{M}$$

Where V is the molar volume and M the molecular weight of the gas. Then by Reech's theorem:

$$\left(\frac{\partial p}{\partial \rho} \right)_S = - \gamma \left(\frac{\partial p}{\partial V} \right)_T \cdot \frac{V^2}{M} \qquad (2)$$

γ being the ratio of the specific heats of the gas. For an ideal gas:

$$\left(\frac{\partial p}{\partial V}\right)_T = -\frac{RT}{V^2},$$

$$\gamma = 1 + \frac{R}{C_v};$$

therefore

$$\left(\frac{\partial p}{\partial \rho}\right)_s = \frac{RT}{M}\left(1 + \frac{R}{C_v}\right) \qquad (3)$$

C_v is the molar heat capacity of the gas at constant volume.

The effect of gas imperfection.

The equation of state of a gas can be expressed as a virial expansion in pressure:

$$pV = RT + Bp + Cp^2 + \ldots\ldots$$

where the second virial coefficient B describes the deviation from the ideal gas equation due to the interaction of the molecules in pairs, the third coefficient C describes the deviation due to the interaction of triads, etc. Ignoring coefficients above the second,

$$pV = RT + Bp,$$

so that neglecting powers of B above the second, using equation (2)

$$(\partial p/\partial \rho)_s = \frac{\gamma(RT + 2Bp)}{M}$$

The molar heat capacities of a gas in terms of the ideal gas values are (Roberts, 1951):

$$C_p = C_p^{id} - T.\frac{d^2B}{dT^2},$$

$$C_v = C_v^{id} - p\left(2\frac{dB}{dT} + T.\frac{d^2B}{dT^2}\right);$$

therefore $$\gamma = \frac{R + C_v^{id} - p\,T\,B''}{C_v^{id} - 2\,p\,B' - p\,T\,B''}$$

Writing the sound velocity in an ideal gas as:

$$v^2_{id} = \frac{\gamma^{id}\,R\,T}{M},$$

we obtain:

$$v = v_{id}\left(1 + \frac{Sp}{RT}\right), \qquad (4)$$

where $$s = B + \frac{T^2 B''}{2c\,(c+1)} + \frac{T\,B'}{c},$$

$$c = \frac{C_v^{id}}{R}.$$

Absorption of Sound.

When viscosity, or some other dissipative force, produces a damping, an extra term is required in the fundamental equation, e.g. when the damping force is proportional to the particle velocity:

$$\frac{\partial^2 y}{\partial x^2} = \frac{1}{v^2}\left\{\frac{\partial^2 y}{\partial t^2} + g\,\frac{\partial y}{\partial t}\right\}$$

If g is small, g^2 may be neglected and the above equation has the approximate solution:

$$y = A \exp(-gt/2) \exp i\, 2\pi f\,(t - x/v),$$

where the effect of the damping occurs as a decay factor. Alternatively, the solution may be expressed in the form:

$$y = A \exp(-\alpha x) \exp i\, w(t - x/v),$$

where/

where the effect of the damping occurs as an attenuation, the amplitude attenuation coefficient being

$$\alpha = \frac{g}{2v}$$

w is the cyclic frequency $2\pi f$.

Another way of taking absorption into account is to use a complex velocity:

$$v_c = v_r - iv_i ,$$

when the solution of the wave equation is:

$$y = A \exp iw (t - x/v_c) ;$$

c.f.

$$y = A \exp (-\alpha x) \exp iw (t - x/v),$$

whence

$$\alpha = \frac{- wv_i}{(v_c)^2} , \quad v = \frac{(v_c)^2}{v_r} , \qquad (5)$$

$$v_c = \frac{v}{1 - i\alpha v/w}$$

For weak absorption, v_i is small and v_i^2 may be neglected (c.f. the neglect of g^2 above) so that $v \approx v_r$.

The formula

$$v = v_r (1 + \alpha^2 v_r^2 / w^2) \qquad (6)$$

gives the change in phase velocity due to absorption.

The "classical absorption" of a gas due to viscosity η and thermal conductivity χ is usually small:

$$\alpha_{cl} = \frac{2\pi^2}{\gamma \rho v} \left\{ \frac{4}{3} \eta + \frac{\gamma - 1}{\gamma} \frac{\chi}{C_v} \right\} f^2$$

The value of the quantity α_{cl}/f^2 at 20°C. and 1 atm. for air is 1.37×10^{-13} cm.$^{-1}$sec.^{2}, so that at a frequency of 100 kc./sec. α_{cl} is 1.37×10^{-3} cm.$^{-1}$. The effect on the phase velocity is negligible (ca. 1 part in 10^8).

A/

A complex velocity is mathematically useful in dealing with $(\partial p/\partial \rho)_s$, which is generally expressed as a complex quantity in relaxation theory (viz:- next section). Let

$$(\partial p/\partial \rho)_s = A - iB$$

But $$(\partial p/\partial \rho)_s = v_c^2 = v_r^2 - i2v_r v_i - v_i^2$$

Hence for weak absorption, when v_i^2 may be neglected, equating real and imaginary parts and using equations (5)

$$v^2 = A \qquad (7)$$

$$\alpha = - \frac{Bw}{2Av} \qquad (8)$$

Relaxation theory.

In a relaxation phenomenon, there are two systems, spatially superimposed on each other, at different temperatures. At constant volume, an infinitessimally small change in entropy is given by:

$$dS = \frac{dU'}{T'} + \frac{dU''}{T''} ,$$

(where the prime and double prime are used to distinguish the two systems).

If the system is a closed one:

$$dU = dU' + dU'' = 0.$$

Therefore

$$\frac{dS}{dt} = \frac{dU'}{dt}\left\{\frac{1}{T'} - \frac{1}{T''}\right\} = \frac{dU'}{dt}\,\frac{T''-T'}{T^2} .$$

This equation may be compared with Onsager's equation:

$$\dot{\Delta} S = \sum_{i=1}^{n} J_i X_i$$

for an irreversible process. He was able to show, on the basis of microscopic reversibility (symmetry of molecular equations of motion) that the "force" X_i produces a change in the "flux" J_i according as the relation:

$$J_i = \sum_{k=1}^{n} L_{ik} X_k \quad ;$$

choosing $\frac{T'' - T'}{T^2}$ as the force and $\frac{du'}{dt} = -\frac{du''}{dt}$ as the "flux", we may write a phenomenological equation:

$$\frac{du'}{dt} = L. \frac{T'' - T'}{T^2}$$

which is usually written:

$$\frac{dT'}{dt} = \frac{1}{\tau}\,(T'' - T')$$

τ has the dimension of time and is called the relaxation time. If $\Delta T'$, $\Delta T''$ are the deviations of T', T'' from equilibrium:

$$\frac{d(\Delta T')}{dt} = \frac{1}{\tau}(\Delta T'' - \Delta T')$$

When the second system remains at equilibrium, and:

$$\frac{d(\Delta T')}{dt} = -\frac{\Delta T'}{\tau} \qquad (9)$$

Unless the frequency is very high, the translational temperature of gas molecules follows synchronously the adiabatic compressions and rarefactions of a propagating sound wave. The vibrational and rotational temperatures are only indirectly affected and so relaxation may be expected for the transfer of energy to these degrees of freedom. For an impressed periodic disturbance y of a sound wave, the temperature of an "indirect degree of freedom" may be expressed as:

$$T' = T_o' + \Delta T_y'$$

where T'_o is the mean temperature. Since the variation of T'_y must be periodic and of the same cyclic frequency w as the sound wave:

$$\Delta T_y' = A_T \exp(iwt)$$

When the frequency of the sound wave is high enough for relaxation to be significant in this particular degree of freedom, application of equation (8) gives

$$\frac{d(\Delta T')}{dt} = \frac{\Delta T_y' - \Delta T'}{\tau}$$

$$\Delta T' = \frac{A_T \exp(-t/\tau)}{\tau} \int_{-\infty}^{t} \exp(\theta/\tau + iw\theta)\, d\theta$$

$$= \frac{\Delta T_y'}{1 + iw\tau}$$

Since the relation between a temperature change of a degree of freedom and its heat capacity is a linear one, the relaxation may be expressed in terms of the heat capacity:

$$C'_{vw} = \frac{C'_{vo}}{1 + iw\gamma}$$

where C'_{vw} is the effective heat capacity of this particular degree of freedom at the frequency w and C'_{vo} is the heat capacity at zero frequency. If just one degree of freedom exhibits relaxation, the total heat capacity is given by:

$$C_w = C_\infty + \frac{C_o - C_\infty}{1 + iw\gamma} \qquad (10)$$

where C_o is the total heat capacity at zero frequency and C_∞ is the effective total, heat capacity at an infinitely high frequency.

Dispersion of sound.

Substituting for the effective C_v in equation (3) and using relation (7) the phase velocity at cyclic frequency w is given by:

$$V_w^2 = \frac{RT}{M}\left(1 + R.\ \frac{C_o + C_\infty w^2 \tau^2}{C_o^2 + C_\infty^2 w^2 \tau^2}\right) \qquad (11)$$

The form of the frequency dependence of the phase velocity for an ideal gas is shown in fig. 1 . The curve has an inflexion at

$$w_{inf} = \frac{1}{\tau}\frac{C_o}{C_\infty} \qquad (12)$$

The velocities at low and high frequencies are given respectively by:

$$V_o^2 = \frac{RT}{M}\left(1 + \frac{R}{C_\infty}\right),$$

$$V_\infty^2 = \frac{RT}{M}\left(1 + \frac{R}{C_\infty}\right).$$

Experimental velocities are reduced to the ideal gas values using equation (4) before plotting the dispersion curve to measure τ . The limiting velocities, which may be calculated from the thermodynamic or spectroscopic data, afford a check on the experiment, e.g. gas purity. Since binary molecular collisions are responsible for the energy transfer process, changes in pressure are complementary to changes in frequency as far as relaxation is concerned. Hence the dispersion curve may be obtained as a plot of log f/p vs. V^2 (fig. 1).

Anomalous absorption.

The absorption coefficient due to relaxation is obtained through relation (8):

$$\alpha = \frac{w}{2V_w} \cdot \frac{w \tau R C_v}{(R + C_o) C_o + w^2 \tau^2 (R + C_\infty) C_\infty}$$

The graph (fig. 1) of α vs. log w shows a maximum at:

$$w_{max} = \frac{1}{\tau} \cdot \frac{V_o}{V_\infty} \cdot \frac{C_o}{C_\infty}$$

Even the strong absorption in a dispersion region is hardly sufficient to affect the phase velocity appreciably. For example, in the vibrational relaxation of CO_2:

α_{max} = 1.00 db. per wavelength (Fricke, 1940)

w_{max} = 13.6 rad./sec.

and V = 274 m/sec. (Leonard, 1940)

The change in velocity from equation (6) amounts to 3 parts in 10,000. CO_2 is an extreme example because the absorption peak occurs at only 20 kc./sec.

Vibrational relaxation.

Even though polyatomic molecules possess several different vibrational modes, it is usual for the dispersion curve to have the characteristics of just a single relaxation process with relaxation time τ. This indicates that a particular mode is capable of transferring energy more easily than the rest and that energy is able to flow from this mode into the others by intramolecular processes which are relatively fast. The latter impliesa strong coupling of anharmonic oscillators in a model of the molecule. The mode responsible for vibrational-trans-:lational energy transfer is normally the one with smallest energy/

energy quanta. The relaxation time resulting from this system is related to the relaxation time of the easily excited mode, ϕ by the equation:

$$\phi = \frac{C'_v}{C_v} \cdot \tau \qquad (12)$$

where C'_v is the heat capacity of the single degree of freedom and C_v is the total vibrational heat capacity.

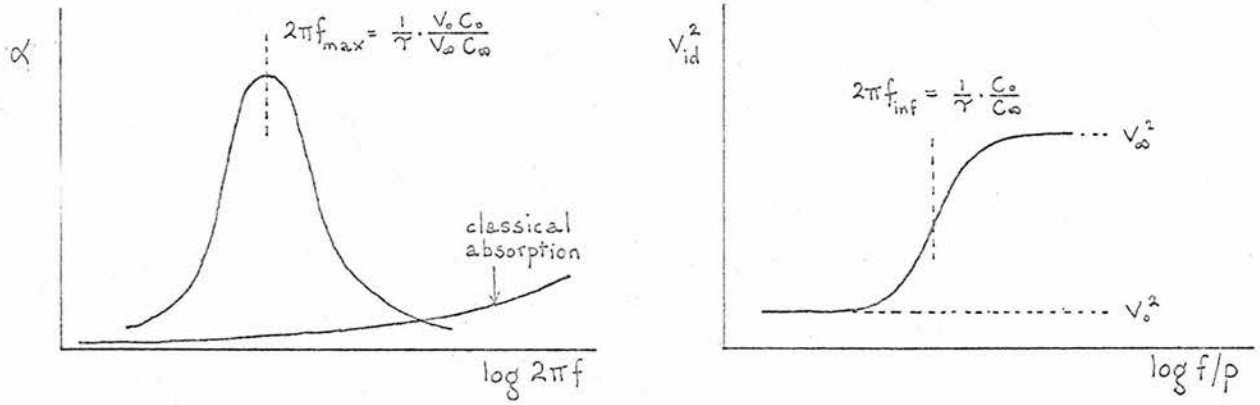

Fig. 1. Sonic anomalous absorption and velocity dispersion curves in a relaxation region.

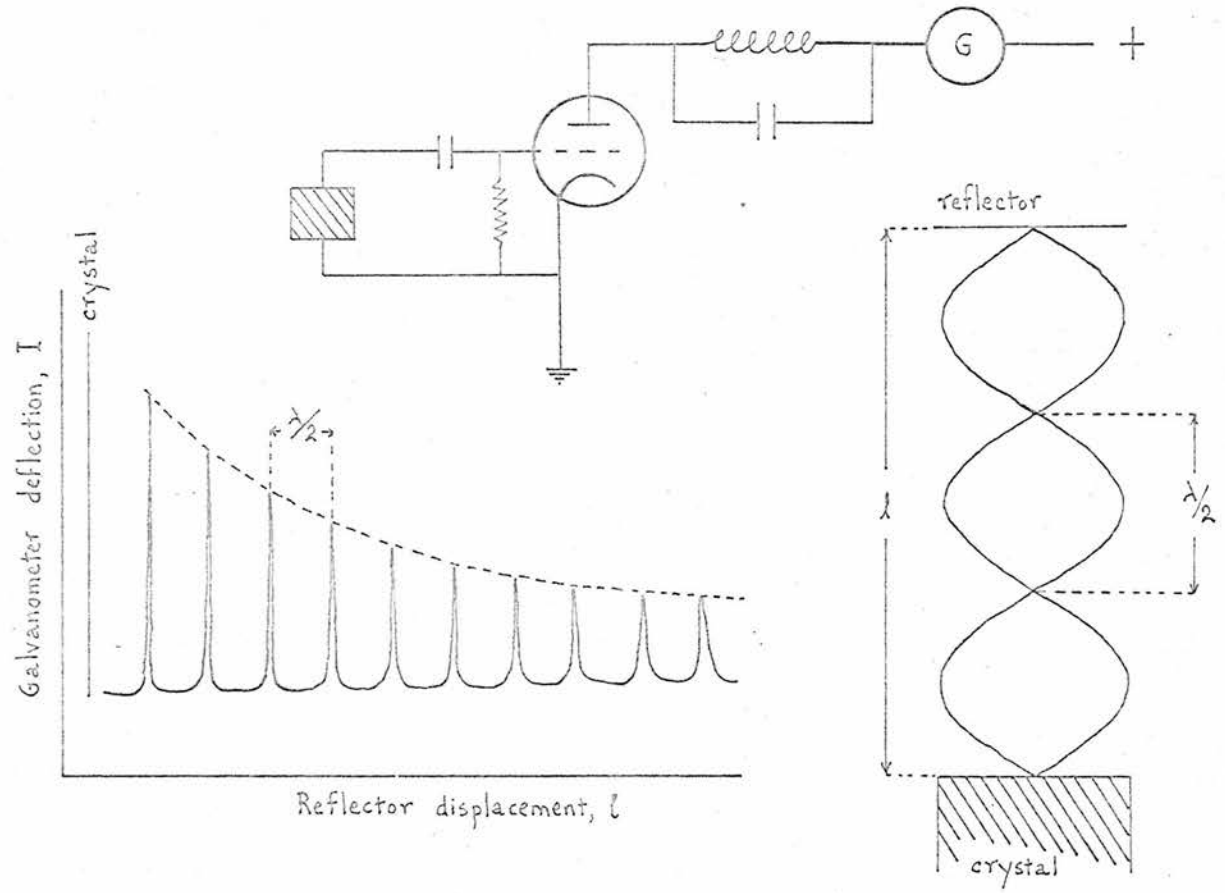

Fig. 2. The Pierce interferometer.

THE ULTRASONIC INTERFEROMETER.

Essentially, an ultrasonic interferometer consists of an ultrasonic transducer with a plane face vibrating at a constant, known frequency and a reflector plate mounted axially parallel to it. The reflector can be moved towards or away from the transducer, its movements causing a series of resonance and anti-resonance conditions in the gas column, fig. 2. In the first apparatus Pierce (1925) used a vibrating quartz crystal. The variations in the plate current of the valve circuit (fig. 2), used to sustain the piezo-electric oscillations, gave a measure of the reactance of the gas column on the crystal face, fig. 2 . Pielemeier (1929, 1932) has shown that the reflector positions for which there are standing waves are those for which the plate current is a maximum: the distance between successive reflection peaks is equal to the half-wavelength of the ultrasound generated in the gas. Hardy (1943) has carried out a thorough theoretical analysis of this experimentally simple system.

Acoustic theory.

If we suppose that only plane waves are generated in the interforometer, then the acoustic impedance per unit area of gas column at the face of the transducer is the same as that of a one-dimensional model along the z-axis (Vigoureux, 1952):

$$Z = \frac{i\rho w}{ik+\alpha} \cdot \frac{1 + \exp(-i2kl - 2\alpha l - \beta)}{1 - \exp(-i2kl - 2\alpha l - \beta)},$$

where k is the propagation constant of the waves, $2\pi/\lambda$, and β is the reflection absorption coefficient. When the absorption coefficient α of the gas is small compared with k :

$$Z = \rho v \cdot \frac{1 + \exp(-i2kl - 2\alpha l - \beta)}{1 - \exp(-i2kl - 2\alpha l - \beta)}$$

As l is varied, Z goes through a series of minima:

Z/

$$Z_{min} = \rho V \frac{1 - \exp(-2\alpha l - \beta)}{1 + \exp(-2\alpha l - \beta)},$$

$$2kl = (2n - 1)\pi, \quad n = 1,2 \ldots\ldots,$$

and a series of maxima:

$$Z_{max} = \rho V \frac{1 + \exp(-2\alpha l - \beta)}{1 - \exp(-2\alpha l - \beta)}$$

$$2kl = 2n\pi, \quad n = 1,2 \ldots\ldots$$

These stationary Z's are purely resistive. The maxima are sharp peaks, whose heights are proportional to $\coth(\alpha l + \beta/2)$.

Electrical theory.

In an ultrasonic interferometer where the transducer controls the frequency (as in the Pierce oscillator) there is a small cyclic change in frequency as the reflector moves away from the transducer (Norton, 1935); the gas column reacting on the face of the transducer changes the electric characteristics of the transducer and affects its natural frequency. The reactance of the gas column changes radically as the reflector passes through successive positions of resonance. Therefore it is better to drive the transducer as a resonator when the frequency may be kept constant independently. This also facilitates the selection of a particular mode of vibration of the crystal from the multiplicity around the natural frequency.

The operation of an electric circuit containing a transducer may be understood in terms of the equivalent electric circuit of the transducer. Van Dyke (1925) determined the equivalent electric circuit of a piezs-electric quartz crystal, fig. 3. The resonant frequency of the crystal is given by:

$$f_R = \frac{1}{2\pi}\sqrt{\frac{L}{C}}.$$

The electric impedance due to the gas column reacting on the transducer is

$$Z' = C_t A Z,$$

where/

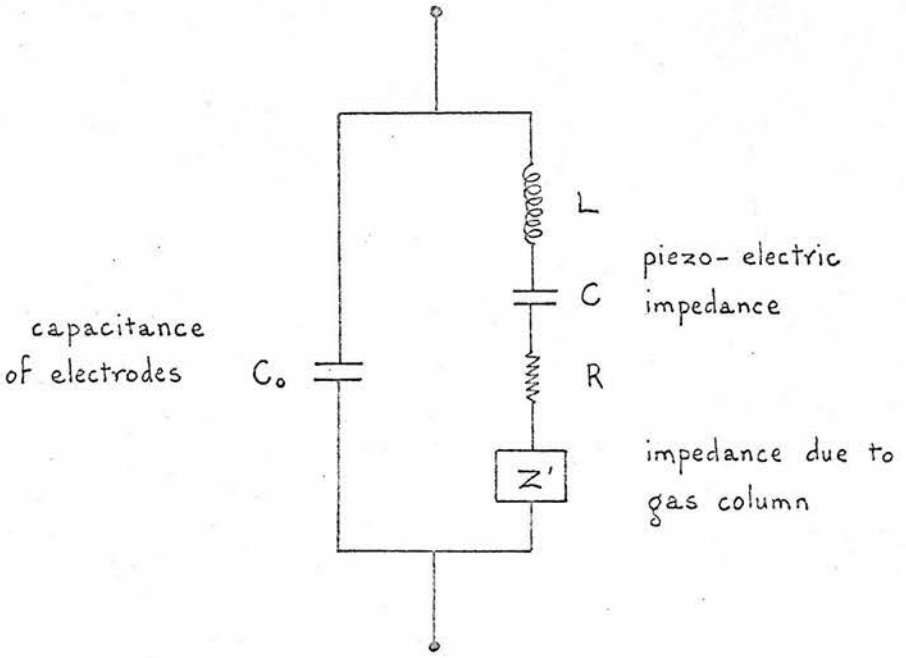

Fig. 3. Equivalent electric circuit of a quartz crystal

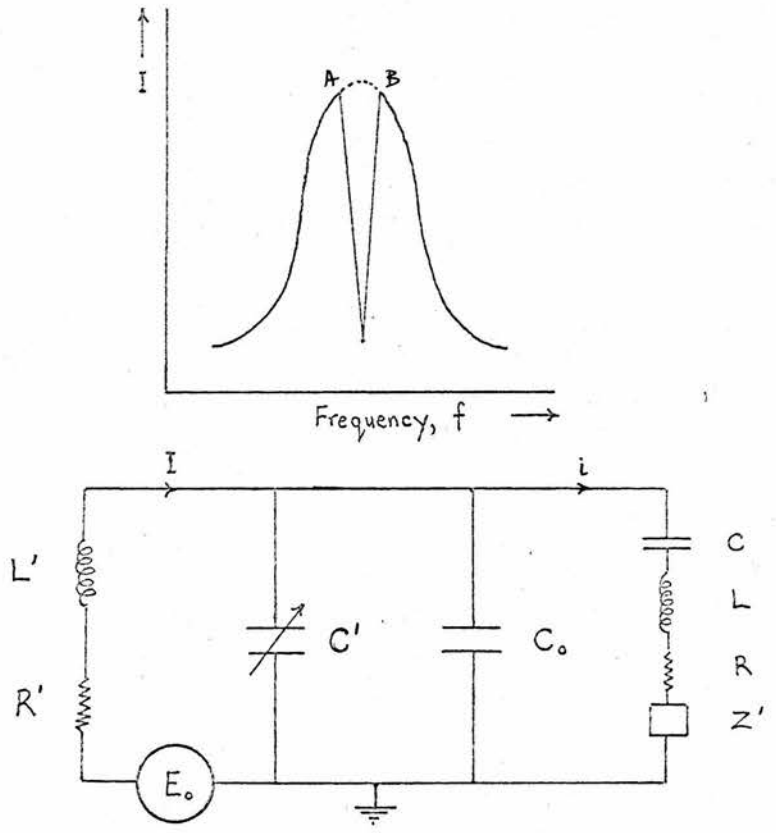

Fig. 4. Acceptor circuit and crystal crevasse

where Z is the acoustic impedance per unit area of the gas column at the transducer, A is the surface area of the transducer and C_t is the electric coupling constant.

The changes in acoustic reaction on a piezo-electric quartz crystal may be detected electrically in several ways:

1. Acceptor circuit.

Dye (1926), in a fundamental paper on piezo-electric quartz resonators, discussed the circuit shown in fig. 4. The circuit may be readily tuned to the resonant frequency of the crystal, (when the current i actually flowing in the quartz circuit is in phase with the voltage applied across the terminals). The current I shows a sharp minimum, called a dip or crevasse, at the resonant frequency of the crystal (fig. 4), and the value of C' may be varied until the crevasse occurs symmetrically in the broad resonance peak of the L - C circuit. When the circuit is thus tuned:

$$iwL + \frac{1}{iwc} + \frac{1}{iw(C'+C_o)} = 0,$$

$$iwL' + \frac{1}{iw(C'+C_o)} = 0,$$

so that:

$$I = \frac{E_o}{R' + 1/w^2(C_o+C')^2 (R + Z')}$$

Maxima in Z' (which are purely resistive) are reflected by maxima in I.

2. Rejector circuit.

In this circuit (fig. 5) I shows a sharp peak in the broad resonance minimum of the L' - C' circuit (tuned to the resonant frequency of the quartz crystal) at the resonant frequency of the crystal. Tuning is facilitated by looking at the circulatory current i which is a maximum at resonance: C' is adjusted to give a maximum at the resonant frequency of the quartz crystal.

When/

When the circuit is thus tuned:

$$iwL' + \frac{1}{iw(C_o+C')} = 0,$$

$$iwL + \frac{1}{iwc} = 0,$$

so that:

$$I = \frac{E_o}{r_o + R_o(R+Z)/(R_o+R+Z)}$$

where $$R_o = \frac{L'}{(C' + C_o)R'}$$

If $$R_o \gg Z,$$

$$I \approx \frac{E_o}{r_o + R + Z}$$

This time, maxima in Z are reflected by minima in I.

3. Admittance bridge.

Bell (1953) has developed an admittance bridge: changes in the resistive component of the acoustic impedance are indicated directly.

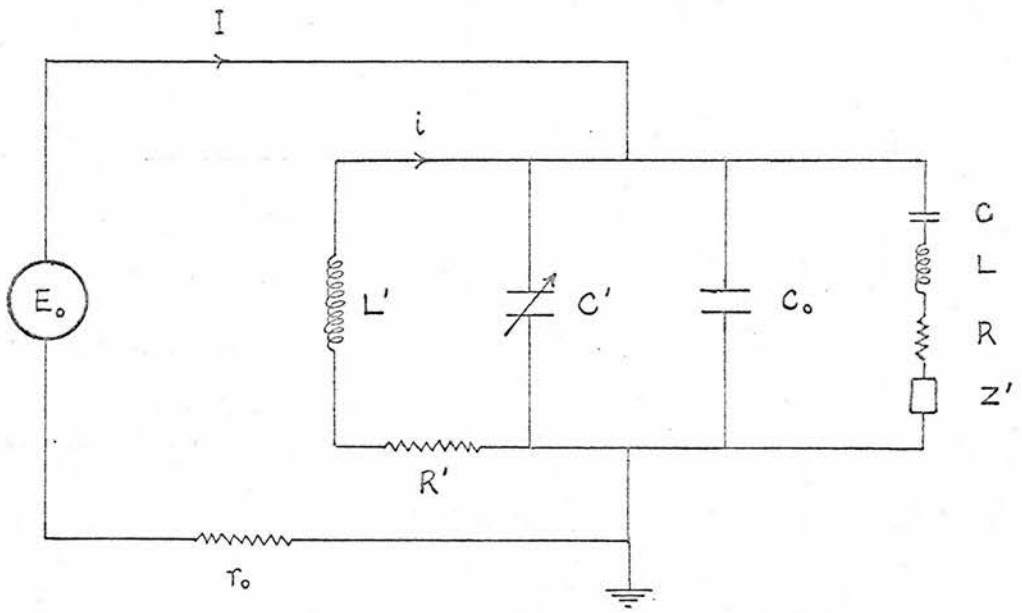

Fig. 5. Rejector circuit.

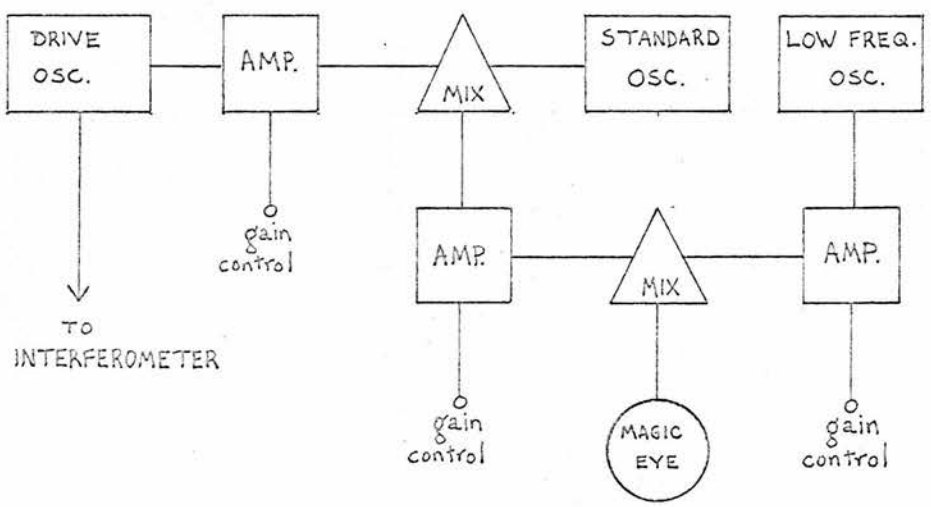

Fig. 6. Block diagram of frequency measurement apparatus.

Frequency measurement.

The frequency of vibration of the interferometer quartz crystal was monitored throughout an experiment by comparing it with a standard crystal of nearly the same resonant frequency. This standard crystal was used to control the frequency of a secondary oscillator; the whole unit was housed in a thermally insulated box. The heat from the valves served to maintain the temperature at about 35°C. with a constancy of 0.1°C. during an experiment.

Edinburgh Observatory kindly measured the standard frequency to 1 part in 10^6, fig. 7.

The standard oscillator was set to beat against the oscillations applied to the interferometer crystal and the resultant low frequency was set to beat against a variable low frequency oscillator; the result was displayed on a magic eye. The low frequency oscillator was adjusted to give zero flicker on the magic eye. Since the low frequency oscillator was calibrated to an absolute accuracy of 1 c/sec., the absolute frequency of the interferometer crystal during an experiment was known to better than 1 part in 50,000. The system was seen to be stable to at least 1 part in 10^6 over a period long enough to take a reading.

A block diagram of the system is shown in fig. 6.

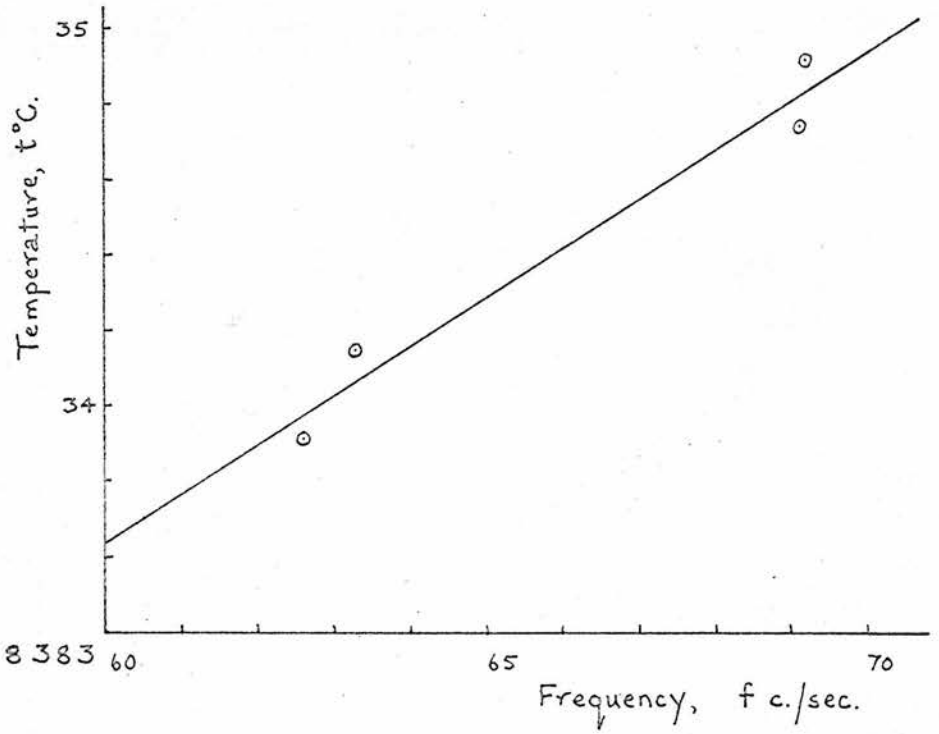

Fig. 7. Frequency calibration of standard crystal

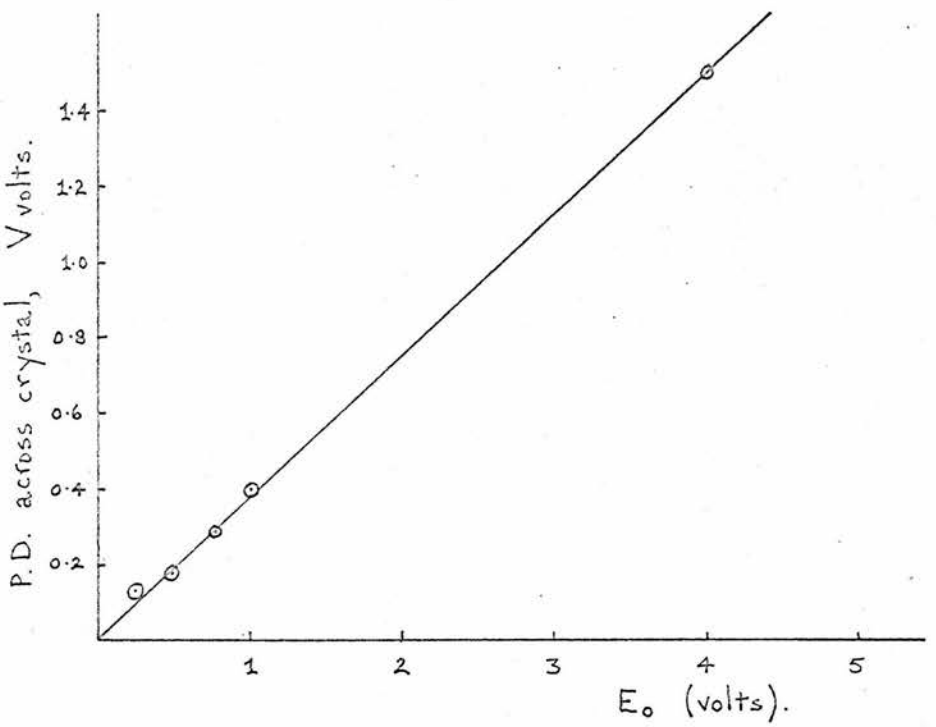

Fig. 8. P.D. across crystal as a function of E_0 (rejector circuit).

Design of the instrument.

The aim was to build an interferometer to operate in the region of 100 kc./sec. at 0-2 atm. pressure and 20 - 200°C. using a small amount of gas, and to measure wavelength to an accuracy of 1 part in 20,000.

A device was obtained from Ferranti Ltd. which was capable of measuring linear traverses of up to 2 cm. with an accuracy of 10^{-5} cm. In this device two optical gratings are aligned so as to produce Moiré fringes from a collimated light beam. A lateral shift of one grating with respect to the other causes a displacement of the fringes; the fringes are counted as they move past a photoelectric head and the total displayed on a linear read-out. The system is arranged so that each count corresponds to a shift of one micron. Tenths of a micron are interpolated on a cathode ray tube whose spot moves round an engraved cursor. Mechanical vibrations of the system also show up on the cathode ray tube. The accuracy of the measurement depends on the gratings: these were ruled by the National Physical Laboratory and guaranteed accurate to 10^{-5} cm. A check was made in situ with a micrometer screw gauge: the maximum discrepancy was 7×10^{-5} cm. over 2 cm.

The interferometer is shown diagrammatically in fig. 9.

The transducer is an X - cut, piezo-electric quartz crystal, supplied by Brookes Crystals Ltd. The crystal, a cylinder 1 inch in diameter, has a circumferential groove in its medial, nodal plane and it is held by three pins with Teflon tips, which rest in the groove. The pins are mounted in a metal ring and one of them is spring loaded so as to hold the crystal securely but without danger of cracking it. The ends of the crystal are coated with gold (by evaporation) to serve as electrodes. The gold is extended down the side as a stripe for a short distance from each end and wires are attached by Devcon (a metal putty) to the stripes. This arrangement relieves the faces of the crystal/

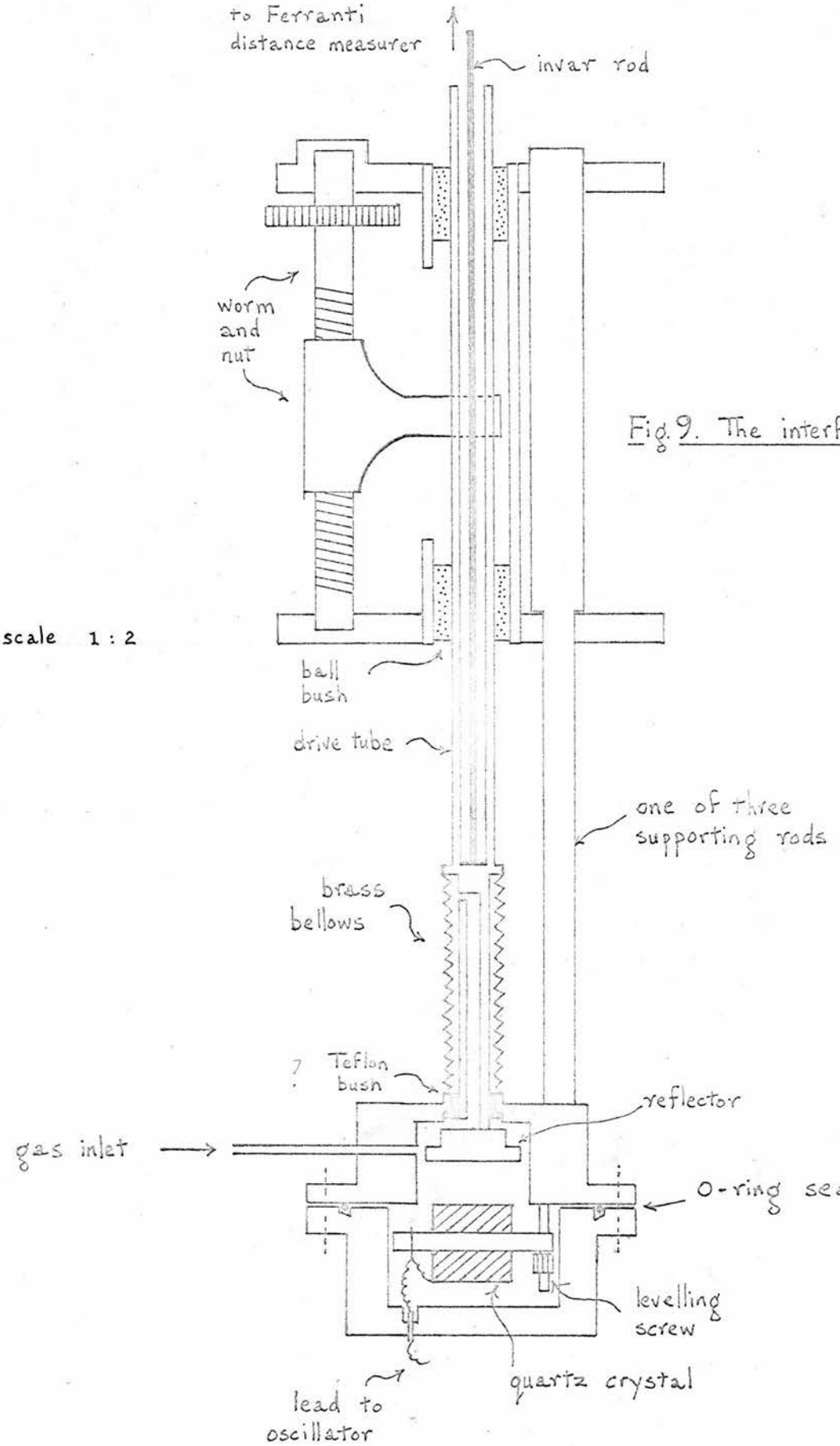

Fig. 9. The interferometer.

crystal of any irregularities which might affect the sound field in front of the crystal. The wire to the upper face of the crystal is taken to earth (the mounting ring), whilst the wire to the lower face is anchored to an insulated tag on the mounting ring and is lead thence out of the vessel via an insulated sleeve. Earthing the upper face eliminates changes in capacitive effects when the reflector moves. The metal mounting ring is suspended on three adjusting screws so that the crystal may be levelled with respect to the reflector.

The polished stainless steel reflector, 1¼ in. in diameter, is fixed to the end of a stainless steel tube, which moves up and down in two ball bushings. The tube is guided into the vessel by a Teflon bush. A Hydroflex brass bellows allows the tube to move in and out of the vessel whilst keeping the vessel gas-tight. Vertical drive for the tube is provided by a worm and nut. The worm has a pitch of 6 turns per inch and is rotated through a worm and wheel reduction gear by a reversible electric motor at a speed which moves the nut at 1/50th inch per minute. Fine control is obtained with microswitches. Microswitches are also arranged to stop the motor automatically when the reflector reaches either end of its 2 cm. traverse. The motor is mounted on the wall and its shaft connected via a rubber tube to reduce vibration.

Movement of the reflector is transmitted by an invar rod, resting at the foot of the drive tube, to the slider of the measuring device. The slider moves under the constant load of its own weight. The invar rod extends into the thermostat so that the temperature gradient from the vessel to the measuring device will have negligible effect.

Measurement to 10^{-5} cm. requires mechanical stability of a high order. To reduce vibration the apparatus is mounted on a half-inch steel plate resting on two brick piers in the basement of the building. The room is also thermostatted at 21°C. to reduce/

reduce thermal effects.

The cylindrical, stainless steel gas vessel is suspended below the plate on three rods. The lower part of the vessel may be removed to expose the crystal assembly. The latter is situated at the bottom of a 1½ inch long, 1½ inch diameter tube, along which the reflector moves. A ¼ inch steel tube leads via a valve to the gas handling system. The total volume of the vessel is about 50 cc. In order to allow measurements with the reflector at extended distances from the crystal face the crystal mounting may be lowered on its adjustment screws. This necessitates the insertion of a stainless steel collar between the two parts of the gas vessel. Rubber O-rings seal the vessel when the parts are bolted together.

A thermally insulated bath of silicone oil is supported from pulleys on the plate and counterbalanced by lead weights. The oil is thermostatted by means of an immersion heater connected to a hard valve relay operated by a toluene regulator. Auxilliary heating is provided by mica elements under the bath. The bath may be raised to cover the gas vessel. A stirrer is mounted on the wall. The temperature of the bath was taken with a thermometer calibrated at the National Physical Laboratory to 0.01°C. The temperature stability of the bath was better than 0.05°C. during the course of an experiment.

The gas handling system.

The general arrangement of the apparatus is as shown in fig. 10. The apparatus consists of a pumping system and vacuum line, to which are connected a collection of gas storage globes with freeze-out traps, a Töpler pump, a distillation line, a U-tube mercury manometer, a Pirani vacuum gauge, several subsidiary mercury manometers to indicate roughly the pressure in their respective parts of the apparatus, and an air purification train. The interferometer is also connected via a glass spiral which protects the glass-metal seal from undue strain due to thermal expansion. The apparatus may be evacuated by a glass, mercury diffusion pump, backed by a rotary oil pump or an evacuated 5 litre globe. A liquid nitrogen trap, between the pumps and the vacuum line, prevents mercury vapour passing into the apparatus and protects the oil pump from condensible vapours.

The glassware is clamped to a metal grid. Pyrex glass is used throughout and all taps lubricated with Apiezon L grease.

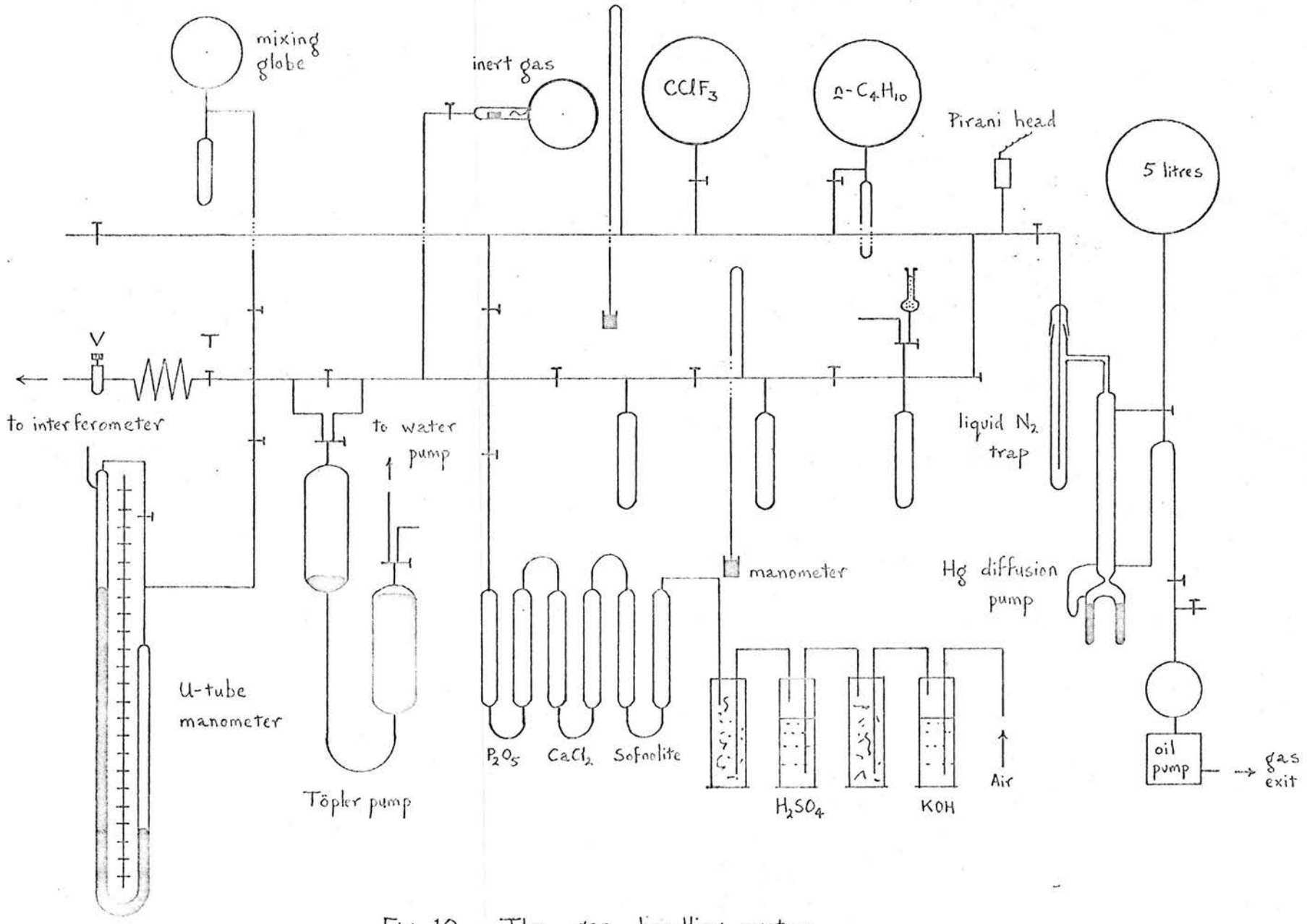

Fig. 10. The gas handling system

Electronics.

Two separate electronic units were built for the interfero-:meter: one based on the acceptor circuit and the other on the rejector circuit. Both units were fed from a stabilized power pack. Simplified circuit diagrams are shown in fig. 11.

1. Acceptor circuit.

A cathode-coupled Colpitts oscillator is loosely coupled through a buffer amplifier to the crystal circuit. The frequency range is 50 - 500 kc./sec. Current I in the tuned circuit is detected by induction, amplified, rectified and displayed on a microammeter of variable sensitivity.

The power from the oscillator is variable and Voltage across the crystal may be crudely measured by a valve voltmeter. However, the valve voltmeter affects the crystal circuit so much at crystal resonance, that it is best to take readings just off tune at the maxima A or B (fig. 4) in order to examine systematically the effect of oscillator power.

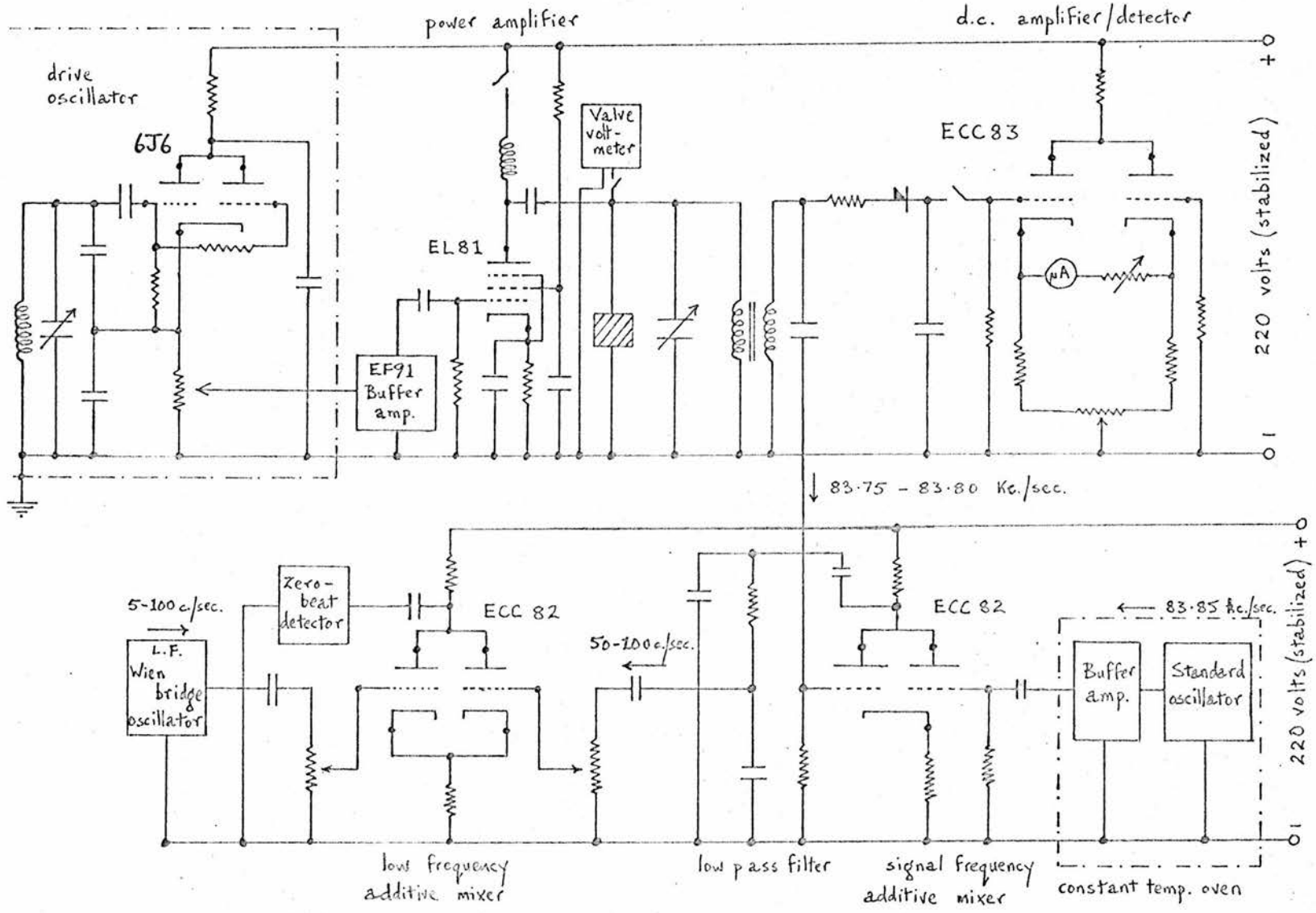

Fig. 11a. Acceptor circuit electronics.

2. Rejector circuit.

A similar oscillator, designed to give frequencies in the region of 83 kc./sec. only, is connected via a cathode follower as a low impedance source of E.M.F., E_o = 0.1 to 10 volts. The voltage across the crystal at resonance vs. E_o is shown in fig. 8, (measured with an Airmec valve voltmeter). The circulating current i in the tuned L' - C' circuit is detected by induction and displayed on a magic eye. Current I is also detected by induction: the signal is amplified and partly backed off in order to detect small changes by means of a microammeter of variable sensitivity.

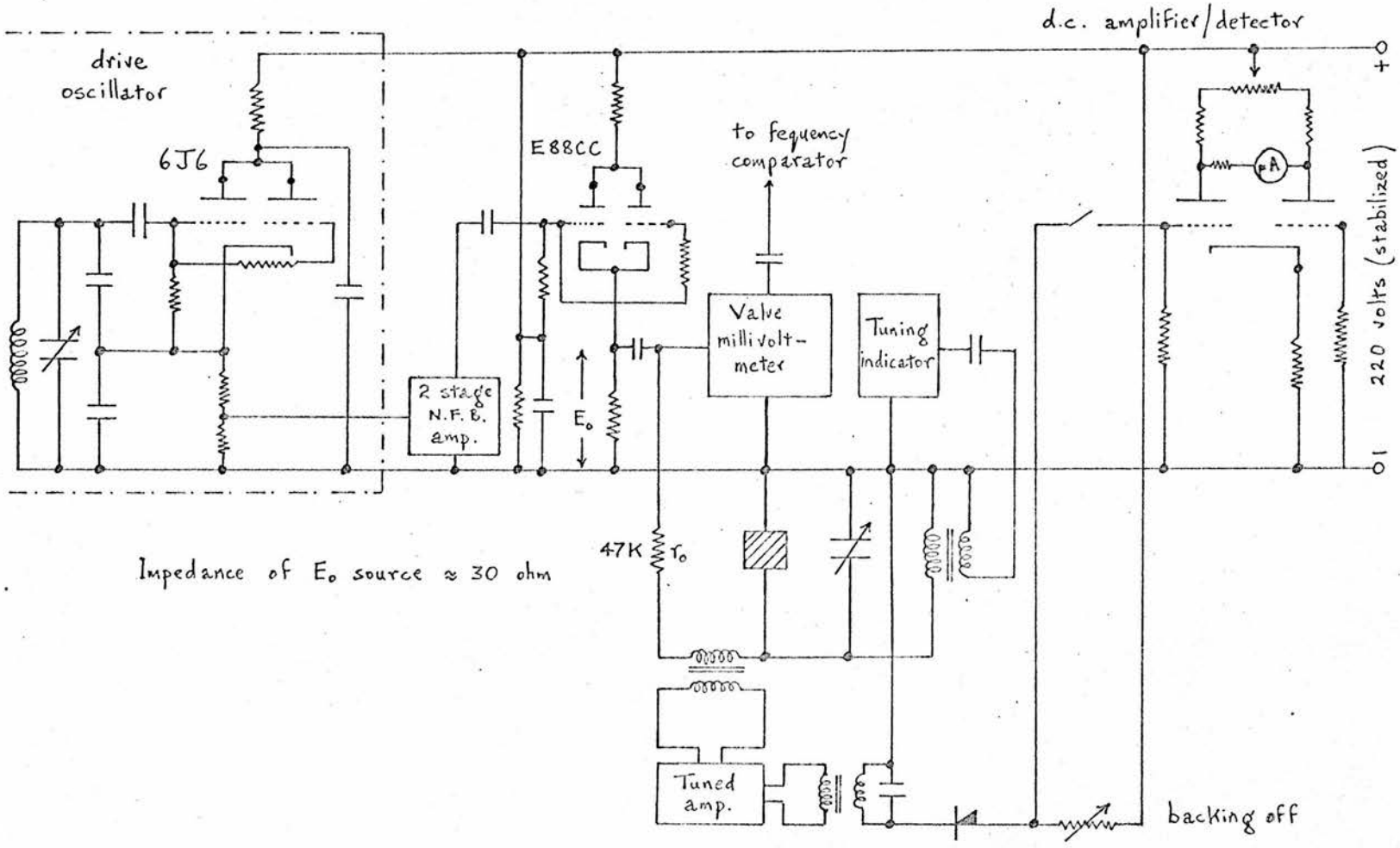

Fig. 11b. Rejector circuit electronics

The gases used.

1. Air.

Dry, CO_2-free air was prepared by drawing atmospheric air slowly through:

(i) an almost saturated aqueous solution of potassium hydroxide, to remove CO_2.

(ii) a glass-wool spray trap.

(iii) concentrated sulphuric acid, to remove water vapour.

(iv) another spray trap.

(v) two tubes of Sofnolite to remove last traces of CO_2.

(vi) two tubes of fused calcium chloride, to remove more water vapour.

(vii) two tubes of phosphorus pentoxide dispersed on glass wool, to complete the drying ($< 2.10^{-5}$ mg./l. at 25°C.)

2. Inert gases.

1¼ litre samples of "spectrally pure" Helium, Neon and Argon were obtained in sealed globes from the British Oxygen Company. Their specifications are listed below:

He: 100% He, 2 v.p.m. CO_2, 4 v.p.m. O_2

Ne: 99.9% Ne, 0.1% He, 2 v.p.m. O_2, 1 v.p.m. H_2.

Ar: 100% Ar, 1 v.p.m. CO_2, 2 v.p.m. O_2.

A 1¼ litre sample of Krypton containing ½% Xenon as the only impurity was also obtained from the B.O.C.

3. Normal butane.

$\underline{n}$ - C_4H_{10} was introduced into the apparatus directly from a cylinder supplied by B.P. The purity was only 99%

4. Chlorotrifluoromethane.

$CClF_3$ (Arcton 13) was introduced directly into the apparatus from a cylinder supplied by I.C.I. The purity was not quoted.

Experimental procedure.

1. Levelling the crystal.

The interferometer crystal was levelled with respect to the reflector by adjusting the three screws supporting the mounting ring, until the height of the first reflection peak in open air was a maximum. This was a trial and error procedure: each adjustment was followed by a movement of the reflector through the reflection peak to observe the height.

2. Preparation of the interferometer.

After replacing the bottom of the interferometer, the metal vessel was degassed by heating in an isomantle to about 200°C. and pumping. After 24 hours the system held a vacuum of 1 μ Hg. for 1 hr.

The isomantle was then removed and the thermostat bath raised into position around the vessel. The apparatus was left overnight to reach temperature equilibrium.

3. Introduction of gas.

Gas was admitted to the interferometer and U-tube mercury manometer via tap T. Air was let slowly into the vacuum line through the purification train until the required pressure (up to 1 atm.) was attained. Tap T and valve V were closed. At the end of a series of experiments on air, the apparatus was thoroughly evacuated for two days.

The other gases were admitted from the storage globes, when the maximum pressure attained was a little below 1 atm. The gases were returned to their respective globes at the end of a series of experiments by freezing out in liquid nitrogen (Ar, Kr, $\underline{n}$ - C_4H_{10}) or by using the Töpler pump (He, Ne, $CClF_3$).

4. Acceptor circuit electronics.

The/

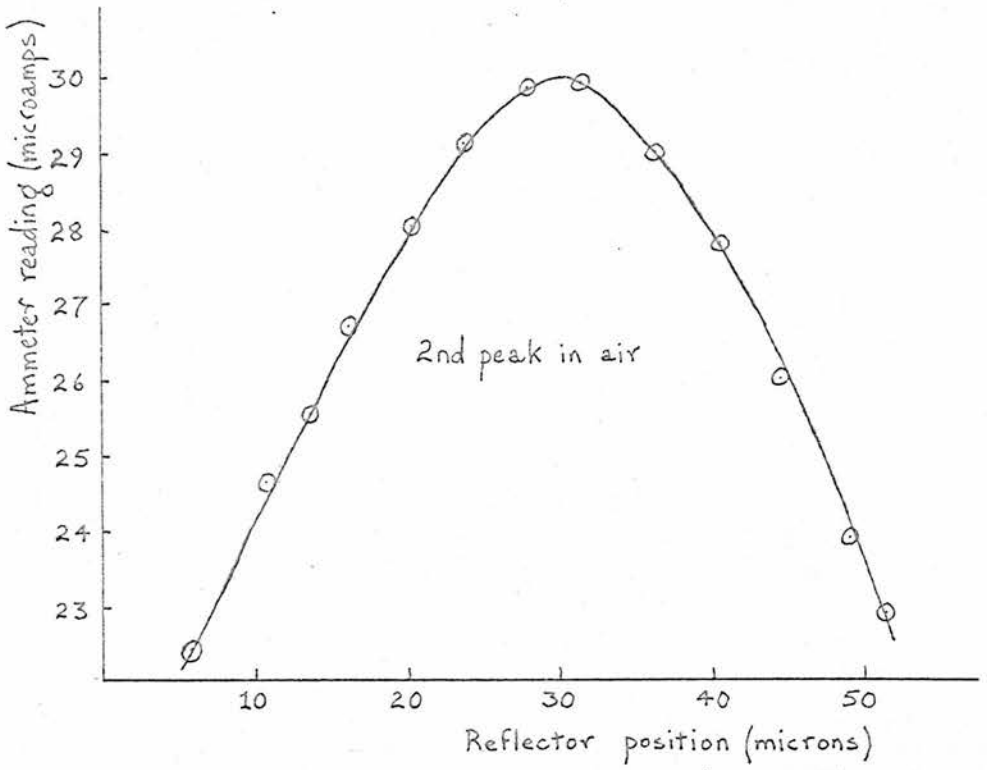

Fig. 12. Typical reflection peak (acceptor circuit).

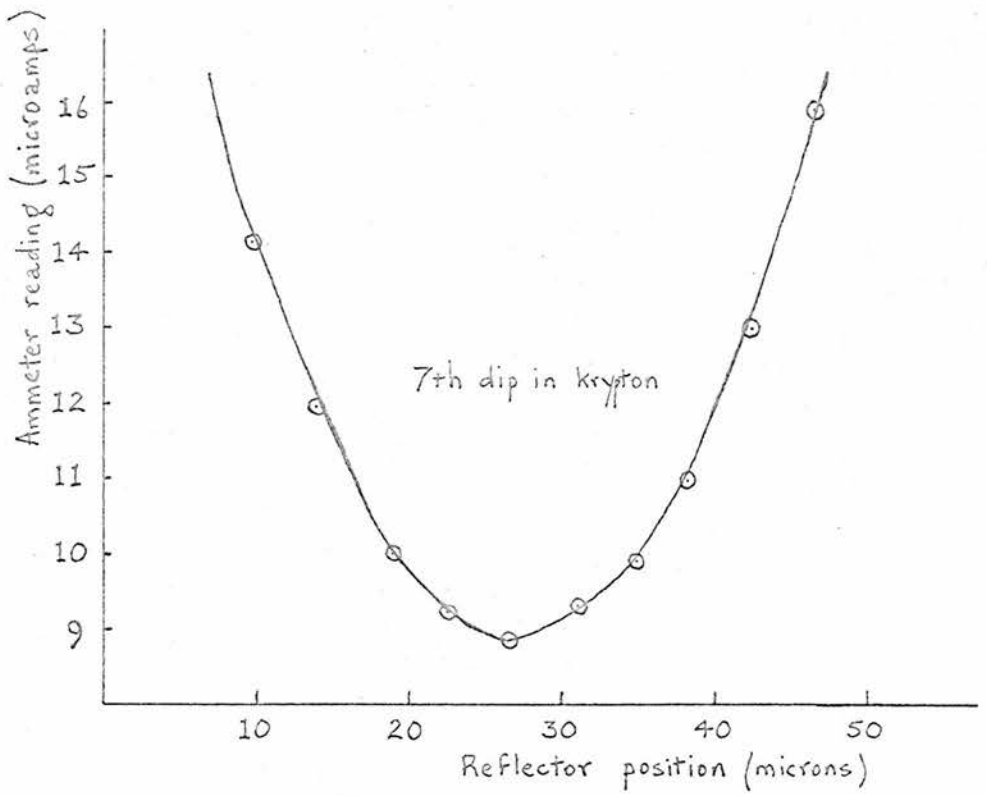

Fig. 13. Typical reflection dip (rejector circuit).

The unit was switched on and left to warm up for several hours. A suitable power and sensitivity were selected. After roughly tuning the circuit to the crystal dip, the interferometer reflector was moved to a position approximately mid-way between two reflection peaks, and the off-tune crystal volts were measured by the valve voltmeter. This voltage was recorded as an indication of the oscillator power. The circuit was retuned accurately. The low frequency oscillator was adjusted to give zero flicker on the magic eye and the dial reading of this oscillator was noted: this dial was not moved again during an experiment.

5. Measurement of reflection peaks.

The reflector was returned to one end of its traverse and the Ferranti distance counter zeroed. The temperatures of the room, standard oscillator, and interferometer thermostat were recorded. After roughly locating the first peak as the reflector was moved on, the top of the peak was examined in detail. At 4 μ intervals the reflector was stopped, the frequency of the drive oscillator adjusted to give zero flicker on the magic eye, and the microammeter and distance readings recorded. A typical crest is shown in fig. 12. (Over some parts of the reflector traverse, there was some "run-on" after the reflector motor was switched off. However, this was never serious enough to prevent the location of a peak in the way described). The rest of the reflection peaks were examined similarly. The temperatures of the room, standard oscillator and interferometer thermostat were recorded at the end of the run. A complete entry in the laboratory book for experiment A2 is given in the results section.

6. Rejector circuit electronics.

A definite value of E_0 was selected and the gain and backing-off arranged to give a suitably large deflection on the microammeter./

microammeter. The Microammeter was put on low sensitivity at first to protect it from excessive currents. With this unit the crystal gave an inverted crevasse at its resonant frequency and reflections in the interferometer produced sharp dips. Accurate tuning was again carried out in between two reflections and the reflection dips were measured in the same way as were the peaks in the previous electronics. A typical reflection dip is shown in fig. 13.

Calculation of results.

1. Apparent wavelength.

The positions of all reflection peaks (or dips) were located on graphs by inspection, (viz:- figs. 12,13), and the distance values tabulated. Since the zero of the Ferranti measuring unit was arbitrary, only relative positions could be compared. Intervals between successive reflection peaks gave the apparent half-wavelength. The graph of these intervals vs. ordinal number was plotted and the root mean square deviation calculated. The mean wavelength was taken as 2x the arithmetic mean of the intervals.

2. Frequency.

The frequency of the vibration of the quartz crystal in the interferometer was given by:

f = (frequency of standard) - (dial reading of low frequency oscillator).

The standard frequency was read from the calibration graph (fig. 7) at the appropriate standard crystal temperature.

3. Velocity.

Velocity was calculated from the formula (1):

$$v = f\lambda .$$

4. Comparison with theory.

The experimentally observed velocities were compared with theoretical values for CO_2-free, dry air and the inert gases. Experimental velocities were corrected to 30°C. using the relation:

$$v^2 \propto T.$$

Theoretical velocities were corrected to the pressure used in the experiment using the relation (4):

$$v = v_{id}(1 + Sp/RT).$$

Experimental/

Experimental and theoretical wavelengths were then calculated for the frequency 83,780 c./sec., using the relation:

$$\lambda = v/f,$$

and the graph of relative error in wavelength, $\frac{\lambda - \lambda_{th}}{\lambda_{th}}$ vs. square of theoretical wavelength, λ_{th}^2, plotted, (fig. 22).

THEORETICAL VELOCITIES.

1. CO_2-free, dry air.

The composition of air was taken from the data of Keenan and Kaye (1945), viz. Table 1. This data leads to a value of the molecular weight of CO_2-free, dry air,

$$M.W. = 28.970$$

The ideal molar heat capacities, at constant pressure, of oxygen and nitrogen were calculated from the spectroscopic data of Johnston and Walker (1933) and Johnston and Davies (1934) respectively, using

$$R = 1.9865 \text{ cal. } (15^0)/\text{mole.}$$

These values, together with the values calculated from them for CO_2-free, dry air of the above composition, are given in Table 2. (The value for argon was taken as $C_P^{id} = 5R/2$).

Ideal sound velocities were then calculated at five degree intervals in temperature using the equations:

$$V_{id}^2 = \gamma^{id} RT/M,$$

$$= 1 + R/(C_p^{id} - R).$$

For the calculation of the effect of gas imperfection, the virial data of Holborn and Otto (1925) were used. The results are given in Table 3.

Tilton (1934) estimates that there is a day to day variation of about 1 part in 1,000 in the density of air. A minimum in density is observed soon after a barometric maximum. He attributes the effect to isotopic changes in the upper atmosphere and subsequent mixing. Thus the velocity of sound in CO_2-free, dry air is not reliable to an accuracy greater than about 1 part in 2,000.

Table 1.

Composition of Air.

	M.W.	% by vol.
N_2	28.016	78.03
O_2	32.000	20.99
A	39.944	0.98

Table 2.

Heat capacities in CO_2-free, dry air.

$t^oC.$	$C_p^{id}(O_2)$ Cal./mole.	$C_p^{id}(N_2)$ Cal./mole.	C_p^{id} (Air) Cal./mole.	γ^{id}
0	6.992	6.958	6.945	1.4007
30	7.023	6.960	6.954	1.4000
45	7.049	6.963	6.961	1.3996
60	7.072	6.966	6.969	1.3989
75	7.096	6.969	6.976	1.3982

Table 3.

Theoretical velocity of sound in CO_2-free, dry air.

t °C	γ^{id}	Vid cm/sec	B cc/mole	$\frac{T}{c} \cdot \frac{dB}{dT}$ cc/mole	$\frac{T^2}{2c(c+1)} \cdot \frac{d^2B}{dT^2}$ cc/mole	Sp/RT x 10^5	v cm/sec
0	1.4007	33138	-13.5	+27.4	-8.99	22	33145
5	1.4006	33438	-12.5	+26.9	-8.99	23	33446
10	1.4005	33737	-11.5	+26.5	-8.98	26	33746
15	1.4004	34032	-10.5	+25.9	-8.99	27	34041
20	1.4003	34325	- 9.5	+25.3	-8.98	28	34335
25.	1.4002	34615	- 8.5	+24.7	-8.88	29	34625
30	1.4000	34901	- 6.8	+23.8	-8.86	30	34911
35	1.3999	35187	- 6.5	+23.3	-8.84	31	35198
40	1.3997	35468	- 5.6	+22.8	-8.79	32	35479
45	1.3996	35749	- 4.2	+22.2	-8.73	35	35761

c = 2.5

p = 1 atm.

2. The inert gases.

The following atomic weights were used:

He	4.00248
Ne	20.183
Ar	39.944
Kr	83.8
Xe	131.3

and γ^{id} was taken as 1.66667.

The following sources of virial data were used:

He, Ne, Ar — Holborn and Otto (1925)

Kr, Xe — Beattie et al. (1952 and 1951)

The results are given in the succeeding tables; the virial correction refers to atmospheric pressure.

A correction for $\frac{1}{2}$ % Xe in the Kr sample was made by calculating an "apparent" molecular weight,

M.W. = 84.037

At 30°C. the ideal velocity of sound in the sample is then:

V_{id} = 22358 cm./sec.

The virial correction factor was assumed to be the same as that for pure Kr. So at 30°C. and 1 atm.:

v = 22379 cm./sec.

A similar correction was made for the 0.1% He in the Ne sample,

M.W. = 20.167

At 30°C. the ideal velocity of sound in the sample is then:

V_{id} = 45641 cm./sec.

The virial correction factor was assumed to be the same as that for pure Ne. So at 30°C. and 1 atm.:

v = 45660 cm./sec.

Table 4.

Theoretical velocity of sound in helium.

t °C	Vid cm/sec	B cc/mole	$\frac{T}{c}\cdot\frac{dB}{dT}$ cc/mole	$\frac{T^2}{2c(c+1)}\frac{d^2B}{dT^2}$ cc/mole	Sp/RT x10^5	Δ v cm/sec	v cm/sec
0	97249	+11.85	-0.42	-0.37	49.4	48	97201
15	99883	+11.81	-0.55	-0.38	46.2	46	99837
30	102450	+11.76	-0.68	-0.38	43.0	44	102406
45	104954	+11.71	-0.80	-0.35	40.5	43	104911
60	107399	+11.65	-0.91	-0.29	38.2	41	107358
75	109791	+11.59	-1.01	-0.20	36.1	40	109751

c = 1.5

p = 1 atm.

Table 5.

Theoretical velocity of sound in neon.

t °C.	Vid cm/sec	B cc/mole	$\frac{T}{c}\cdot\frac{dB}{dT}$ cc/mole	$\frac{T^2}{2c(c+1)}\frac{d^2B}{dT^2}$ cc/mole	Sp/RT x10^5	v cm/sec	v cm/sec
0	43307	+10.60	+4.28	-2.12	56.9	25	43332
15	44480	+10.92	+3.94	-2.03	52.1	24	44504
30	45622	+11.21	+3.64	-1.90	52.1	24	45646
45	46738	+11.47	+3.37	-1.73	50.3	23	46761
60	47827	+11.69	+3.15	-1.57	48.6	23	47850
75	48892	+11.89	+2.97	-1.37	47.2	23	48915

c = 1.5

p = 1 atm.

Table 6.

Theoretical velocity of sound in argon.

t °C	Vid cm/sec	B cc/mole	$\frac{T}{c}\cdot\frac{dB}{dT}$ cc/mole	$\frac{T^2}{2c(c+1)}\frac{d^2B_2}{dT^2}$ cc/mole	Sp/RT x10^5	v cm/sec	v cm/sec
0	30784	-22.1	+47.0	-21.2	16.5	5	30779
15	31618	-18.2	+43.4	-21.6	14.8	5	31613
30	32430	-15.0	+38.2	-21.9	5.2	2	32428
45	33223	-11.8	+36.7	-21.3	13.8	5	33228
60	33997	- 9.5	+33.8	-19.8	16.1	5	33991
75	34754	-7.3	+31.1	-17.5	22.1	8	34746

c = 1.5

p = 1 atm.

Table 7.

Theoretical velocity of sound in krypton.

t °C	Vid cm/sec	B cc/mole	$\frac{T}{c}\cdot\frac{dB}{dT}$ cc/mole	$\frac{T^2}{2c(c+1)}\frac{d^2B_2}{dT^2}$ cc/mole	Sp/RT x10^5	v cm/sec	v cm/sec
0	21253	-60.5	+84.1	+ 3.5	121	26	21279
15	21829	-54.0	+78.9	+ 3.4	120	26	21855
30	22390	-47.7	+74.4	+ 3.3	120	27	22417
45	22937	-42.4	+69.8	+ 3.2	118	27	22964
60	23471	-37.6	+65.5	+ 3.2	114	27	23498
75	23994	-33.5	+61.7	+ 3.1	110	26	24020

c = 1.5

p = 1 atm.

EXPERIMENTAL RESULTS.

The experimental results fall into two parts:

A. Measurements using the acceptor circuit electronics. In this series of experiments the crystal was arranged to be almost touching the reflector when the latter was at the bottom of its traverse. The valve voltmeter was not introduced until the effect of power was examined in experiment A 4 .

B. Measurements using the rejector circuit electronics. In this series of experiments the depth of the gas vessel was extended by means of the collar and the crystal lowered by ca. ½ cm. Thus, in the case of air, the first reflection dip corresponded to the third nodal position in front of the crystal.

The reflection peaks (dips) are numbered starting from the one with the reflector nearest the crystal.

Exp. A1. Examination of the first reflection peak in CO_2-free, dry air.

An extended examination was made of the first reflection peak in CO_2-free, dry air, after levelling the crystal. The satellite peak was most pronounced on this first peak. The results are given in Table 8, and the plot of ammeter reading vs. reflector position shown in fig. 14a.

Temperature	29.30°C.
Pressure	747 mm. Hg.
Frequency	83,787 c./sec.

Reflector going UP .

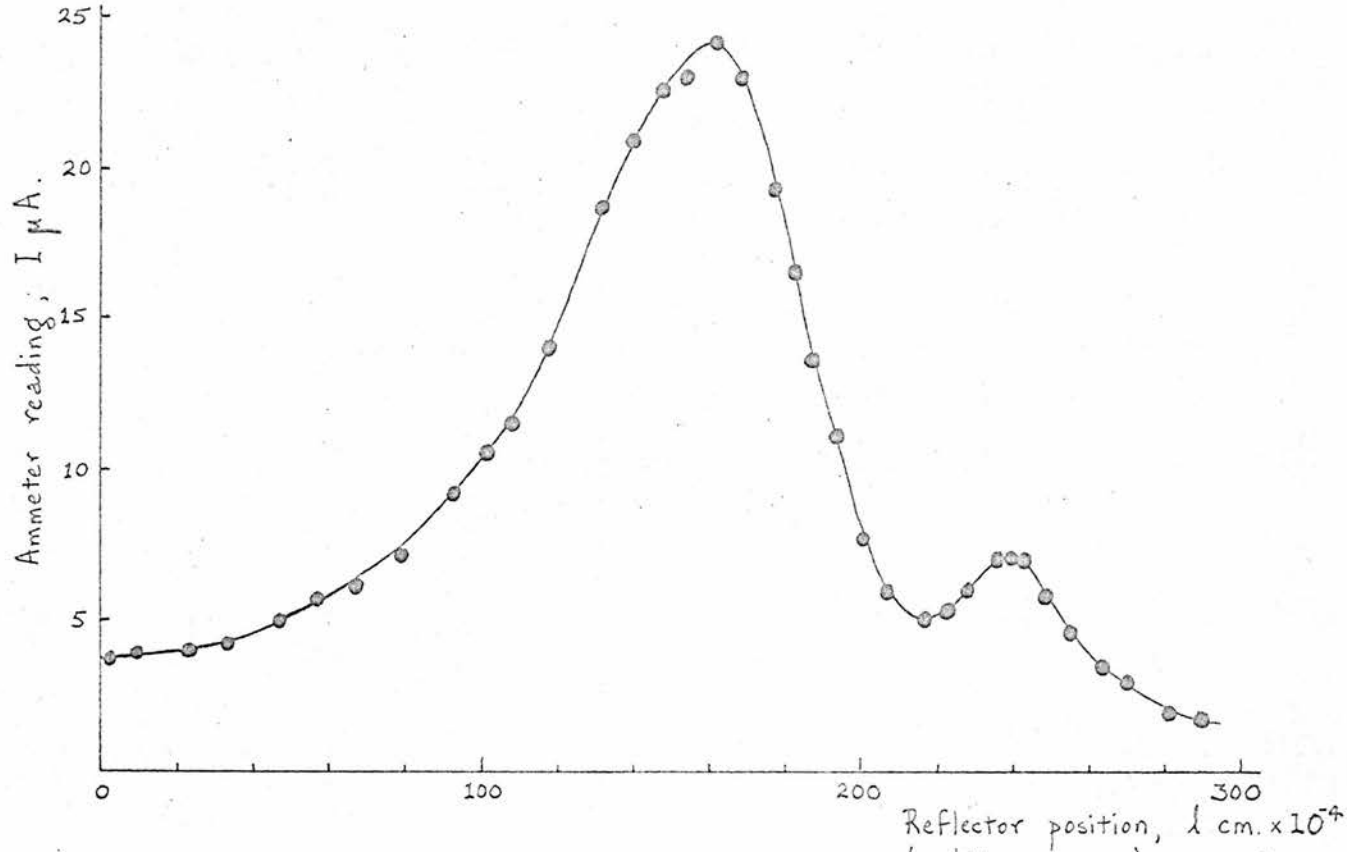

Fig. 4a. The first reflection peak (exp.)

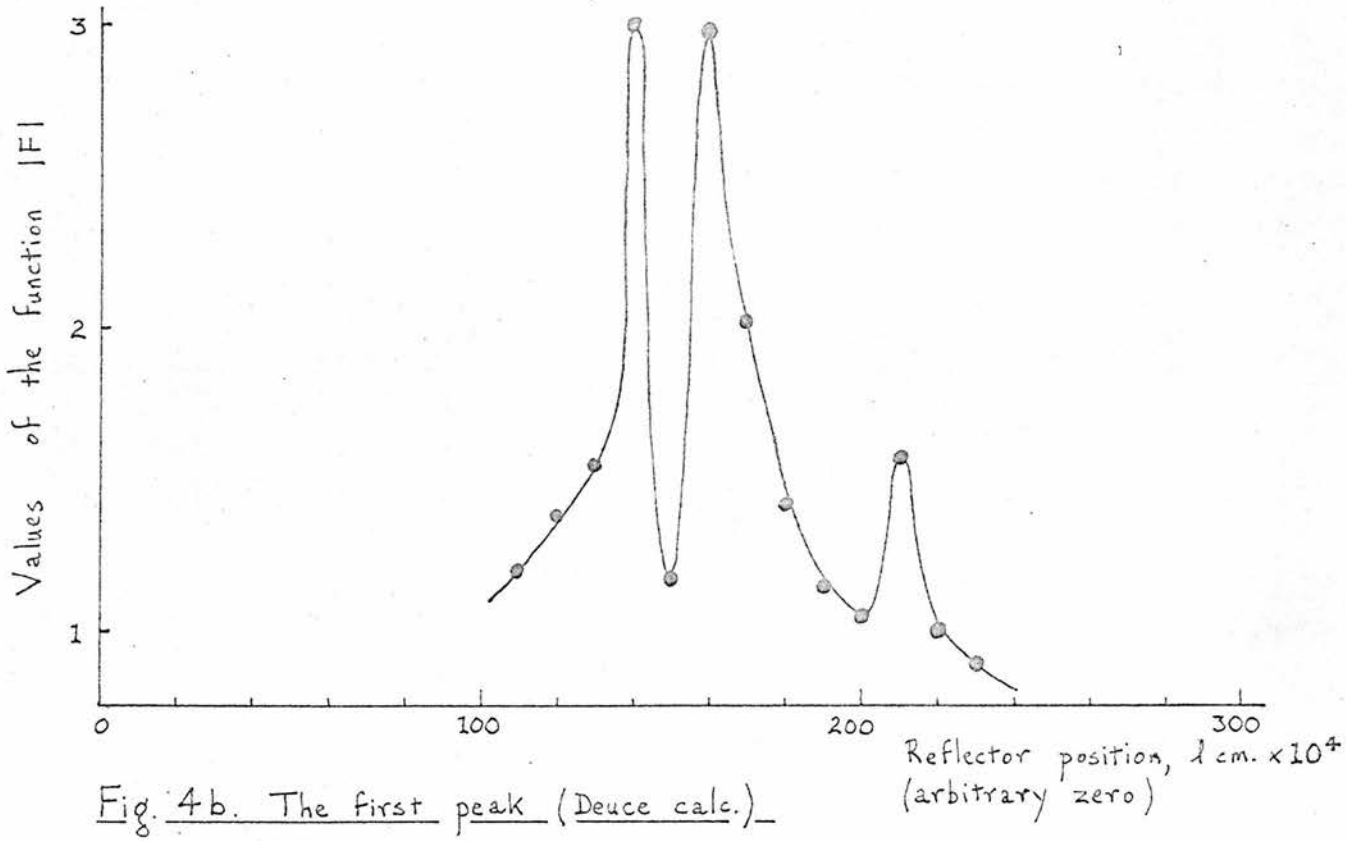

Fig. 4b. The first peak (Deuce calc.)

Table 8.

Results of Experiment A 1.

Ammeter reading μA	Reflector position x10^4cm.	Ammeter reading μA	Reflector position x10^4cm.	Ammeter reading μA	Reflector position x10^4cm.	Ammeter reading μA	Reflector position x10^4cm
3.7	202.5	10.6	301.5	19.2	377.6	7.0	436.2
3.9	209.5	11.5	308.6	16.4	382.5	7.0	438.5
4.0	223.1	13.9	318.9	13.4	387.5	6.9	442.4
4.2	233.4	18.8	331.9	11.0	394.4	5.7	448.6
4.9	246.9	20.9	339.9	7.8	400.2	4.4	455.5
5.7	247.3	22.5	348.7	5.9	406.9	3.4	463.3
6.1	267.1	23.2	354.9	5.0	417.6	2.9	470.4
7.1	278.7	23.9	362.4	5.2	423.3	2.1	481.4
9.0	291.5	23.0	369.9	6.0	427.7	1.8	490.1

Exp. A2. Examination of reflection peaks in CO_2-free, dry air.

The complete entry in the laboratory note-book is given below for this experiment. In a single run, using CO_2-free, dry air, peaks 1-8 (inclusive) were located. The observations are given in Table 9. The positions of the reflection peaks are collected in Table 10, together with the intervals between successive peaks (apparent half-wavelengths) and the deviations of these intervals from the mean value. The deviation vs. ordinal number is shown graphically in fig. 15.

	At beginning of experiment.	At end of experiment.
Room temperature	20.7°C.	20.8°C.
Standard crystal temperature	34.0°C.	34.0°C.
Interferometer temperature	29.38°C.	29.42°C.

Reflector going UP

Pressure 737 mm. Hg.

Frequency difference 49 c./sec.

The apparent velocity is compared with the theoretical value.

Mean temperature	29.40°C.
Frequency	83,787 c./sec.
Mean half-wavelength	0.20936 cm.
Velocity (corrected to 30°C.)	35132 cm./sec.
Theoretical velocity	34911 cm./sec.
Difference in velocity	0.63%

Table 9.

Results of Experiment A 2.

	Ammeter reading. μA.	Reflector position $x10^4$ cm.		Ammeter reading. μA.	Reflector position $x10^4$ cm.
1st peak	29.1	417.2	2nd peak	27.0	2518.1
	29.7	419.8		27.7	2520.6
	30.6	423.4		28.3	2523.6
	31.1	425.6		29.2	2527.2
	31.9	428.4		29.9	2531.4
	32.2	430.9		29.9	2533.7
	32.0	435.5		29.4	2537.0
	31.7	437.6		28.9	2538.7
	30.0	441.2		27.6	2543.4
	29.1	443.0		25.9	2546.6
1st satellite	11.9	493.2	2nd satellite	6.4	2651.6
	12.3	496.0		6.7	2653.5
	13.4	499.8		6.8	2655.2
	13.9	501.8		7.0	2659.9
	13.8	505.0		6.8	2665.6
	13.9	507.2		6.4	2668.3
	13.4	509.5		6.4	2670.9
	13.1	511.8		6.2	2675.8
	12.3	514.8		5.8	2677.3
	11.8	516.7		5.6	2680.5
3rd peak	23.1	4608.0	5th peak	22.3	8805.7
	24.0	4611.6		22.9	8808.5
	24.9	4614.9		23.7	8812.2
	26.1	2620.2		24.1	8815.9
	27.0	4623.5		24.8	8819.5
	27.8	4628.7		25.0	8823.7
	27.6	4633.1		24.6	8826.8
	27.0	4637.2		24.2	8829.4
	25.9	4640.8		23.4	8832.5
	24.1	4645.5		22.0	8836.4

Table 9 (contd.)

	Ammeter reading. μA.	Reflector position $x10^4$ cm.
4th peak	22.0	6708.4
	22.9	6712.3
	23.6	6715.4
	24.2	6718.9
	25.1	6723.9
	25.6	6725.8
	25.7	6729.0
	25.4	6731.7
	25.2	6734.3
	24.9	6736.8
7th peak	18.3	12994.2
	18.7	12997.3
	19.3	13002.8
	19.9	13006.6
	20.0	13011.6
	20.0	13015.8
	20.0	13019.3
	19.8	13022.9
	19.0	13026.4
	18.2	13029.8

	Ammeter reading μA.	Reflector position $x10^4$ cm.
6th peak	19.5	10899.8
	20.1	10904.7
	20.7	10907.8
	21.0	10911.2
	21.3	10915.6
	20.9	10919.7
	20.7	10923.8
	20.0	10927.8
	19.8	10929.6
	18.8	10933.5
8th peak	17.0	15077.0
	17.6	15081.3
	17.9	15085.2
	18.1	15087.7
	18.3	15091.9
	18.3	15097.2
	18.0	15101.3
	17.8	15105.0
	17.0	15109.8
	16.3	15113.2

Table 10.

Half-wavelengths in Experiment A 2.

Peak no.	Reflector position $x10^4$cm.	Interval $x10^4$cm.	Deviation of interval from mean $x10^4$cm.	Interval No.
1	433.0			
		2099.7	+ 5.2	1
2	2532.7			
		2099.2	+ 4.7	2
3	4630.5			
		2097.8	+ 3.3	3
4	6729.7			
		2093.0	- 1.5	4
5	8822.7			
		2093.0	- 1.5	5
6	10915.7			
		2099.3	+ 4.8	6
7	13015.0			
		2079.5	-15.0	7
8	15094.5			

Satellites:		
1	504.7	
		2155.8
2	2660.5	

Exp. A 3. To check the reproducibility of results.

A series of runs was done using the same sample of CO_2-free, dry air at the same temperature and pressure. Only reflection peaks 3, 4, 6 and 7 were located. The apparent half-wave-lengths are given in Table 11 (the interval between peaks 4 and 6 is divided by two for this purpose).

Temperature	29.34°C.
Pressure	736 mm. Hg.
Frequency	83,787 c./sec.

The averages of the measured half-wavelengths are:

3	2098.2	$x10^{-4}$cm.
4/5	2092.9	$x10^{-4}$cm.
6	2096.6	$x10^{-4}$cm.

Table 11.

Half-wavelengths in Experiment A 3.

Reflector going UP			Reflector going DOWN		
Peak No.	Reflector posn. x10^4 cm.	½-wavelength x10^4 cm.	Reflector posn. x10^4 cm.	½-wavelength x10^4 cm.	Interval No.
3	4561.5		1053.2		
		2098.2		2100.0	3
4	6659.7		3149.0		
		2093.6		2093.5	4/5
6	10847.0		7336.0		
		2095.0		2095.8	6
7	12942.5		9436.0		
3	4195.7		1065.0		
		2096.8		2098.8	3
4	6292.5		3161.2		
		2092.4		2092.7	4/5
6	10477.3		7346.7		
		2097.2		2096.2	6
7	12574.5		9445.5		
3	2096.5		2096.0		
		2098.0		2097.5	3
4	4194.5		4193.7		
		2092.0		2093.1	4/5
6	8378.5		8380.8		
		2097.2		2097.7	6
7	10476.0		10477.5		

Exp. A 4. The effect of crystal power.

A series of runs was done, using the same sample of CO_2-free, dry air, changing the power supplied to the crystal. The off-resonance crystal voltage (see above) was recorded for each run. Reflection peaks 1-7 (inclusive) were located. The experimental conditions and the apparent half-wavelengths (intervals between successive reflection peaks) are given in Table 12. The mean velocities (corrected to 30°C.), together with the root mean square deviation in the half-wavelength values, are collected in Table 13.

The average observed velocity (30°C., 1 atm.) of this series is 35129 cm./sec.

Table 12.

Half-wavelengths in Experiment A 4.

Peak No.	Reflector posn. $x10^4$ cm.	Interval $X10^4$ cm.	Deviation of interval from mean, $x\ 10^4$ cm.		
2	10499.7			Reflector going	DOWN
		2094.7	+0.6	Temperature	29.33°C.
3	8405.0			Pressure	719 mm.Hg.
		2094.8	+0.7	Frequency	83,788 c./sec.
4	6310.2			Crystal voltage	14 V.
		2092.0	-2.1	Mean half-wavelength	0.20941 cm.
5	4218.2				
		2096.0	+1.9		
6	2122.2				
		2093.0	-0.9		
7	29.2				
2	1092.2			Reflector going	UP
		2094.5	+0.1	Temperature	29.43°C.
3	3186.7			Pressure	730 mm.Hg.
		2094.3	-0.1	Frequency	83,787 c./sec.
4	5281.0			Crystal voltage	25 V.
		2093.7	-0.7	Mean half-wavelength	0.20944 cm.
5	7374.7				
		2095.3	+0.9		
6	9470.0				
		2094.2	-0.2		
7	11564.2				

Table 12 (Contd.)

Peak No.	Reflector posn. $x10^4$ cm.	Interval $x10^4$ cm.	Deviation of interval from mean $X\ 10^4$ cm.		
2	11505.7			Reflector going	DOWN
		2094.7	+0.5	Temperature	29.44°C.
3	9411.0			Pressure	720 mm. Hg.
		2095.5	+1.3	Frequency	83,787 c./sec.
4	7315.5			Crystal voltage	35 V.
		2092.0	-2.2	Mean half-wavelength	0.20942 cm.
5	5223.5				
		2094.8	+0.6		
6	3128.7				
		2093.7	-0.5		
7	1035.0				
2	1046.3			Reflector going	UP
		2096.5	+1.8	Temperature	29.45°C.
3	3142.8			Pressure	729 mm. Hg.
		2095.7	+1.0	Frequency	83,786 c./sec.
4	5239.5			Crystal voltage	47 V.
		2092.2	-2.5	Mean half-wavelength	0.20947 cm.
5	7331.7				
		2093.8	-0.9		
6	9425.5				
		2095.3	+0.6		
7	11520.8				

Table 12 (Contd.)

Peak No.	Reflector posn. $x10^4$ cm.	Interval $x10^4$ cm.	Deviation of interval from mean $x\ 10^4$ cm.		
2	11519.4			Reflector going	DOWN
		2097.6	+2.9	Temperature	29.46°C.
3	9421.8			Pressure	722 mm. Hg.
		2096.1	+1.4	Frequency	83,786 c./sec
4	7327.7			Crystal voltage	62 V
		2095.0	+0.3	Mean half-wavelength	0.20947 cm.
5	5232.0				
		2091.1	-3.6		
6	3137.0				
		2093.7	-1.0		
7	1045.9				

EX BIBL. UNIV. EDINBURGEN

Table 13.

Velocities in Experiment A 4.

Off-resonance crystal voltage	Mean velocity (corrected to 30°C.) cm./sec.	R.m.s.d. in half-wavelengths $\times 10^4$ cm.
14	35130	1.39
25	35129	0.52
35	35125	1.21
47	35132	1.53
62	35132	2.21

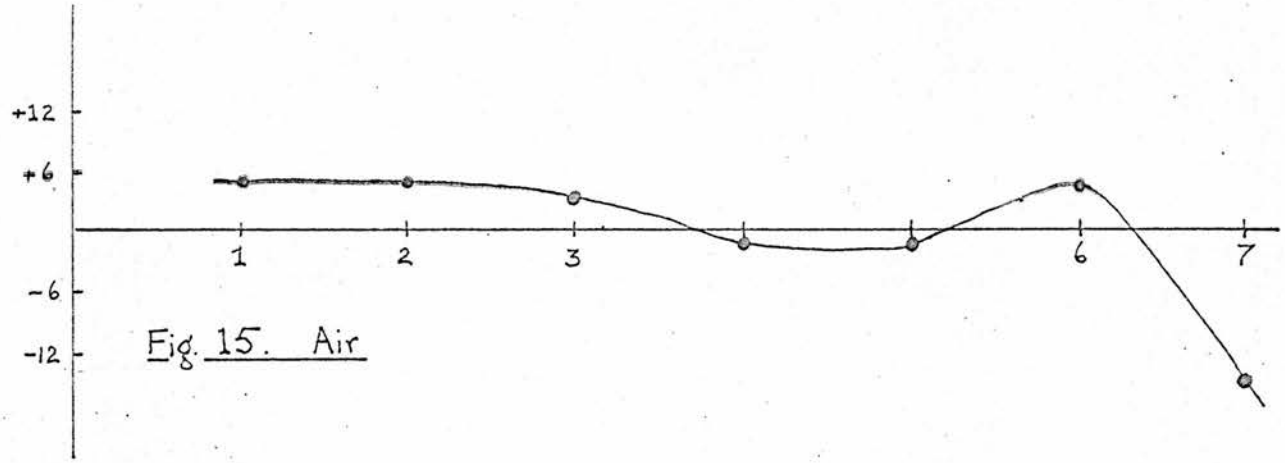

Fig. 15. Air

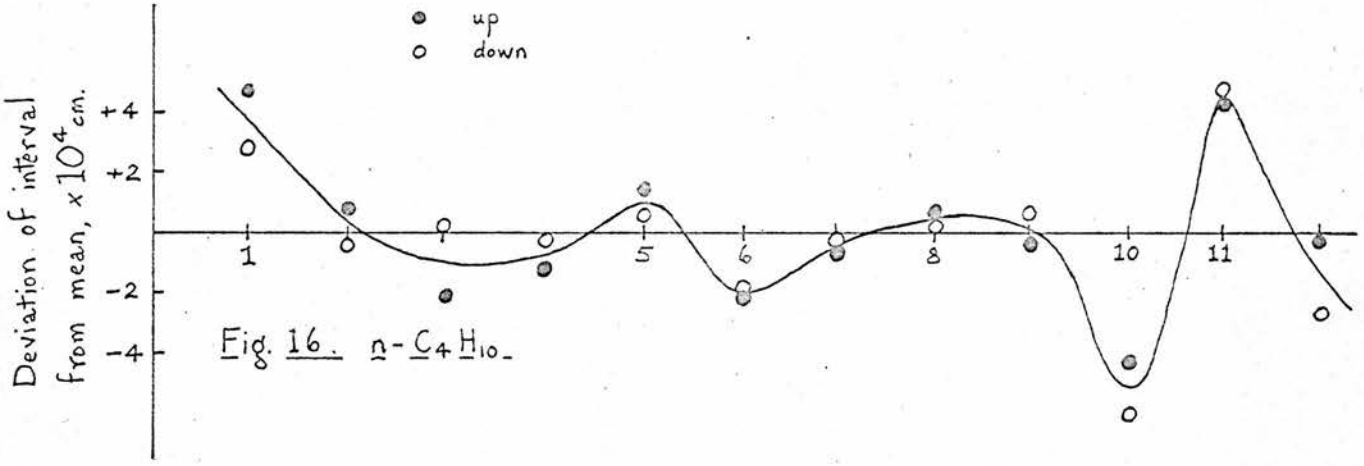

Fig. 16. n-C_4H_{10}

Ordinal no. of interval ⟶

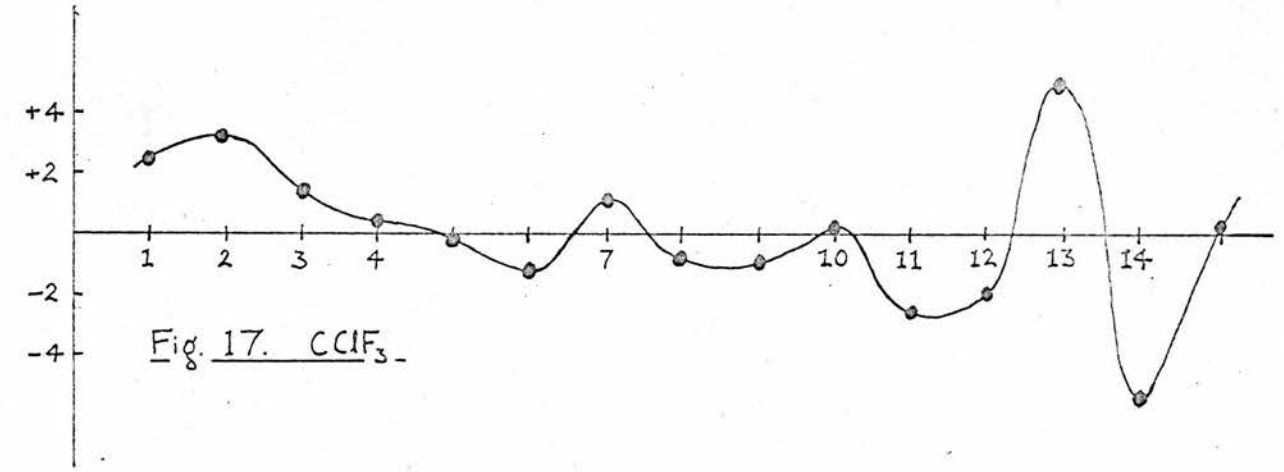

Fig. 17. $CClF_3$

Variation of intervals with ordinal number

Exp. A 5. Half-wavelengths in $\underline{n}$ - C_4H_{10}.

The reflection peaks were examined in normal butane in which sound velocity is low. With the same experimental conditions a run up and down run was done, without zero-ing the distance measurer in between. The results are given in Table 14, and the variation in the interval between successive reflection peaks vs. ordinal number is shown graphically in fig. 16.

Temperature	29.63°C.
Pressure	746 mm. Hg.
Frequency	83,789 c./sec.
Crystal voltage	30 v.
Mean half-wavelength (down)	0.12748 cm.
Mean half-wavelength (up)	0.12747 cm.
Average velocity (corrected to 30°C.)	21375 cm./sec.

Table 14.

Half-wavelengths in Experiment A 5.

Peak No.	Reflector posn. $x10^4$cm.	Interval $x10^4$cm.	Deviation of interval from mean $x10^4$cm.	Reflector posn. $x10^4$cm.	Interval $x10^4$cm.	Deviation of interval from mean $x10^4$cm.	Interval No.
1	816.0			816.2			
		1279.5	+4.7		1277.5	+2.8	1
2	2095.5			2093.7			
		1275.5	+0.7		1274.3	-0.4	2
3	3370.5			3368.0			
		1272.7	-2.1		1275.0	+0.3	3
4	4643.2			4643.0			
		1273.5	-1.3		1274.5	-0.2	4
5	5916.7			5917.5			
		1276.3	+1.5		1275.2	+0.5	5
6	7193.0			7192.7			
		1272.7	-2.1		1272.8	-1.9	6
7	8465.7			8465.5			
		1274.0	-0.8		1274.5	-0.2	7
8	9739.7			9739.0			
		1275.5	+0.7		1275.0	+0.3	8
9	11015.2			11014.0			
		1273.3	-1.5		1275.5	+0.8	9
10	12288.5			12290.5			
		1270.7	-4.1		1268.5	-6.2	10
11	13559.2			13558.0			
		1279.3	+4.5		1279.5	+4.9	11
12	14838.5			14837.5			
		1274.5	-0.3		1273.2	-2.5	12
13	16113.0			16110.7			

Reflector going UP

Reflector going DOWN

Exp. A 6. Half-wavelengths in $CClF_3$.

The reflection peaks were examined in chloro-trifluoro-Methane in which sound velocity is very low. A single upward run was done. The results are given in Table 15, and the variation in the intervals between successive reflection peaks vs. ordinal number is hown graphically in fig. 17.

Temperature	29.90°C.
Pressure	718 mm. Hg.
Frequency	83,788 c./sec.
Crystal voltage	30 v.
Mean half-wavelength	0.09884 cm.
Velocity (corrected to 30°C.)	16566 cm./sec.

Table 15.

Half-wavelengths in Experiment A 6.

Peak no.	Reflector posn. $\times 10^4$ cm.	Interval $\times 10^4$ cm.	Devn. of interval from mean $\times 10^4$ cm.	Interval no.	Peak no.	Reflector posn. $\times 10^4$ cm.	Interval $\times 10^4$ cm.	Devn. of interval from mean $\times 10^4$ cm.	Interval no.
1	498.5				8	7424.6			
		991.0	+2.6	1			987.5	-0.9	8
2	1489.5				9	8412.0			
		991.7	+3.3	2			987.5	-0.9	9
3	2481.2				10	9399.5			
		989.8	+1.4	3			988.5	+0.1	10
4	3471.0				11	10388.0			
		988.8	+0.4	4			985.0	-2.4	11
5	4459.8				12	11373.0			
		988.2	-0.2	5			986.5	-1.9	12
6	5448.0				13	12359.5			
		987.2	-1.2	6			993.5	+5.1	13
7	6435.2				14	13353.0			
		989.3	+0.9	7			983.0	-5.4	1 4
8	7424.6				15	14336.0			
		987.5	-0.9	8			989.0	+0.6	15
9	8412.0				16	15325.0			

Exp. B 1. The effect of crystal power.

A series of runs was done, using the same sample of Co_2-free, dry air, changing the power supplied to the crystal. The value of E_o was recorded for each run. Reflection peaks 1 - 8 (inclusive) were located; these corresponded to the nodal positions 3 - 10 (inclusive) in front of the crystal. The experimental conditions remained the same throughout the series. The apparent half-wavelengths (intervals between successive reflection dips) are given in Table 16, and the mean values collected in Table 17.

Temperature	30.40°C.
Pressure	737 mm. Hg.
Frequency	83,780 c./sec.

These results were taken by Mr. M.A. Day.

Table 16.

Half-wavelengths in Experiment B 1.

Interval No.	Interval $x10^4$cm.	Deviation of interval from mean $x10^4$ cm.	
1	2098	+5	E_o= 0.1v.
2	2098	+5	
3	2098	+5	
4	2085	-8	
5	2095	+2	
6	2093	-10	
7	2092	-1	
1	2096	+4	E_o= 0.4v.
2	2093	+1	
3	2098	+6	
4	2091	-1	
5	2094	+2	
6	2080	-12	
7	2093	+1	
1	2096	+3	E_o= 2.0v.
2	2092	-1	
3	2098	+5	
4	2094	+1	
5	2094	+1	
6	2088	-5	
7	2091	-2	

Table 17.

Mean half-wavelengths in Experiment B 1.

E_o volts	Mean half-wavelengths $\times 10^4$ cm.
0.1	2093
0.4	2092
2.0	2093

Exp. B 2. The effect of pressure.

Two runs were done, using the same sample of CO_2-free, dry air, at different pressures. The half-wavelengths are given in Table 18 and the mean velocities (corrected to 30°C.) collected in Table 19. The variation of the half-wavelengths vs. ordinal number is shown graphically in fig. 18.

Temperature	30.03°C.
Frequency	83,782 c./s.
E_o	2 v.

Table 18.

Half-wavelengths in Experiment B2.

	726 mm. Hg. (UP)			385 mm. Hg. (DOWN)			
Peak No.	Reflector posn. $x10^4$cm.	Interval $x10^4$cm.	Deviation of interval from mean $x10^4$cm.	Reflector posn. $x10^4$cm.	Interval $x10^4$cm.	Deviation of interval from mean $x10^4$ cm.	Interval No.
1	42.2			14685.7			
		2095.0	+2.2		2095.3	+2.6	1
2	2137.2			12590.4			
		2095.6	+2.8		2095.6	+2.9	2
3	4232.8			10494.8			
		2092.4	-0.4		2092.8	+0.1	3
4	6325.2			8402.0			
		2092.6	-0.2		2094.0	+1.3	4
5	8417.8			6308.0			
		2087.5	-5.3		2090.0	-2.7	5
6	10505.3			4218.0			
		2091.0	-1.8		2085.5	-7.2	6
7	12596.3			2132.5			
		2095.7	+2.9		2095.8	+3.1	7
8	14692.0			36.7			

Table 19.

Velocities in Experiment B 2.

Pressure mm.Hg.	Theoretical vel. cm./sec.	Experimental vel. cm./sec.	R.m.s.d. of intervals. $x10^4$ cm.
726	34910	35066	2.7
385	34906	35064	3.5

Exp. B 3.

Argon.

The half-wavelengths for a single run are given in Table 20, and the variation in half-wavelengths vs. ordinal number is shown graphically in fig. 19.

Temperature	30.20°C.
Pressure	566 mm. Hg.
Frequency	83,780 c./sec.
E_o	2 v.
Mean half-wavelength	0.19415 cm.
R.m.s.d. of half-wavelength	0.00025 cm .
Mean velocity (30°C.)	32522 cm./sec.
Theoretical velocity	32436 cm./sec.

Reflector going UP

These results were confirmed by Mr. M.A. Day.

Table 20.

Half-wavelengths in Experiment B 3.

Peak No.	Reflector posn. $x10^4$cm.	Interval $x10^4$cm.	Deviation of interval from mean $x10^4$cm.	Interval No.
1	648.0			
		1942.0	+0.5	1
2	2590.0			
		1944.0	+2.5	2
3	4534.0			
		1941.0	-0.5	3
4	6475.0			
		1941.0	-0.5	4
5	8416.0			
		1941.0	-0.5	5
6	10357.0			
		1936.0	-5.5	6
7	12293.0			
		1943.0	+1.5	7
8	14236.0			
		1944.5	+3.0	8
9	16180.5			

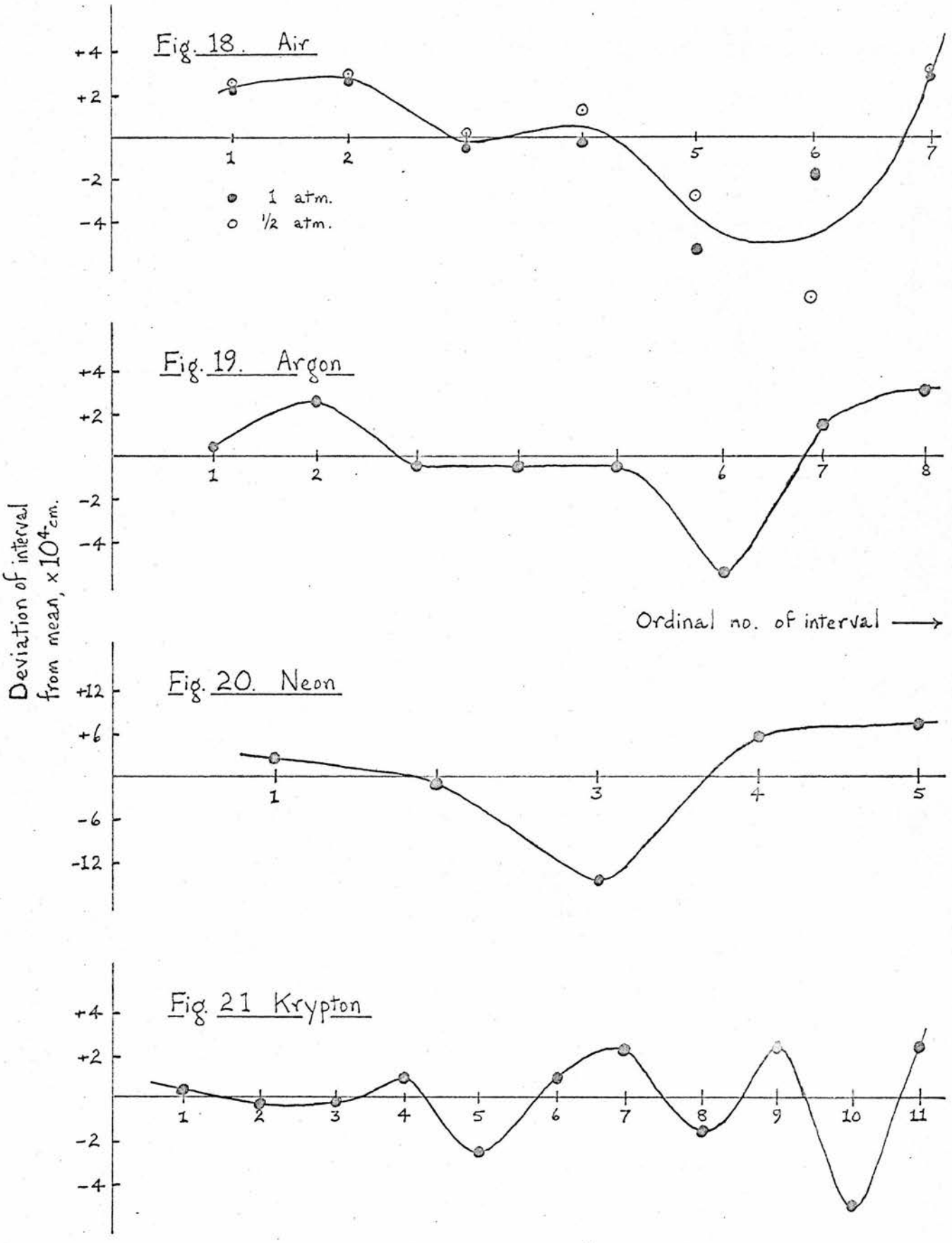

Variation of intervals with ordinal number

Exp. B 4.

Neon.

The half-wavelengths for a single run are given in Table 21, and the variation in half-wavelength vs. ordinal number is shown graphically in fig. 20.

Temperature	30.46°C.
Pressure	587 mm. Hg.
Frequency	83,780 c./sec.
E_o	2 v.
Mean half-wavelength	0.27531 cm.
R.m.s.d. of half-wavelength	0.00079 cm.
Mean velocity (30°C.)	46097 cm./sec.
Theoretical velocity	45660 cm./sec.

Reflector going UP

These results were confirmed by Mr. M.A. Day.

Table 21.

Half-wavelengths in Experiment B 4.

Peak No.	Reflector posn. $x10^4$cm.	Interval $x10^4$cm.	Deviation of interval from mean $x10^4$ cm.	Interval No.
1	28.0			
		2755.5	+2.4	1
2	2773.5			
		2752.0	-1.1	2
3	5525.5			
		2738.5	-14.6	3
4	8264.0			
		2759.0	+5.9	4
5	11023.0			
		2760.5	+7.4	5
6	13783.5			

Table 22.

Half-wavelengths in Experiment B 5.

Peak No.	Reflector posn. $x10^4$cm.	Interval $x10^4$cm.	Deviation of Interval from mean $x10^4$cm.	Interval No.
1	145.7			
		1339.0	+0.4	1
2	1484.7			
		1338.3	-0.3	2
3	2823.0			
		1338.5	-0.1	3
4	4161.5			
		1339.5	+0.9	4
5	5501.0			
		1336.2	-2.4	5
6	6837.2			
		1339.5	+0.9	6
7	8176.7			
		1340.8	+2.2	7
8	9517.5			
		1337.0	-1.6	8
9	10854.5			
		1341.0	+2.4	9
10	12195.5			
		1333.5	-5.1	10
11	13529.0			
		1341.0	+2.4	11
12	14870.0			

Exp. B 5.

Krypton.

The half-wavelengths for a single run are given in Table 22, and the variation in half-wavelength vs. ordinal number is shown graphically in fig. 21.

Temperature	30.26°C.
Pressure	594 mm. Hg.
Frequency	83,780 c./sec.
E_o	2 v.
Mean half-wavelength	0.13386 cm.
R.m.s.d. of half-wavelength	0.00016 cm.
Mean velocity (30°C.)	22426 cm/sec.
Theoretical velocity	22379 cm/sec.

Reflector going UP

Exp. B 6.

Helium.

The half-wavelengths of a single run are given in Table 23. Only three peaks could be located due to the long wavelength. Absorption was very strong and the third peak could not be located very accurately ($\pm 10^{-3}$ cm., say).

Temperature	29.99°C.
Pressure	662 mm. Hg.
Frequency	83,782
E_o	2 v.
Mean half-wavelength	0.6299 cm.
R.m.s.d. of half-wavelength	0.0120 cm.
Mean velocity (30°C.)	105560 cm./sec.
Theoretical velocity	102412 cm./sec.

Reflector going UP

Table 24.

Half-wavelengths in Experiment B 6.

Peak No.	Reflector posn. $\times 10^4$ cm.	Interval $\times 10^4$ cm.	Deviation of interval from mean. $\times 10^4$ cm.	Interval No.
1	1171			
		6423	+124	1
2	7594			
		6176	-123	2
3	13770			

The calibration curve.

The data for the $\Delta\lambda/\lambda$ vs. λ^2 plot is assembled in Table 25. The graph is shown in fig. 22.

Table 25.

The calibration data.

Frequency	=	83,780 c./sec.
Temperature	=	30°C.
Pressure	≈	1 atm.

	Dry, CO_2-free air.	He	Ne	Ar	Kr	
λ (theory)	0.41669	1.2223	0.54500	0.38715	0.2671	cm.
λ (exp)	0.41855	1.260	0.55021	0.38818	0.2676	cm.
$\Delta\lambda$	0.00186	0.038	0.00521	0.00103	0.0005	cm.
$\Delta\lambda/\lambda$	44.69	3o7	95.60	26.50	18.3	$x10^{-4}$
λ^2 (theory)	0.1736	1.494	0.2970	0.1499	0.0714	$cm.^2$

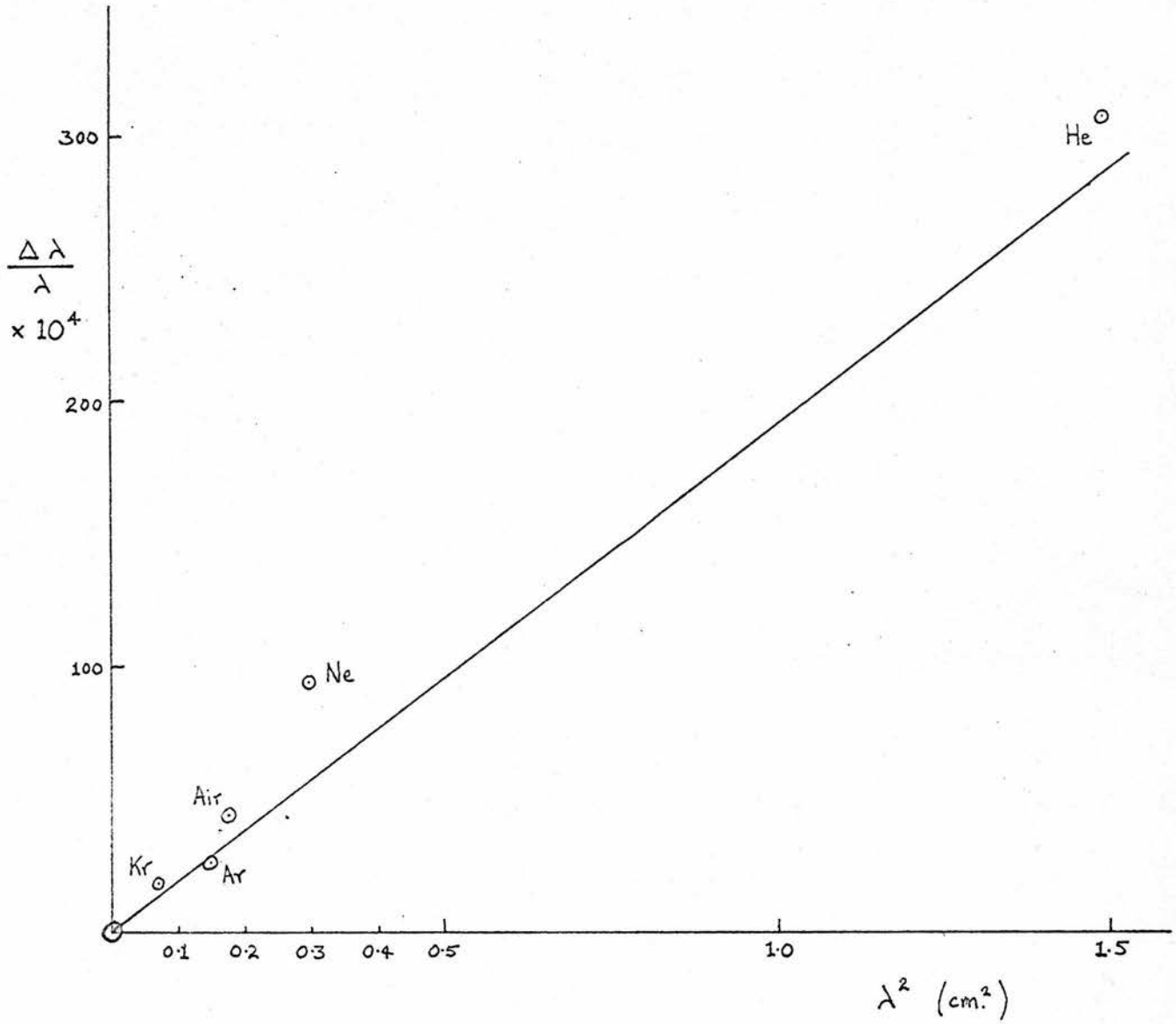

Fig. 22. The calibration curve

Discussion of Results.

The first results obtained for air showed two general features which later appeared to be characteristic of all results from this interferometer:

(a) a mean sound velocity greater than the theoretical free-space, plane-wave value; in the case of air the difference was ca. ½ %.

(b) an irregular, but reproducible, variation of the intervals between successive reflection peaks (these intervals are equal to the half-wavelength in the elementary theory of the interferometer); in the case of air the maximum deviation from the mean was ca. 15 microns in 2,000.

The rest of the results were taken in order to elucidate the effects leading to these spurious results and to calibrate the instrument sufficiently accurately for the determination of relaxation times.

The first part of the discussion deals with the effects of tube dispersion, reflection and high intensity of sound. This is followed by a review of side-effects in interferometers recorded in the literature. The last part attempts to analyse theoretically a simple model of the interferometer. To obtain agreement between the results of this analysis and experiment, a new hypothesis about the propagation of sound in an interferometer is suggested.

Tube dispersion.

In a small tube, the viscosity of the gas, as influenced by the walls, and increased heat conduction from the gas, produce a decrease in sound velocity. The theoretical Helmholtz-Kirchhoff formula, based on a simple model, relates the velocity of a plane-wave in a narrow tube to the free-space velocity:

$$v = v_s \left\{ 1 - \frac{\eta^{\frac{1}{2}} + (C_v \gamma)^{\frac{1}{2}} (\gamma - 1)}{2 r (\pi f \rho)^{\frac{1}{2}}} \right\}$$

where η = coefficient of viscosity of gas,

κ = thermal conductivity of gas,

and v_s = free-space sound velocity.

Henry (1931) has critically examined the assumptions and approximations of this formula. Although it underestimates the tube effect, the formula is good enough to indicate the order of magnitude of the velocity reduction. Many workers have investigated the tube effect experimentally (e.g. Kaye and Sherratt, 1933; Norton, 1935; Lawley, 1952). The later results confirm the form of the relation:

$$v = v_s \left\{ 1 - \frac{C}{2r (\pi f)^{\frac{1}{2}}} \right\},$$

and the constant C agrees with the theoretical value to within 5 %.

For a tube diameter of $1\frac{1}{2}$ in. and a sound frequency of 100 kc./sec. the predicted decrease in velocity is less than 1 part in 10,000:

CO_2 at $20^{\circ}C$. (from theoretical Helmholtz-Kirchhoff formula) $\quad \frac{\Delta v}{v} \times 100 = 0.0083$

Air at $18^{\circ}C$ (from Kaye and Sherratt experimental parameters) $\quad \frac{\Delta v}{v} \times 100 = 0.0077$

Reflection.

The very large difference in compressibility between a gas and steel produces a reflection coefficient of very nearly unity for sound at the reflector in the interferometer. However, the thermal conductivity of a metal is very large and Herzfeld (1938) considered the effect of the temperature changes accompanying the adiabatic/

adiabatic compressions and rarefactions in front of a reflector. Heat flows in and out of the metal; a temperature wave is set up in the gas and a dissipative loss arises from the interference of this temperature wave with the incident and reflected sound waves. All solids are infinitely good conductors compared with a gas, so that the material of the reflector should not influence the reflection coefficient much. For air, Herzfeld calculates that the reflection coefficient of intensity γ^* due to the temperature wave effect is given by:

$$1 - \gamma^* = 4.4 \times 10^{-5} \cdot f^{\frac{1}{2}},$$

so that at 100 kc./sec. the exponential reflection coefficient of amplitude is:

$$\beta = 0.013.$$

However, both Alleman (1939) and Borgnis (1952) have shown theoretically that the reflection coefficient does not affect the separation of successive reflection peaks in an interferometer, although the whole series of reflection peaks is shifted towards the transducer for a finite reflection coefficient.

Intensity.

For an adiabatic sound wave of finite amplitude we have exactly that (Richards, 1939):

$$\frac{\partial^2 y / \partial t^2}{\partial^2 y / \partial x^2} = \frac{\gamma p}{\rho_0} \left(1 + \frac{\partial y}{\partial x} \right)^{-(\gamma + 1)}$$

for a wave propagated in the x-direction with displacement y. For waves of large amplitude the adiabatic compressibility (which determines $\partial y / \partial x$) changes with pressure in such a way that "crests tend to overtake troughs". Fay (1931) has shown how viscosity damping then leads to a stable saw-tooth wave-form. For this wave-form the second term in the expansion of the above expression is zero and, neglecting terms beyond the third, the velocity is given, in terms of the velocity v_0 of waves of infinitely small amplitude, by:

v /

$$v = v_o \left\{ 1 + \frac{\gamma(\gamma+1)}{4} \left(\frac{\partial y}{\partial x} \right)^2 \right\}$$

Richards (1939) has used this equation to calculate the change in velocity in an interferometer where the maximum intensity does not exceed 130 db. (0.1 watt/cm.^{2}). Pielemeier (1935) gives this figure as a reasonable maximum for the intensity in an interferometer, and supports this with observations of particle motion in a Kundt's tube at resonance (Andrade and Lewer, 1929). Richards finds that the velocity is not increased by more than 0.001%.

There is a much larger effect on the absorption coefficient. A saw-tooth wave may be resolved into harmonics of the fundamental frequency. Since

$$\alpha \propto f^2$$

the harmonics are strongly absorbed and the mean absorption coefficient of the saw-tooth wave is enhanced.

Side-effects noted in the literature.

Many workers have reported secondary effects in measurements in an interferometer or similar instrument. The significant observations and interpretations are reviewed below.

(i) Satellites.

An extraneous effect was discovered right from the very beginning of ultrasonic interferometry, when small subsidiary peaks were observed in association with the main reflection peaks which were recorded as the reflector receded from the transducer. (Pielemeier, 1935, gave an explanation in terms of multiple reflections between the reflector and transducer). The position of the maximum of the main peak must surely be affected when the satellites are very close. Kaye and Sherratt (1933) found in their experiments in tubes that at their highest frequency (27,422 c./sec.) it was impossible to locate the reflection peaks because/

because of these satellites; but the satellites disappeared if the diameter of the tube was reduced or the wavelength increased (either by lowering the frequency or by changing the gas to one in which the velocity is higher).

Alleman (1939) demonstrated that the satellites are greatly reduced by levelling the reflector with respect to the transducer. He further suggested that alignment is best achieved by adjustment for maximum height of the main reflection peak. This has been confirmed by Mr. A.J. Matheson in this laboratory. Using a cathetometer he obtained a graph of angle of tilt vs. peak height: the curve showed a maximum at zero tilt.

Even after levelling, satellites usually still remain to a small extent on the side of the main peak corresponding to larger displacement of reflector from transducer, viz:- fig. 14a. The separation of successive, corresponding satellites is greater than the separation of the main peaks.

(ii) Increase in peak separation near the source.

Reid (1930) and Pielemeier (1929) found that the spacing of the reflection peaks is increased when the reflector is near the source. Grabau (1933) studied this effect extensively as a function of frequency, diameter of source and diameter of reflector. He interpreted his results in terms of diffraction of sound from the source, which had a diameter comparable with the wavelength of the sound.

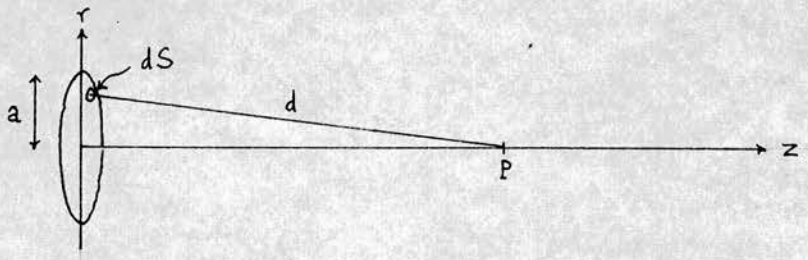

The velocity potential at a point P on the axis of a piston source is given by Rayleigh's formula:

$$\phi(z) = -\frac{\exp(iwt)}{2\pi} \iint \frac{\partial\phi}{\partial z} \frac{\exp(-ikd)}{d}\, ds,$$

where ds is an element of the source surface distance d from P on the axis. If the source is a circular piston of radius a, evaluation of the double integral yields:

$$\text{R.P.}\left[\phi(z)\right] = \frac{1}{k}\frac{\partial\phi}{\partial z}\left[\sin\left\{wt - k(z^2-a^2)^{\frac{1}{2}}\right\} - \sin(wt-kz)\right]$$

Maxima in the amplitude of ϕ occur at

$$z = n\lambda - \frac{a^2}{4n\lambda}, \quad n = 1, 2 \ldots\ldots$$

The sound intensity I along the axis varies as

$$I \propto \sin^2\left[\tfrac{1}{2}k\left\{(a^2 - z^2)^{\frac{1}{2}} - z\right\}\right]$$

The graph of I vs. z for $a = 1.5$ cm., $k = 15$ cm.$^{-1}$ is shown in fig. 23. The near-region, which exhibits maxima, is analogous to the optical Fresnel diffraction region, whilst the far-region, where the attenuation becomes exponential, is analogous to the Fraunhofer region. Suckling (1959) has experimentally verified these diffraction phenomena of sound.

Assuming that the reflector in an interferometer is small enough to produce negligible diffraction, reflection peaks occur at separations l between the source and reflector given by:

$$l = n\frac{\lambda}{2} - \frac{a^2}{8n\lambda}, \quad n = 1, 2 \ldots.$$

This formula is in fair agreement with experiment except for very small separations, when the assumptions are incorrect.
Von Grossmann (1934) has modified the treatment to take account of diffraction due to the reflector.

Examination of Grabau's experimental data indicates that the effect is very small at the frequency and source and reflector diameters used in the present interferometer. In fact no systematic decrease has been detected in intervals between successive/

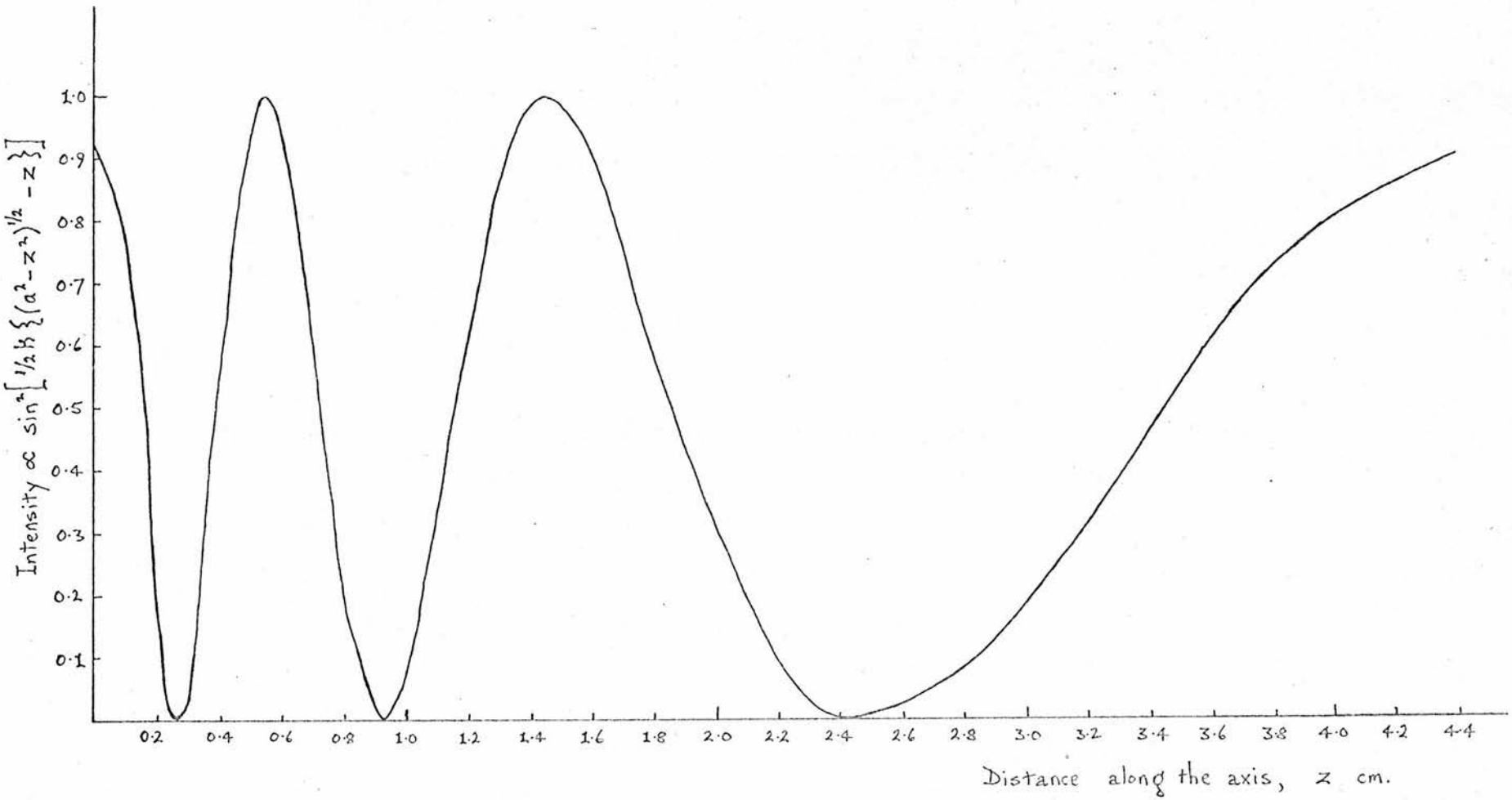

Fig. 23. The intensity along the axis of a piston source (3 cm. in diameter).

successive reflection peaks.

(iii) Fluctuation of intervals with ordinal number n.

Grabau (1933) observed irregular variations in the intervals between successive reflection peaks (fig. 24). Von Grossmann (1934) attempted a qualitative explanation in terms of the contour picture of the sound field in front of a circular piston source in the Fresnel region.

A statistical analysis of the results of Mr. A.J. Matheson in this laboratory revealed a similar curve (fig. 25). These results were taken on an interferometer, which, like that of Grabau , had no close side-walls.

(iv) Rayleigh modes of a waveguide.

The wave equation for the propagation of sound in a gas may be written in cylindrical polar co-ordinates:

$$\frac{\partial^2\phi}{\partial r^2} + \frac{1}{r}\frac{\partial\phi}{\partial r} + \frac{1}{r^2}\frac{\partial^2\phi}{\partial\theta^2} + \frac{\partial^2\phi}{\partial z^2} = \frac{1}{v^2}\frac{\partial^2\phi}{\partial t^2}$$

Separating variables, the real solutions independent of z are:

$$\phi = J_n(g_n r)\left[A\cos n\theta + B\sin n\theta\right]\sin wt$$

where A, B are arbitrary constants and n = 0, 1, 2 ...
Applying the boundary conditions of a rigid cylinder of radius b,

$$V_r = \left(\frac{\partial\phi}{\partial r}\right)_{r=b} = 0,$$

we obtain a set of normal modes characterized by the roots of the first derivative of Bessel functions of the first kind:

$$g_n b = j_{mn}, \quad m = 1, 2 \ldots$$

These are called "radial" or "transverse" waves since they have a particle velocity in the r - direction. The complete, general, real solution of the wave equation can then be expressed as:

$$\phi = \left[A\cos n\theta + B\sin n\theta\right] J_n(j_{mn}\, r/b)\sin(w t - k\psi_{mn} z),$$

$$\psi_{mn} = \left\{1 - (j_{mn}/kb)^2\right\}^{\frac{1}{2}},$$

so/

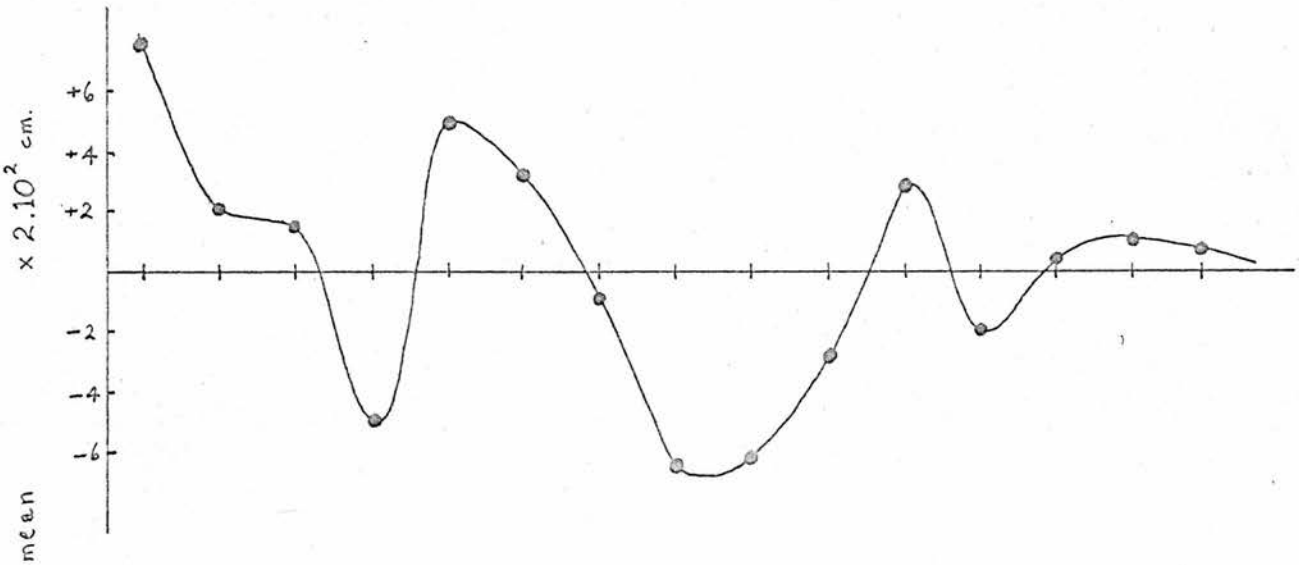

Fig. 25. Variation of intervals with ordinal number

Grabau : air , 20 kc./sec.

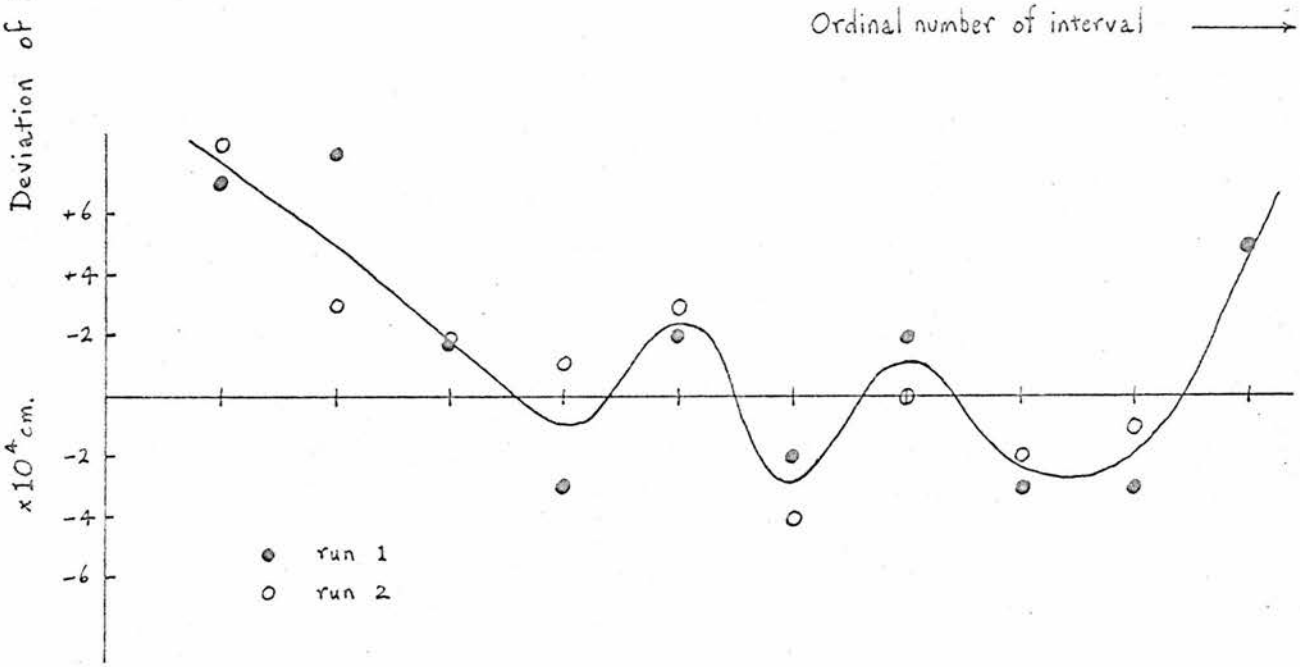

Fig. 26. Variation of intervals with ordinal number

Matheson : air , 125 kc./sec.

so that the propagation constant of a transverse wave along the cylinder may be defined as:

$$k_{mn} = k \left\{ 1 - (j_{mn} / kb)^2 \right\}^{\frac{1}{2}},$$

where k is the plane-wave propagation constant.

When $(j_{mn}/kb)^2 < 1$, progressive waves are possible in the mn th mode. The cut-off frequency f_{mn} for the mode is that frequency for which $(j_{mn}/kb)^2 = 1$, i.e.

$$f_{mn} = j_{mn} v / 2 \pi b$$

Below this frequency progressive waves are not possible in this mode.

When $(j_{mn}/kb)^2 \ll 1$, the relative increase in wavelength of the mn th mode over that of the plane-wave is given by:

$$\frac{\Delta\lambda}{\lambda} = \frac{\lambda_{mn} - \lambda}{\lambda} \approx \frac{j_{mn}^2}{8\pi^2 b^2} \lambda^2$$

Hartig and Swanson (1938) investigated the propagation of transverse waves of audio-frequencies in cylindrical waveguides. Individual modes were excited by applying the appropriate pressure profile at the end of the cylinder. Complete agreement with the above theory was obtained. Hartig and Lambert (1950) developed a transverse wave detector and examined stationary transverse waves, particularly the (0,1) mode, in great detail. Lambert (1953) has calculated the dissipative losses for resonance in a transverse mode.

Transverse waves may be excited in an interferometer; this may happen in two ways:

(a) a piston source vibrating at the end of a waveguide of larger diameter.

(b) the source operating not as a piston, but vibrating in some more complicated fashion.

In an experiment described by Zühlke (1934) two quartz crystals/

crystals were used (presumably to give a larger surface area) side by side. This system strongly excites transverse waves and, in fact, the main observed reflection peak corresponded to a transverse wave; the plane-wave showed up as a satellite. But this time, in accordance with the velocity of a plane-wave being smaller than any transverse wave, the satellite appeared on the side of the main peak corresponding to a smaller displacement of the reflector from the crystal, and the interval between successive satellites was smaller than the interval between successive main peaks. This interferometer had no close side-walls so that it is not meaningful to speak of a particular transverse mode in this case. This does not mean, however, that transverse waves may not propagate in unrestricted space.

Hubbard and his school aim to eliminate transverse waves by using a source where $b \gg \lambda$ and ensuring that the whole of the cylinder cross-section is covered by the source. Nevertheless, Stewart and Stewart (1952), using an interferometer of this type, report a velocity increase in helium (5 parts per 1,000) and they attribute this increased velocity to transverse waves.

Krasnooshkin (1944) suggested that in reality a group of transverse waves is always generated in an interferometer, and that this group remains unresolved in the main reflection peaks. The position of a maximum is slightly shifted from that of a pure plane-wave, producing an apparent increase in velocity. He recommended that an interferometer should therefore be calibrated with gases of known velocities. Due to interference between the members of a group of normal modes the signal at a non-selective receiver (sensitive to all modes) will be decreased (after leaving the source the normal modes are never all in phase again). Thus the absorption coefficient will be effectively increased too.

Bell (1950) examined satellite structure of an interferometer which had a 1 in. diameter, 250 kc./sec. quartz crystal axially mounted in a tube 1½ in. in diameter. Assuming that the main reflection/

reflection peak corresponded to the plane-wave, he identified the satellites by comparing their respective intervals with the half-wavelengths of possible transverse waves. Thisindentification was not very convincing since many modes are available when cylindrically asymmetric ones are considered, and the numerical agreement was only fair. The gases were not pure enough for a comparison to be made between the measured velocities and the theoretical values. Bell tried to stop the propagation of transverse waves by lining the interferometer tube with cotton-wool. The result was inconclusive: there was merely a reduction in height of both main peak and satellites.

Van Itterbeek and Verhagen (1951) tried to detect the presence of transverse waves in an interferometer by the increased absorp-:tion. They measured the absorption coefficient of o-and p -H_2 as a function of pressure. The total absorption coefficient is given by:

$$\alpha = \frac{\alpha_o p_o}{P} + \alpha_1$$

where α_o is the absorption coefficient due to the gas at pressure p_o and α_1 is the parasitic absorption coefficient due to inter-:ference of a group of transverse waves. α_1 was found to be zero. Similarly for He.

Guptill's approach.

Guptill (1953) has derived an analytic expression for the velocity potential in front of a piston source in an infinite, rigid baffle and parallel to an infinite, rigid reflector. Integrating pressure over a finite-area, co-axial receiver, the largest maxima in the signal of the receiver occur at half-wave-:length positions corresponding to the plane-wave.

Graham (1953), experimentally imitating these ideal conditions, using a two-crystal interferometer with water as medium (ka = 20, f= 0.6 -5.0 mc./sec., t= 10 - 20°C), has confirmed Guptill's/

Guptill's predictions. The plane-wave component predominates.

Vibration of quartz crystals.

Dye (1932) examined the vibrations of X - cut quartz crystals by means of optical interferometry. He found that:

(a) there are no absolutely pure modes.

(b) at the natural frequency (resonance) the modes are purely compressional - no torsional or flexural oscillations in the mixture.

(c) nodal patterns are generally of the type:

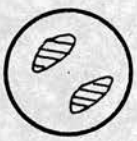

(d) when the edge is bevelled to give increased piezo-electric reaction a circumferential node is produced:

Nixon and Williams (1950) have more recently confirmed the circumferential nodes. At 0.5 mc./sec. — 1 mc./sec. they find that "when the reflection coefficient between quartz and fluid approaches unity (radiation into air) only some 5% of the surface vibrates with appreciable amplitude..."

Alleman (1939) detected uneven radiation from the quartz crystal of his interferometer by schlieren photography. Zartmann (1949) trimmed his crystals until no unevenness could be detected. However, Zartmann's results for CO_2-free, dry air are still high by 1/3 % above the plane-wave, free-space value.

Pielemeier (1939) at one time suggested that quartz crystal does not necessarily vibrate at the same frequency as the applied electric potential difference; there seems to be neither reason nor evidence for this.

Definitive/

Definitive experimental absolute ultrasonic velocities.

There are very few accurate determinations of absolute velocities reported in the literature. Interferometers are usually calibrated using air as standard.

Very accurate comparison of an experimental velocity with a theoretical velocity is worthwhile only when the gas is non-relaxing, and when its specific heat, molecular weight, virial data are well established. CO_2-free, dry air is suitable for comparative purposes, especially as it is readily available with a purity guaranteeing its velocity to 1 part in 2,000. The inert gases can also be used as standards; the velocity of sound in argon can be calculated to 1 part in 20,000.

Kneser (1938) has reviewed the literature up to 1938. His estimate of the velocity of sound in CO_2-free, dry air at $0^{\circ}C.$ and 1 atm. is:

$$33160 \pm 5 \text{ cm./sec.}$$

Kneser takes into account values obtained at low frequencies ($< 1{,}000$ c./sec.) and values corrected for CO_2 content.

Two careful determinations of velocity in CO_2-free, dry air have been made in the 1-100 kc./sec. region in narrow tubes by Kaye and Sherratt (1933) and Norton (1935). These authors worked below the cut-off frequencies of their tubes and extrapolated a "universal" Helmholtz-Kirchhoff type curve,

$$v = v_s \left\{ 1 + \frac{c}{2r\,(\pi f)^{\frac{1}{2}}} \right\},$$

to obtain the free-space, plane-wave velocity.

More recently Boyer (1951) and Ener, Gabrysh and Hubbard (1952), using a conventional interferometer, have reported measurements in the 1 - 2mc./sec. region. The authors, in calculating their average values, have assumed that the velocity in CO_2-free, dry air is constant over the pressure range 15-76 cm. Hg. whereas the change due to gas imperfection is appreciable. Accordingly/

Accordingly their experimental values have been corrected to a pressure of 1 atm. before taking the averages quoted below. The classical absorption at 2mc./sec. and 1 atm. is 0.5664 cm.$^{-1}$ so that the effect of absorption on velocity is 0.5 cm./sec., which is just outside the experimental accuracy of these later workers. At these sound frequencies the low order Rayleigh modes of the interferometer tubes used by them have wavelengths which differ negligibly from the plane-wave value.

The results for CO_2-free, dry air are collected in Table 26, for comparison with the theoretical values. It may be noted that all the experimental values are slightly high.

Greenspan (1950), using a two-crystal interferometer at 11 mc./sec. has obtained good agreement with theory in the case of helium. At 0°C. and 1 atm.:

experimental velocity = 97220 cm./sec.
theoretical velocity = 97200 cm./sec.

Table 26.

Velocities in CO_2-free, dry air.

Temperature °C.	Theoretical velocity cm./sec.	Experimental velocity cm./sec.	Reference
20	34335	34371	Norton (1935)
18	34219	34240	Kaye & Sherratt (1933)
32	35028	35045	Ener, Gabrysh and Hubbard (1952)
0	33145	33167	Boyer (1951)

Experimental conclusions.

Before describing the theoretical analysis of the ultrasonic interferometer, the main conclusions derived from the experimental results of the present interferometer are summarized below.

(a) the relative increase in mean wavelength above the theoretical, free-space, plane-wave value shows an approxi-:mately linear dependence on the square of the wavelength (fig. 22).

(b) The variation in the intervals between successive reflection peaks is irregular and the mean square deviation from the mean increases with wavelength. It is not possible to be more specific here because the variation of successive intervals is itself very irregular.

(c) The intensity of the sound has no effect within the experimen-:tal range employed.

(d) Change of pressure has no effect (non-dispersive gas).

(e) There is no systematic decrease in the intervals as the reflector recedes from the crystal.

A theoretical analysis.

An attempt has been made to examine theoretically the acoustic impedance at the face of the transducer in an interfero-:meter. The following simple model was chosen: a vibrating circular piston axially situated at the end of a rigid tube which has a larger diameter than the piston and which is closed at the other end, by a reflector normal to the axis, viz:- fig. 24.

Recently Seki, Granato and Truell (1956) gave an improved calculation of sound absorption taking into account diffraction due to a circular source. The application of their approach to the above model did not lead to any usable formula.

Another approach is that of normal modes of a waveguide, as used by Redwood (1957). In this method the velocity potential is expressed as a linear combination of orthogonal eigen-functions which correspond to the normal Rayleigh modes of the gas in the tube. The form of these modes is determined by the boundary conditions applicable to the side-wall of the tube and by the diameter of the tube. The coefficients of the terms in the expansion/

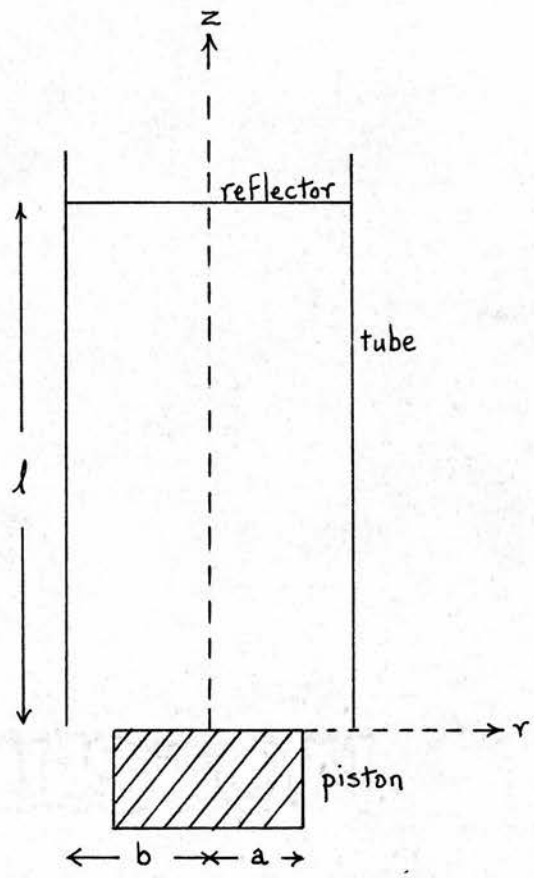

Fig. 24. Theoretical model

expansion are determined by the boundary conditions at the source; in the above model the coefficients are determined by the ratio a/b. This method only works when there are sufficient Rayleigh modes allowed (this is determined by the velocity of sound in the gas, the frequency of the source and the diameter of the tube) to render a reasonable approximation to the velocity profile across the face of the source. The model considered has cylindrical symmetry so that only cylindrically symmetric eigenfunctions are used.

Normal mode theory.

The velocity potential of the system may be expressed in the form:

$$\Phi(r,z,t) = \Psi(r,z)\exp(iwt)$$
$$= \sum_m G_m J_o(j_{mi} r/b)\exp i(wt - k_{mi} z)$$

where summation is over all members of the set of allowed modes (viz:- p.78).

The amplitude factors G_m may be determined by investigating the boundary conditions at the source. If the source behaves like a piston, at $z = 0$ the particle velocity has only a z component, given by

$$v_z = -\frac{\partial}{\partial z}\Phi(r,o,t) = V_o \exp(iwt),\ a \geq r > o$$

$$v_z = o,\quad r > a .$$

The velocity potential at the source may be expressed as the superposition of two waves:

$$\Phi(r,o,t) = \Phi_p + \Phi_s ;$$

Φ_p is the velocity potential of the primary wave emitted from the source and Φ_s is the velocity potential of the secondary wave reflected back to the source. The potential of the latter is taken as that of a primary wave distance $2l$ from the source. Therefore the particle velocity in the z-direction at the source is:

$$v_z = \left[-\frac{\partial}{\partial z}\Psi(r,0) - \left\{ -\frac{\partial}{\partial z}\Psi(r,2l) \right\} \right] \exp(iwt)$$

$$\therefore \quad v_z = \sum_m ik_{mi} G_m J_o(j_{mi}\, r/b) \left\{ 1 - \exp(-i2k_{mi} l) \right\} \exp(iwt)$$

Multiply each side by $J_o(j_{m'_1} r/b)r$ and integrate over r from o to b. Noting the boundary condition consequence,

$$\int_o^b v_z J_o(j_{mi} r/b)\, r\, dr = V_o \int_o^a J_o(j_{mi} r/b)\, r\, dr$$

$$= Vo \; \frac{a\, b}{j_{mi}} \; J_1(j_{mi}\, a/b),$$

and the orthogonality of the Bessel functions,

$$\int_o^b J_o(j_{mi}\, r/b)\, J_o(j_{m'_1} r/b)\, r.\, dr = \tfrac{1}{2} b^2 J_o^2(j_{m'_1}), \quad m=m'$$

$$= o, \qquad m \neq m'$$

it follows that:

$$G_m = \frac{2Vo}{i} \; \frac{a}{b} \; \frac{1}{k_{mi}} \; \frac{1}{1 - \exp(-i2k_{mi} l)} \; \frac{J_1(j_{mi}\, a/b)}{j_{mi} J_o^{\,2}(j_{mi})}$$

The effective or net pressure on the source is defined by:

$$P_o = \int_o^a \frac{p\,(r,o,t)\; 2\pi\, r\, dr}{\pi\, a^2} = \frac{2}{a^2} \int_o^a p(r,o,t)\, r\, dr$$

$$p\,(r,o,t) = \rho \frac{\partial}{\partial t} \left\{ \Phi(r,o,t) + \Phi(r, 2l, t) \right\}$$

$$= \rho\, i\, w \exp(iwt) \sum_m G_m J_o(j_{mi}\, r/b) \left\{ 1 + \exp(-i2k_{mi} l) \right\}$$

$$\therefore \quad p_o = 4 \rho w V_o \exp(iwt) \sum_m \frac{1}{k_{mi}} \; \frac{1+\exp(-i2k_{mi} l)}{1-\exp(-i2k_{mi} l)} \left\{ \frac{J_1(j_{mi}\, a/b)}{j_{m'} J_o(j_{mi})} \right\}^2$$

The acoustic impedance per unit area at the face of the source is given by:

$$Z_o = \frac{P_o}{V_o \exp(iwt)}$$

$$= 4\rho w \sum_m \frac{1}{k_{ml}} \frac{1 + \exp(-i2k_{ml}l)}{1 - \exp(-i2k_{ml}l)} \left\{ \frac{J_1(j_{ml}\, a/b)}{j_{ml} J_o(j_{ml})} \right\}^2$$

The plane-wave ($m = o$) component must be considered separately since for the plane wave:

$$J_o(z = o) = 1,$$

$$J'_o(z = 0) = 0,$$

whence, due to the plane-wave alone, the impedance per unit area is:

$$Z_{oo} = \rho w \frac{1}{k_{10}} \frac{1 + \exp(-i2kl)}{1 - \exp(-i2kl)} \left(\frac{a}{b}\right)^2$$

$$k_{10} = k = w/v$$

Taking into account absorption by the gas and the exponential reflection coefficient β the final expression is:

$$Z_o = \frac{i\rho w}{ik + \alpha} \frac{1 + \exp(-i2kl - 2\alpha l - \beta)}{1 - \exp(-i2kl - 2\alpha l - \beta)} \left(\frac{a}{b}\right)^2$$

$$+ 4 \sum_m \frac{i\rho w}{ik_{ml} + \alpha} \frac{1 - \exp(-ik_{ml}l - 2\alpha l - \beta)}{1 + \exp(-ik_{ml}l - 2\alpha l - \beta)} \left\{ \frac{J_1(j_{ml}\, a/b)}{j_{ml} J_o(j_{ml})} \right\}^2$$

$m = 1, 2 \ldots\ldots m.$

When $a = b$, the expression reduces to that for a pure plane-wave.

Normal mode calculation.

The constants in the formula for acoustic impedance per unit area of source were given the values corresponding to CO_2-free, dry/

dry air in the experimental interferometer at 30°C. and 1 atm.

α = 0.001 cm.$^{-1}$
β = 0.013
a = 1.270 cm.
b = 1.905 cm.
a/b = 0.6667
v = 34,911 cm./sec.
f = 85,787 c./sec.
w = 52.645 rad./sec.
k = 15.080 cm.$^{-1}$
$\lambda/2$ = 0.20833 cm.

Only 8 Rayleigh modes are allowed in this case; the roots of the first order Bessel functions and the corresponding mode data are given in Table 27, where the abbreviations,

$$J = \left\{ \frac{J_1(j_{m1}\, a/b)}{j_{m1}\, J_o(j_{m1})} \right\}^2 , \lambda_{m1} = \frac{2\pi}{k_{m1}}$$

are used.

Values of

$$|F| = \left| \frac{i}{ik + \alpha} \left(\frac{a}{b}\right)^2 \frac{1}{4} \frac{1 + \exp(-i2kl - 2\alpha l - \beta)}{1 - \exp(-i2kl - 2\alpha l - \beta)} \right.$$

$$\left. + \sum_m \frac{i}{ik_{m1} + \alpha} \left\{ \frac{J_1(j_{m1}\, a/b)}{j_{m1} J_o(j_{m1})} \right\}^2 \cdot \frac{1 + \exp(-i2k_{m1} l - 2\alpha l - \beta)}{1 - \exp(-i2k_{m1} l - 2\alpha l - \beta)} \right|$$

were calculated for various values of l. $|F|$ is related to $|Z_o|$ by:

$$Z_o = 4 \rho w F$$

Taking

$$v^2 = \frac{\gamma p}{\rho} ,$$

$$Z_o = \frac{4 \gamma p w}{v^2} \cdot F$$

At/

At 30°C. and 1 atm.:

$$\frac{4\gamma_p w}{v^2} \doteq 3240 \text{ c.g.s. units.}$$

The Bessel functions and their roots were taken from Gray, Matthews and MacRobert (1931). The values of $J_1(j_{m1}a/b)$ for the last two modes were calculated from the asymptotic formula for J_1.

The calculations were done on Deuce (an English Electric digital electronic computer) using an α-code programme.

Since the plane-wave component is the most important, peaks in $|F|$ were expected in the vicinities of $l = \lambda/2$, λ, $3\lambda/2$ etc. $|F|$ was therefore calculated for sets of 10 points (at intervals of 2 microns in l) in each of the first 7 half-wavelength regions.

Table 27.

Normal mode data (rigid wall).

m	j_{m1}	k_{m1}	m1	J
1	3.8317	14.945	0.42042	0.098025
2	7.0156	14.623	0.42968	0.016947
3	10.173	14.103	0.44552	0.000775
4	13.324	13.360	0.47030	0.007834
5	16.471	12.355	0.50856	0.002882
6	19.616	11.017	0.57032	0.000232
7	22.760	9.2012	0.68286	0.002686
8	25.904	6.5198	0.96371	0.001100

Results of the normal mode calculation.

A peak was found at each of the expected positions; a typical one is shown in fig. 27. The peaks have a rather irregular appearance, presumably due to the way in which the phases of the component waves happen to add up at each point. The positions of the peaks and the intervals between successive peaks are given in Table 28. There is a fluctuation in the spacing of the main peaks which is similar in kind to that observed experimentally, viz:- fig. 28. It may be noted that all the peaks are displaced slightly towards the source from the half-wavelength positions; this is presumably due to the reflection coefficient β .

The mean value of the intervals, 0.20843 cm., is very close to the plane-wave half-wavelength, 0.20833 cm. This calculation does not predict, then, the increased mean velocity observed experimentally.

It is also clear from the results that there are no grounds for Krasnooshkin's suggestion that a group of modes would give a mean separation of the main peaks greater than the plane-wave half-wavelength. The inclusion of asymmetric modes would not alter the picture in kind, since there are few modes whose wavelengths are near to that of a plane-wave, viz:- Table 29.

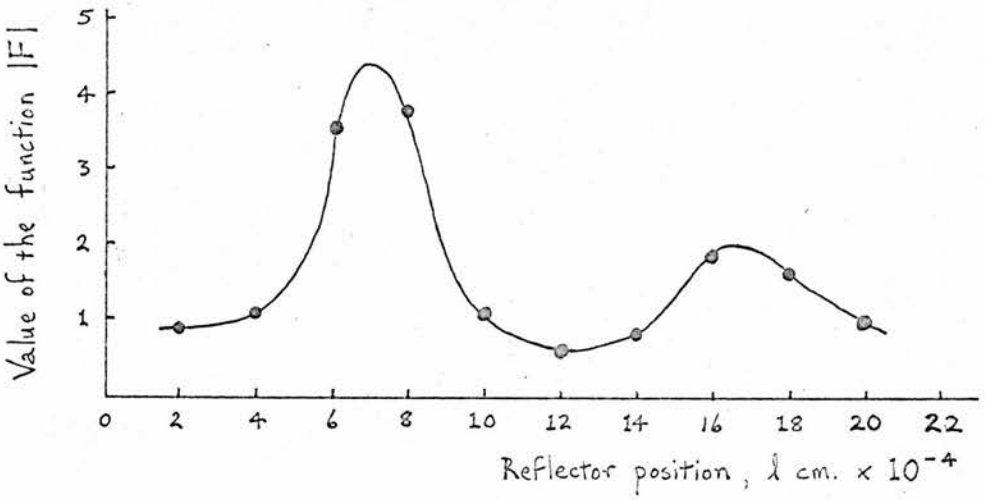

Fig. 27. Typical peak (3rd)
Deuce calc. (rigid wall)

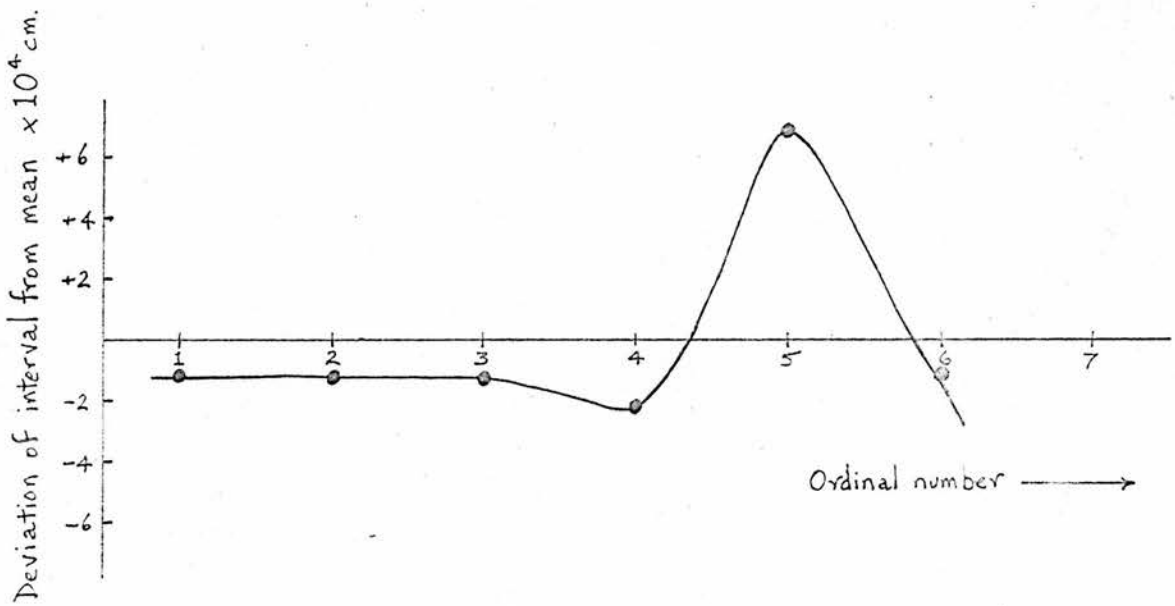

Fig. 28. Variation of intervals with ordinal number
Deuce calc. (rigid wall)

Table 28.

Results of the normal mode calculation (rigid wall).

Peak No.	Peak posn. $x10^4$ cm.	Interval $x10^4$ cm.	Deviation of interval from mean $x10^4$ cm.	Interval No.
1	2078.6			
		2083.3	-1.1	1
2	4161.9			
		2083.3	-1.3	2
3	6245.0			
		2083.2	-1.2	3
4	8328.2			
		2082.3	-2.1	+
5	10410.5			
		2091.3	+6.9	5
6	12501.8			
		2083.3	-1.1	6
7	14585.1			

Table 29.

Asymmetric normal modes (rigid wall).

m, n	j	k	λ
1,1	1.841	15.049	0.41752
2	5.332	14.818	0.42402
3	8.536	14.399	0.43636
4	11.706	13.771	0.45626
1,2	3.054	14.994	0.41905
2	6.705	14.663	0.42851
3	9.965	14.144	0.44423
1,3	4.201	14.918	0.42118
2	8.015	14.481	0.43389
3	11.344	13.854	0.45353

Free-wall boundary conditions.

Although theory indicates that the plane-wave component is the most important in the interferometer, the experimentally observed reflection peaks are well removed from the plane-wave positions. Only the (1,2) Rayleigh mode has a comparable half-wavelength. It is possible that this mode is preferentially excited by an uneven vibration of the quartz crystal.

An alternative explanation lies in the boundary conditions at the side-wall of the tube. In the theory of the Rayleigh modes given above, a rigid side-wall was assumed, when the radial particle velocity of the sound wave at the wall must be zero:

$$v_r = -(\partial/\partial r)\Phi = 0, \text{ at } r = b.$$

The other extreme boundary condition is that called "free-wall", which is appropriate to a solid medium in air; the pressure at the side-wall must be zero in this case:

$$p = \rho(\partial/\partial t)\Phi = 0 \text{ at } r = b.$$

For axially symmetric modes, the solution of the wave equation is of the form:

$$\Phi(r,z,t) = \sum_m G_m J_o(j_{mo} r/b) \exp i(wt - k_{mo} z),$$

where the j_{mo} are roots of the zeroth order Bessel function:

$$J_o(j_{mo}) = 0, \quad m = 1,2 \ldots.$$

There is no plane-wave component since

$$J_o(z = o) = 1.$$

The expression for the acoustic impedance per unit area at the source for a "free-wall" model takes the form:

$$Z_o = 4\rho w \sum_m \frac{i}{ik_{mo} + \alpha} \left\{ \frac{J_1(j_{mo} a/b)}{j_{mo} J_1(j_{mo})} \right\}^2 \frac{1 + \exp(-i2k_{mo} 1-2\alpha 1-\beta)}{1 - \exp(-i2k_{mo} 1-2\alpha 1-\beta)}$$

There may be a spectrum of normal modes even when a = b.

Free-wall calculation.

The/

The constants in the formula for acoustic impedance per unit area of source were given the values corresponding to CO_2-free, dry air in the experimental interferometer at 30°C. and 1 atm. except that $\beta = 0$ was taken for simplicity.

9 Rayleigh modes are allowed; the roots of the zeroth order Bessel functions and the corresponding mode data are given in Table 30, where the abbreviations,

$$J = \left\{ \frac{J_1(j_{mo}\, a/b)}{j_{mo}\, J_1(j_{mo})} \right\}^2, \quad \lambda_{mo} = \frac{2\pi}{k_{mo}},$$

are used.

Values of

$$|F| = \left| \sum_m \frac{i}{ik_{mo}+\alpha} \left\{ \frac{J_1(j_{mo}\, a/b)}{j_{mo} J_1(j_{mo})} \right\}^2 \cdot \frac{1+\exp(-i2k_{mo}-2\alpha l)}{1-\exp(-i2k_{mo}-2\alpha l)} \right|$$

were calculated for sets of l values in the vicinities of the half-wavelength positions corresponding to the first mode. The details of this calculation are similar to those for the previous "rigid-wall" case.

Table 30.

Normal mode data (free-wall).

m	j_{mo}	k_{mo}	λ_{mo}	J
1	2.4048	15.027	0.41813	0.83459
2	5.5201	14.799	0.42457	0.00437
3	8.6537	14.380	0.43694	0.07207
4	11.7915	13.723	0.45786	0.02403
5	14.9309	12.883	0.48771	0.00127
6	18.0711	11.723	0.53597	0.01683
7	21.2116	10.170	0.61782	0.00708
8	24.3525	7.999	0.78550	0.00016
9	27.4935	0.437	1.4607	0.00185

Free-wall results.

A peak was found at each of the expected positions; a typical one is shown in fig. 29. The positions of the peaks and the intervals between successive peaks are given in Table 31. The fluctuation in the intervals vs. ordinal number is shown in fig. 30.

The first mode contributes the largest component by far and its half-wavelength corresponds closely to the experimentally observed interval between reflection peaks. The mean value of the intervals from the "free-wall" calculation is 0.20906 cm., c.f. 0.2093 cm. observed experimentally.

An extended examination was made of the first peak in $|F|$, viz:- fig. 4b. This peak shows a satellite at about the same position as the experimental reflection peak. The comparison of the two main peaks is not very satisfactory, however, since the theoretical one shows a dip in the middle. This dip must arise from some coincidental addition of phases of the Rayleigh modes at that point. Such a feature shows how the normal mode treatment sometimes fails badly in describing the system.

The theoretical slope of the graph of $\Delta\lambda/\lambda$ vs. λ^2 was calculated from the equation:

$$\frac{\Delta\lambda}{\lambda} \doteq \frac{j^2}{8\pi^2 b^2} \cdot \lambda^2$$

substituting $j = j_{10}$, corresponding to the first Rayleigh mode with free-wall boundary conditions. The theoretical line is shown in fig. 22 where the experimental points are also plotted. The agreement is fair, except for Neon.

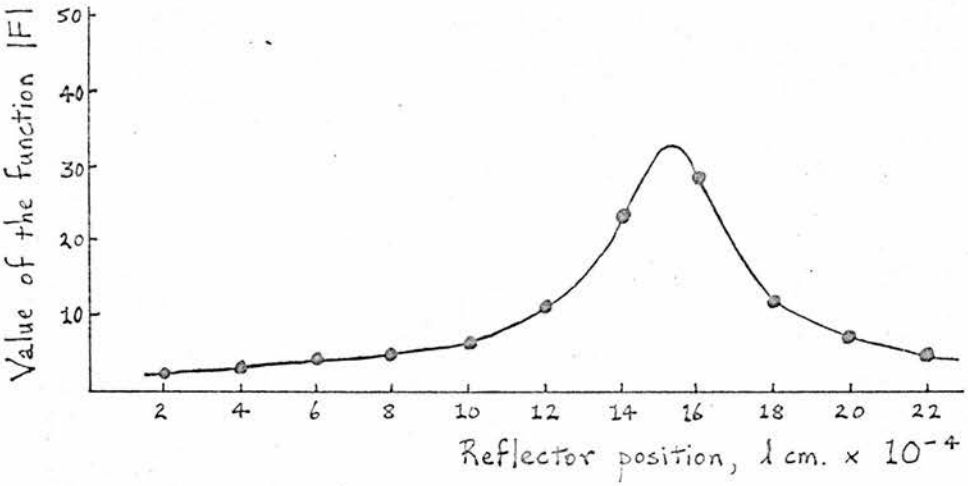

Fig. 29. Typical peak (5th)
Deuce calc. (free-wall)

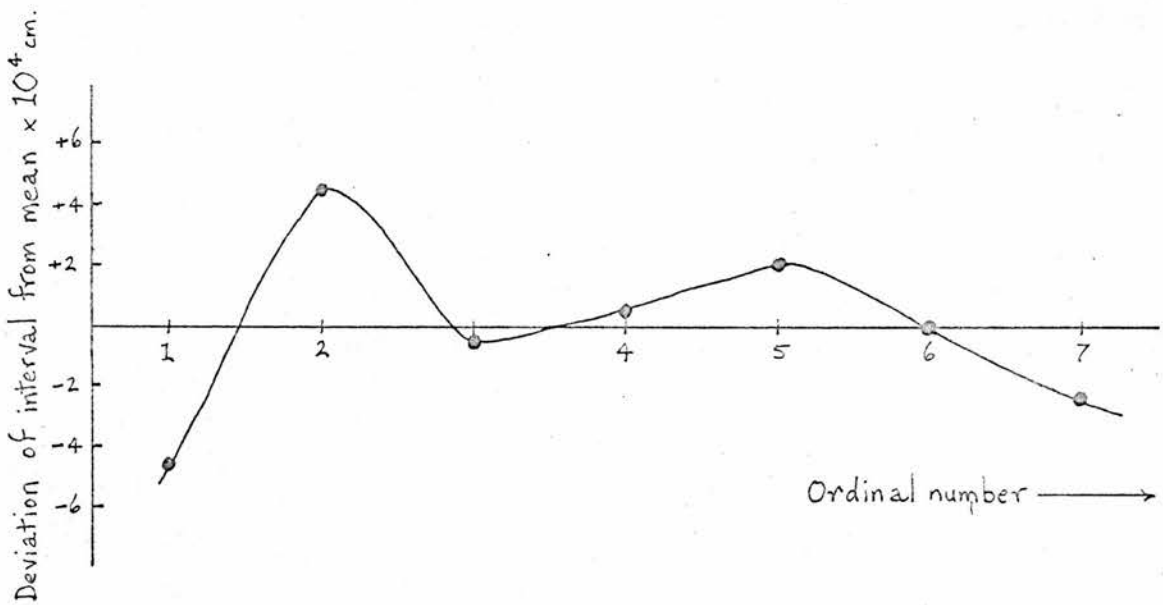

Fig. 30. Variation of intervals with ordinal number
Deuce calc. (free-wall)

Table 31.

Results of normal mode calculation (free-wall).

Peak No.	Peak posn. $x10^4$ cm.	Interval $x10^4$ cm.	Deviation of interval from mean $x10^4$ cm.	Interval No.
1	2090.2			
		2086.1	-4.5	1
2	4176.3			
		2095.1	+4.5	2
3	6271.4			
		2090.0	-0.6	3
4	8362.3			
		2091.1	+0.5	4
5	10453.4			
		2092.6	+2.0	5
6	12546.0			
		2090.6	0	6
7	14636.6			
		2088.4	-2.2	7
8	16725.0			

Discussion of the free-wall hypothesis.

The experimental results from the present interferometer are consistent with the hypothesis of "free-wall" propagation of sound in the interferometer tube.

The hypothesis is somewhat supported by the work of Carome, Witting and Fleury (1961), who have recently reported absorption experiments in liquids contained in a thick-walled metal tube. They showed that "free-wall" rather than "rigid-wall" boundary conditions were indicated, but no definite explanation of the phenomenon was offered.

The increased velocity observed by Stewart and Stewart (1952) in their conventional ultrasonic interferometer in the case of helium is also explained by the hypothesis. Taking their values

$$v = 97200 \text{ cm./sec.}$$
$$f = 1.95 \text{ mc./sec.}$$
$$b = 0.4 \text{ cm.}$$

the wavelength of the first Rayleigh, free-wall mode is in excess of the plane-wave wavelength by 5 parts in 1,000. This is just the difference they observed. The difference would be negligible for air, $v = 33100$ cm./sec. This agrees with the experiments of Ener, Gabrysh and Hubbard (1952).

A possible explanation of the "free-wall" propagation lies in a boundary layer. For a normal mode in which the radial particle velocity at the side-wall, $(\partial \Phi / \partial r)_{r=b}$, is zero, the tangential particle velocity at the side-wall, $(\partial \Phi / \partial z)_{r=b}$, is a maximum and vice versa. Friction between the gas and the side-wall may lead to a boundary layer stationary in the z-direction but providing a "free-wall" effect in the r-direction. In fact, Weston (1953) has studied such a boundary layer in the case of plane-wave propagation in a tube. His profiles of particle velocity are shown in fig. 31. Nielsen (1949) has given a formula for the thickness of such a boundary layer:

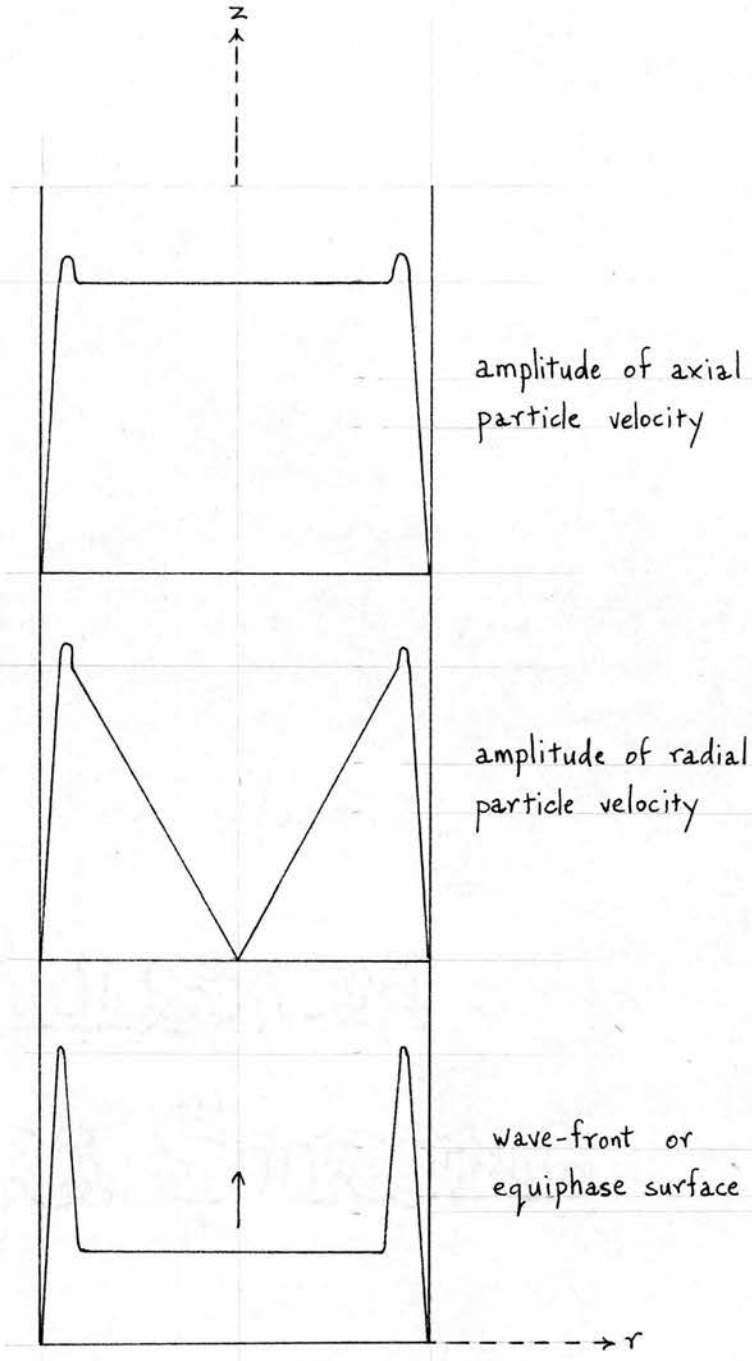

Fig. 31. Profiles of a plane-wave in a tube

$$\Delta r = \tfrac{1}{2}\sqrt{\frac{2\eta}{\rho w}}$$

$$\therefore \quad \Delta r = \frac{0.5}{f^{\frac{1}{2}}} \quad \text{for air.}$$

In the present interferometer the thickness would be ca. 0.002 cm.

There is another way of considering the boundary. The side-wall has a large thermal conductivity so that heat flows into and out of the wall when the temperature of the gas adjacent to the wall rises and falls in accompaniment with the "adiabatic" compressions and rarefactions of the sound wave. Thus as far as the sound energy is concerned the wall is "soft".

Clearly more work is required to test the "free-wall" hypothesis. It is necessary to distinguish between a Rayleigh mode excited by an uneven vibration of the quartz crystal and a Rayleigh mode due to free-wall boundary conditions. This can only be achieved by using several different transducers, different quartz crystals and possibly a magnetostriction oscillator and a ceramic transducer.

Future research.

If the detailed working of the interferometer is to be completely understood, measurements must be made over a range of frequencies and source diameters in non-dispersive gases.

As it stands, the interferometer has been empirically calibrated to measure wavelengths to an accuracy of 1 part in 2,000 to 1 part in 4,000 (at 80 kc./sec.) for a gas with molecular weight greater than 30. The f/p range is 40-800 kc./sec/atm. so that relaxation times in the 1 - 2 microsec. region could be determined. Thus CO_2/Ar mixtures could be examined, as originally planned.

It should also be possible to say whether the relaxation time of H_2S is greater or less than 1 microsec., simply by comparing/

comparing v with v_o(calc.) and v_∞ (calc.).

The temperature range 20-200°C. is also available. This would allow an extension of the results for CH_4 and CD_4 to higher temperatures to be made. At the highest temperatures it might be possible to detect the dispersion of some diatomics, e.g. C O (at 500°K. $C_{vib} \doteq 0.1$ cal./mole). The interferometer is capable of measuring changes in velocity with an accuracy of 1 part in 10,000.

Measurements of heat capacities are also possible for a number of molecules which have very short relaxation times: at 80 kc./sec./atm. the velocity is then definitely v_o rather than v_∞. Ethane, and higher hydrocarbons, are possibilities.

Finally the second virial coefficient of a gas could be measured in the interferometer. This may be useful for a polar gas like CH_3Br which is strongly absorbed on surfaces. The gas must have a short relaxation time to avoid the effects of dispersion due to energy transfer processes.

The interferometer could be used at higher frequencies to measure the relaxation times of PH_3 and AsH_3.

A THEORETICAL CALCULATION OF THE VIBRATIONAL RELAXATION OF METHYL CHLORIDE.

Previous theoretical calculations of the probability of vibrational-translational energy transfer in molecular encounters have, in general, given unsatisfactory agreement with experiment in that the calculated temperature dependences are rather too steep in the important practical region, 300-1000°K (Arnold, McCoubrey and Ubbelohde, 1957). Most authors have used an exponential repulsive intermolecular potential function, following the original work of Landau and Teller (1936), and only introduced the effect of an attractive term in an indirect way. In low-energy collisions the attractive term may be important and it was therefore decided to investigate the effect of including it directly. The semi-classical methods are based on those of Cottrell and Ream (1955) who showed in principle how to take account of attractive forces, but did not do so in their numerical calculations. The results were confirmed using the fully quantum-mechanical distorted wave technique of Mott and Massey (1949). Some investigation of the effect of the attractive term has been made by Takayanagi (1958), but he did not examine the temperature dependence of the results.

Methyl chloride was chosen for study. The following points are important for this example:

1. The molecule is strongly polar so that the attractive term is relatively large.
2. Vibrational energy transfer generally proceeds via the mode of lowest frequency; in the case of methyl chloride, this is the simple C-Cl stretching mode. The naïve theoretical model for de-excitation of a vibration is much more realistic for a stretching mode than for a more complicated mode.
3. Relaxation times are available from a variety of experimental methods over a wide temperature range and the results are fairly consistent. The virial data are also well established. Therefore/

Therefore the results of the theoretical treatment may be tested by comparison with experiment.

The work has been reported in a paper by Blythe, Cottrell and Read (1961).

The potential energy function.

The attractive term can be included explicitly, and the results for head-on collisions calculated analytically, assuming a Morse potential function,

$$V(r) = D \exp\left[-2\alpha(r-r_e)\right] - 2D \exp\left[-\alpha(r-r_e)\right] \qquad (1)$$

The constants in this function for methyl chloride were obtained by fitting it to a Krieger potential function,

$$V(r) = 4u\left[(r_o/r)^{12} - (r_o/r)^6\right] - 2\mu^2/r^3 \qquad (2)$$

where the angle-dependent contribution of the Stockmayer potential has been replaced by the expression for the interaction of two point-dipoles which are aligned so as to exert a maximum mutual attraction. The parameters of the Stockmayer potential were obtained from the second virial coefficient data (Hamann and Pearse, 1952; Whytlaw-Gray, Reeves and Bottomley, 1958) by the method of Rowlinson (1949). The electric dipole moment of a methyl chloride molecule was taken as $\mu = 1.86$ D. Hence:

$$u/k = 380^{\circ}K, \quad r_o = 3.43\ \text{Å}$$

Tanczos (1956) used the Krieger potential function,

$$V(r) = 4u\left[(r_o/r)^{12} - (r_o/r)^6 - \delta(r_o/r)^3\right]$$

as a basis for his calculation of transition probabilities in methyl chloride. But he used parameters consistent with viscosity and thermal conductivity data, and these parameters differ from the ones above which only relate to perfectly aligned molecules.

u/k°,K/

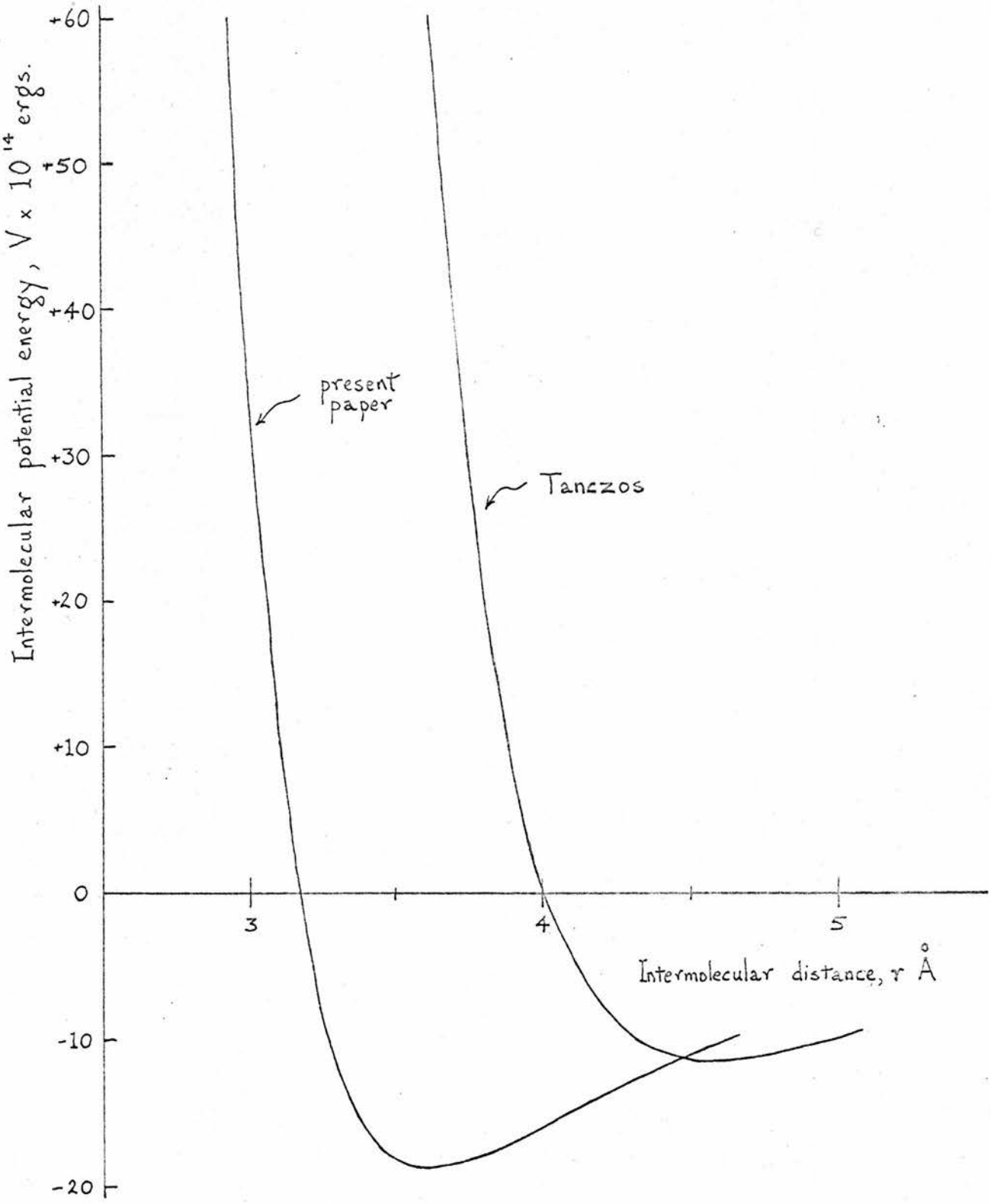

Fig. 32. The Krieger potential of CH_3Cl.

	u/k°, K.	r_o, Å	δ
Tanczos	244	4.332	0.761
present work	383	3.43	0.816

A simple method of fitting (1) to (2) is to make each pass through the points $(r_e, -D)$, $(r_z, 0)$, where the Krieger potential crosses the r - axis at $(r_z, 0)$, when

$$\alpha = \ln 2/ (r_e - r_z).$$

However, this does not give very good agreement in slope in the important repulsive region. A better fit is obtained by arranging a common potential minimum $(r_e, -D)$ and setting

$$\alpha = 6/2^{1/6} r_z .$$

Hence:

$D = 18.9 \times 10^{-14}$ ergs, $r_e = 3.61$ Å, $\alpha = 1.69 \times 10^{8}$ cm.$^{-1}$

(A Lennard-Jones potential,

$$V(r) = 4u \left[(r_o/r)^{12} - (r_o/r)^{6} \right],$$

may be fitted to a Morse potential by arranging a common potential mimimum $(r_e, -D)$, when

$$r_e = 2^{1/6} r_o ,$$

and equating the second derivatives of the potential w.r.t. r at this minimum, when

$$\alpha = 6/r_e = 6/2^{1/6} r_o).$$

The potential functions are compared in Fig. 32.

The double exponential function used by Cottrell and Ream (1955),

$$V(r) = \lambda \exp(-2\alpha r) - \mu \exp(-\alpha r),$$

was obtained from the Morse function through the relations:

$$\lambda = D \exp(2\alpha r_e), \quad \mu = 2D \exp(\alpha r_e).$$

Semi-classical calculation.

Substitution was made in the formula for the probability,

P_{10}/

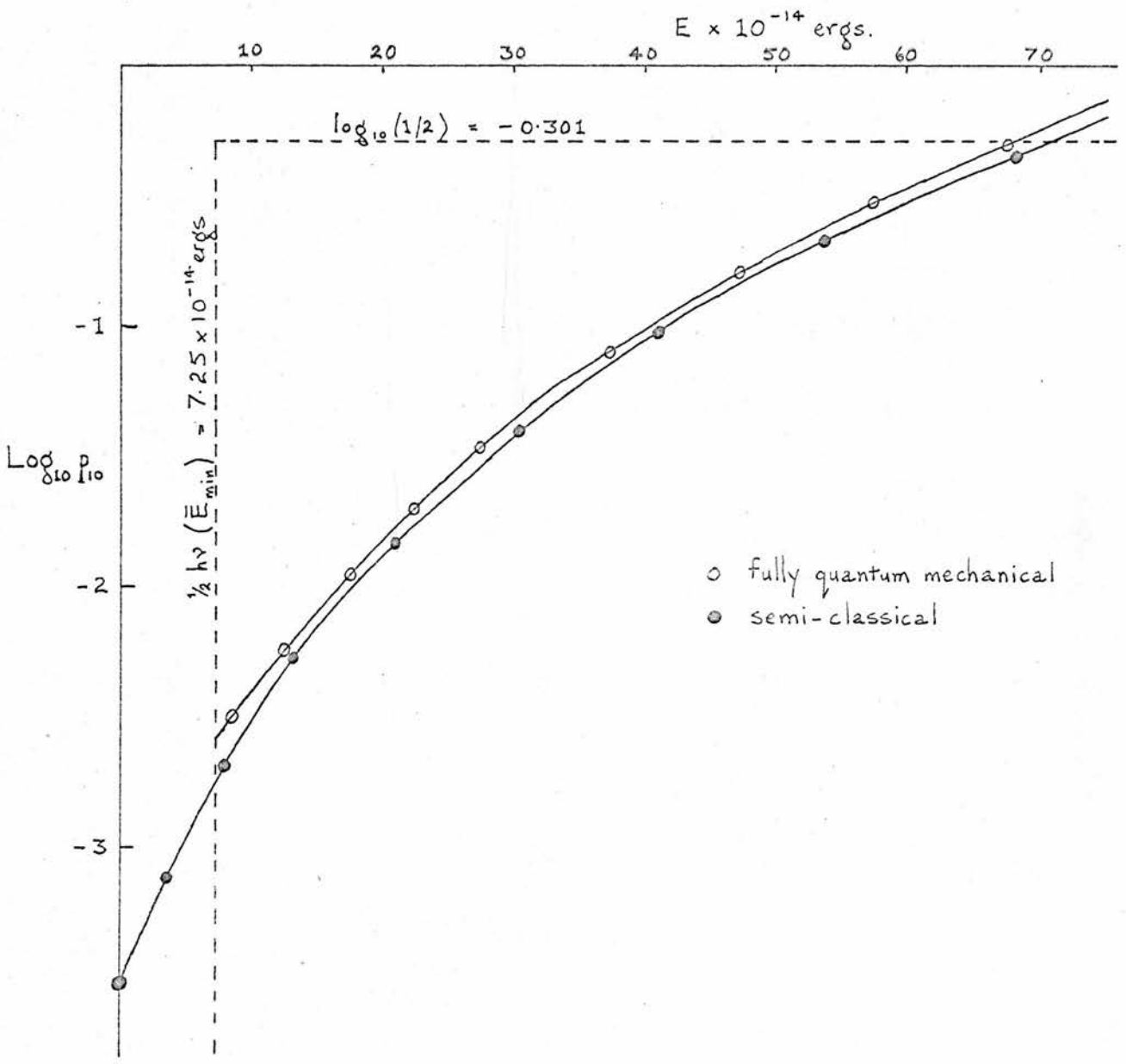

Fig. 33. $\text{Log}_{10} P_{10}$ against relative kinetic energy.

p_{10}, of the transition $1 \longrightarrow 0$ in the lowest vibrational mode of an excited molecule in a head-on collision with another molecule of relative velocity v:

$$p_{10} = \frac{16\pi^2}{h^2} X_{10}^2 I^2$$

Assuming the C-Cl stretching mode to be a simple harmonic oscillation ($\nu = 732$ cm.$^{-1}$) we obtain for the matrix element of co-ordinates between the first excited state and the ground state:

$$X_{10} = \left[\frac{h}{8\pi^2 M \nu}\right]^{\frac{1}{2}}$$

where M is the "effective" mass of the system, the maximum value of M, shown by Arnold, McCoubrey and Ubbelohde (1957) to be one-half the reduced mass m of the colliding system, was used here. For a collision between two methyl chloride molecules m is equal to one-half the mass of a single methyl chloride molecule (M.W. = 50.5).

Since $\pi^2\nu / \alpha v > 3$, we can use the approximation,

$$I = \frac{2\pi^2 m\nu}{\alpha} \exp -\frac{\pi\nu(\pi - 2\phi)}{\alpha v}$$

where $\tan^2 \phi = \mu^2 / 2 m v^2 \lambda$,

for the perturbation integral.

The results are given in Table 32, and the curve for $\log_{10} p_{10}$ as a function of the relative kinetic energy E of a collision shown in fig. 33. The rise of the probability above unity is physically unreasonable and is due to the failure of the normalization for large perturbations; the curve was arbitrarily cut off at $\log_{10} (\frac{1}{2})$.

Quantum mechanical calculation.

The distorted wave method of calculating p_{10} is given for a purely repulsive intermolecular potential energy function in the book/

Table 32.

Semi-classical calculation.

v x 10^{-5} cm./sec.	E x 10^{14} ergs.	$\log_{10} p_{10}$
0	0	-3.527
0.05	0.105	-3.534
0.1	0.210	-3.485
0.2	0.838	-3.414
0.4	3.353	-3.119
0.6	7.545	-2.721
0.8	13.413	-2.275
1.0	20.957	-1.831
1.2	30.179	-1.408
1.4	41.077	-1.016
1.6	53.651	-0.676
1.8	67.902	-0.358
2.2	101.434	+0.162

book of Cottrell and McCoubrey (1961). Only the modifications arising from the use of a Morse potential are explained in this section.

A diagrammatic representation of the transition model in terms of particles is shown below.

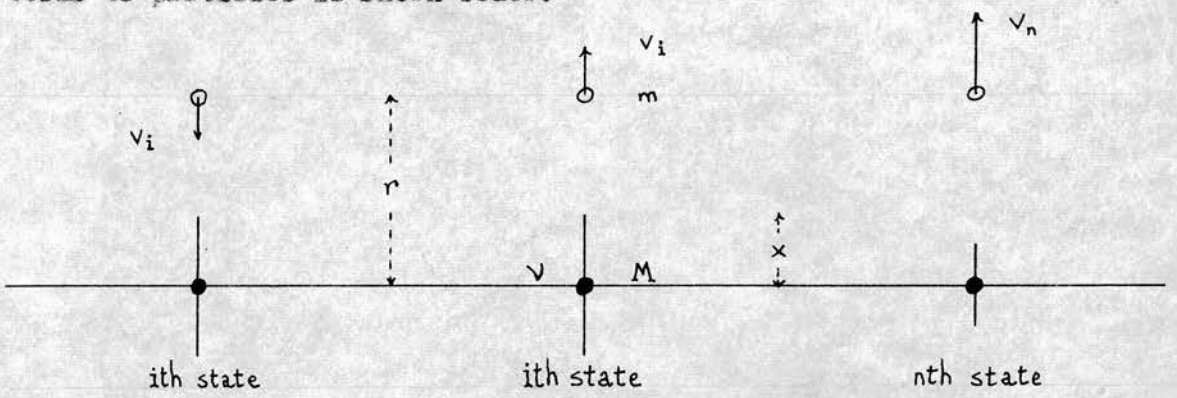

The interaction potential between the vibrating atom (normal co-ordinate x, effective mass M) and the bombarding molecule (trajectory co-ordinate r, reduced mass M) is given in Morse form by:

$$V(r,x) = D \exp\left[-2\alpha(r-r_e-x)\right] - 2D \exp\left[-\alpha(r-r_e-x)\right].$$

for low vibrational levels (small amplitude in x):

$$\exp(\alpha x) \doteq 1 + x,$$

so that the interaction potential may be written:

$$V(r,x) \doteq \left\{D \exp\left[-2\alpha(r-r_e)\right] - 2D \exp\left[-\alpha(r-r_e)\right]\right\} + 2\alpha Dx\left\{\exp\left[-2\alpha(r-r_e)\right] - \exp\left[-\alpha(r-r_e)\right]\right\}$$

$$\doteq V(r) + V'(r,x).$$

The term $v'(r,x)$ is relegated to a perturbation and is conveniently factorized:

$$V'(r,x) = Y(x)\,U(r)$$

where $Y(x) = 2\alpha D x,$

and $U(r) = \exp\left[-2\lambda(r-r_e)\right] - \exp\left[-\lambda(r-r_e)\right]$

The Schodinger equation for the whole system is:

$$\left\{-\frac{\hbar^2}{2M}\frac{\partial^2}{\partial x^2} + 2\pi^2 M\nu^2 x^2 - \frac{\hbar^2}{2m}\frac{\partial^2}{\partial r^2} + V(r,x) - \mathcal{E}\right\}\Psi(x,r) = 0$$

where/

where $\mathcal{E}$ is the stationary total energy (vibrational and translational) of the system. The solution may be expanded in terms of the unperturbed oscillator functions, i.e. solutions of the equation

$$\left\{ \frac{-\hbar^2}{2M} \frac{\partial^2}{\partial x^2} + 2\pi^2 M \nu^2 x^2 - W_n \right\} \phi_n(x) = 0,$$

and functions of r only:

$$\Psi(x,r) = \sum_n \phi_n(x) f_n(r).$$

The functions f_n are asymptotes of the particle waves outside the region of interaction; the normalized incident and reflected waves are given respectively by:

$$f_i = \exp(-i k_i r) + A_i \exp(i k_i r)$$

$$f_n = A_n \exp(i k_n r).$$

Here

$$k_i = m v_i / \hbar, \quad k_n = m v_n / \hbar;$$

v_i is the velocity of the molecule before collision, and v_n is the velocity after collision and energy transfer. The probability of a transition $i \longrightarrow n$ of the oscillator in a collision is:

$$p_{in} = \frac{k_n}{k_i} |A_n|^2 .$$

By first order perturbation theory it may be shown that:

$$f_n(r) \doteq \frac{4m}{\hbar^2 k_n} X_{in} R_{in} \exp\left[-i(k_n r + a)\right]$$

where $X_{in} = \int_{-\infty}^{+\infty} \Psi(x) \phi_i(x) \phi_n(x) dx,$

and $R_{in} = \int_{-\infty}^{+\infty} U(r) F_n F_i dr.$

The F_n denote solutions of the equation:

$$\left\{ \frac{d^2}{dr^2} + k_n^2 - U(r) \right\} F_n(r) = 0.$$

In deriving the formula for R_{in}, the perturbation transition matrix element in the co-ordinate of the bombarding molecule, use

was/

was made of the integration worked out by Devonshire (1936) in his paper on the interaction of atoms with solid surfaces.

$$R_{in}^2 = \frac{\pi^4 \nu^2 \hbar^2}{4 \alpha^2 D^2} \frac{\sinh 2\pi\mu_i \sinh 2\pi\mu_n}{(\cosh 2\pi\mu_i - \cosh 2\pi\mu_n)^2} \frac{(A\mu_i - A\mu_n)^2}{A\mu_i A\mu_n},$$

$$A\mu_i = \left|\Gamma(-\eta + i\mu_i + \tfrac{1}{2})\right|^2, \quad A\mu_n = \left|\Gamma(-\eta + i\mu_n + \tfrac{1}{2})\right|^2,$$

$$\eta = (2mD)^{\frac{1}{2}}/\alpha\hbar \qquad \mu_i = (2mE_i)^{\frac{1}{2}}/\alpha\hbar \qquad \mu_n = (2mE_n)^{\frac{1}{2}}/\alpha\hbar,$$

$$\left(k_i = \alpha\mu_i, \quad k_n = \alpha\mu_n\right)$$

E_i is the relative kinetic energy of the system before collision, and

$$E_n = E_i + h\nu .$$

The final formula for p_{10} is:

$$p_{10} = \frac{1}{k_1 k_o} \left(\frac{4m}{\hbar^2}\right)^2 X_{10}^2 \, R_{10}^2$$

In this calculation, the values of μ_1, μ_o, are sufficiently large for the approximation,

$$\frac{\sinh 2\pi\mu_1 \sinh 2\pi\mu_o}{(\cosh 2\pi\mu_1 - \cosh 2\pi\mu_o)^2} = \exp 2\pi(\mu_1 - \mu_o),$$

to be satisfactory, and also for the gamma functions to be calculated from the first four terms of Stirling's expansion,

$$\ln \Gamma(z) = (z - \tfrac{1}{2}) \ln z - z + \tfrac{1}{2} \ln(2\pi) + 1/12\, z - \ldots.$$

The perturbation transition matrix element in the co-ordinate of the vibrating atom is given by:

$$X_{10} = 2\alpha D \left(\frac{\hbar}{4\pi M\nu}\right)^{\frac{1}{2}}$$

The results are given in Table 33; In fig. 33 the curve of $\log_{10} p_{10}$ vs. the mean relative kinetic energy $\bar{E} = (E_o - E_1)/2$ is compared with that from the semi-classical method.

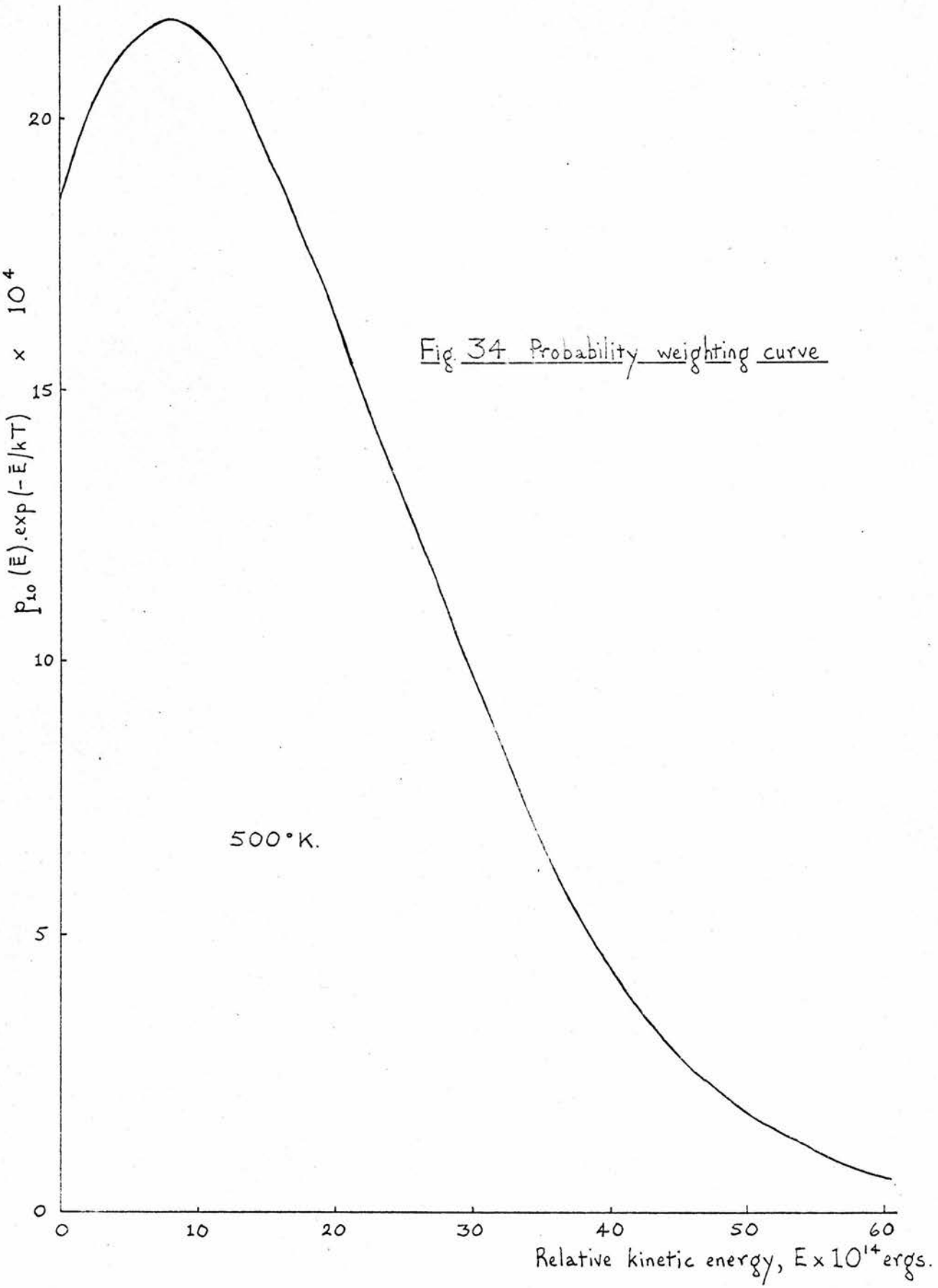

Fig. 34 Probability weighting curve

Table 33.

Quantum mechanical calculation.

E_1 x 10^{14} ergs.	$\bar{E}$ x 10^{14} ergs.	$\log_{10} p_{10}$
1	8.265	-2.495
5	12.265	-2.254
10	17.265	-1.940
15	22.265	-1.684
20	27.265	-1.454
30	37.265	-1.083
40	47.265	-0.784
50	57.265	-0.529
60	67.265	-0.334

Averaging over all encounters.

Encounters between two molecules are characterized by two statistically independent quantities: the relative kinetic energy $E = \frac{1}{2} mv^2$ and the "impact" parameter b (the distance separating the asymptotes to the paths of the molecules). The number of encounters of a molecule per second in which the relative kinetic energy lies between E, E + dE and the impact parameter between b, b + db is (Fowler, 1936):

$$\frac{8N}{s} \left(\frac{\pi}{2mkT}\right)^{\frac{1}{2}} b E \exp(-E/kT)\, dbdE,$$

where/

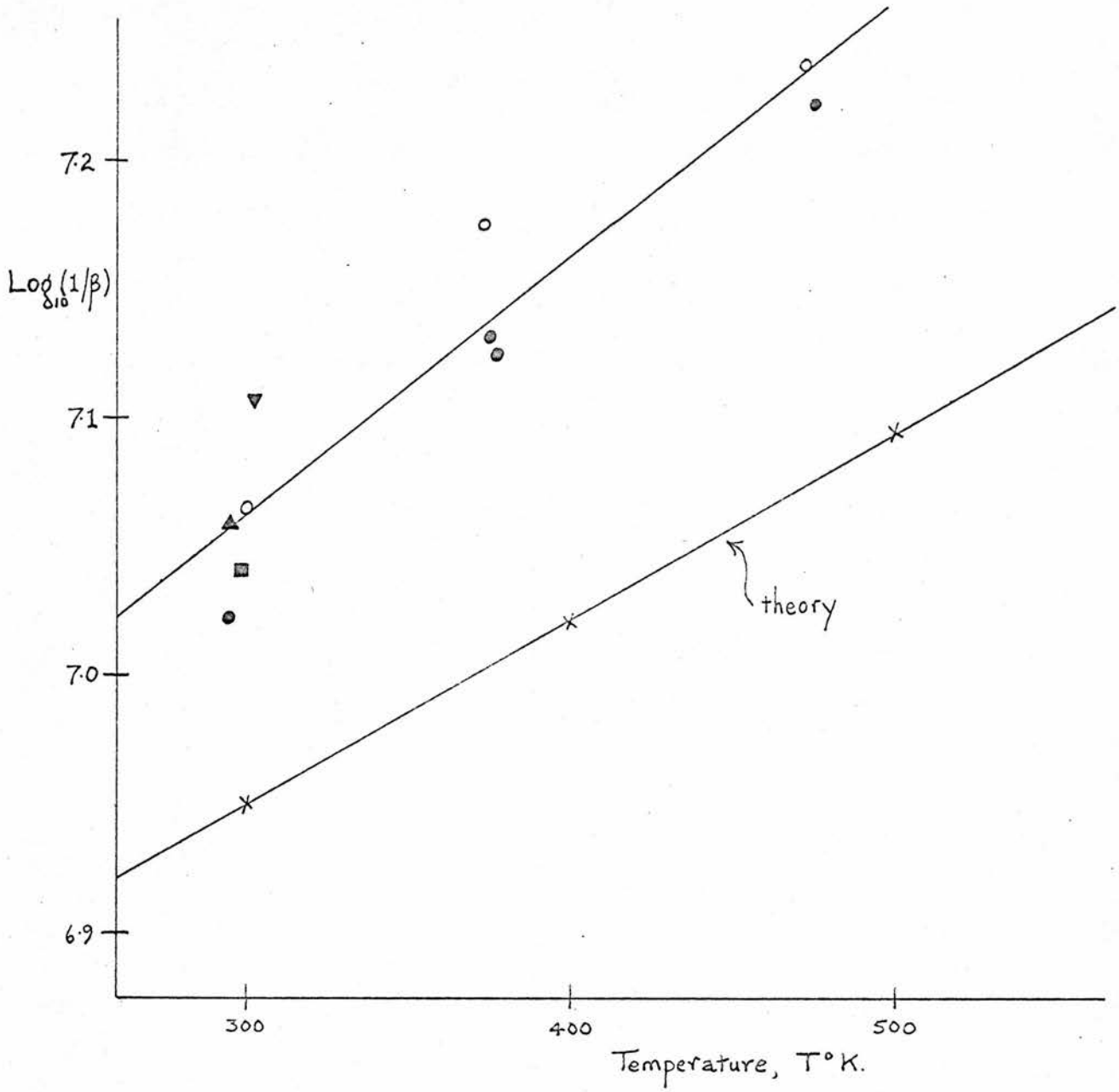

Fig. 35. Relaxation time of methyl chloride.

where N is the molecule density and s is a symmetry number, equal to 2 for identical molecules. If $p_{10}(E,b)$ is the probability of transition of an excited molecule to the ground state in an encounter detailed by E, b, then the overall probability of de-excitation of such a molecule per second is:

$$f_{10} = 4N\left(\frac{\pi}{2mkT}\right)^{\frac{1}{2}} \int_0^\infty \int_0^\infty p_{10}(E,b)\, b\, E \exp(-E/kT) db\, dE.$$

The evaluation of f_{10} thus depends on knowledge of the complete surface $p_{10}(E,b)$. Unfortunately it is very laborious to calculate p_{10}, except for head-on collisions (b=0) (as in the preceding sections). But it appears that in general encounters p_{10} is largely determined by the distance of closest approach r_c, so we may write:

$$p_{10}(E,b) \doteq p_{10}(r_c).$$

Widom and Bauer (1953) examined three-dimensional encounters in terms of the "effective" potential which determines the trajectory of the equivalent one-body problem:

$$V_{eff} = V(r) + E^2 b^2 / r^2$$

For $E < 4D/5$ they showed that there is, for a particular relative kinetic energy E, a critical impact parameter $b_{crit.}$, such that for collisions with $b > b_{crit}$, the molecules do not pass into close contact because of a "centrifugal hump". This leads to a discontinuity in the r_c vs. E curve. However, the potential well for CH_3Cl molecular interaction is not deep enough to make this effect important at the temperatures considered here.

With certain other approximations Cottrell and Ream (1955) showed that:

$$f_{10} = 2N\left\{\frac{\pi}{2mkT}\right\}^{\frac{1}{2}} \int_0^\infty r_c^2\, p_{10}(E,0) \exp(-E/kT)\, dE.$$

The value of r_c varies slowly over the region where the integrand/

integrand is large and so it may be put outside the integral as a constant; the value $r_c = 3.16$ Å was used.

In evaluating the integrand in the expression for f_{10}, energy exchange was allowed for by using $p_{10}(\bar{E}, 0)$ values where $\bar{E}$ is the "symmetrized" relative kinetic energy of an inelastic collision of initial relative kinetic energy E_1:

$$\bar{E} = (E_o - E_1) / 2 = E_1 + \tfrac{1}{2} h\nu .$$

A typical $p_{10}(\bar{E}, 0) \exp(-E/kT)$ vs. E curve is shown in fig. 34. The integrals were evaluated by applying Simpson's rule.

The relaxation time.

The relaxation time β for energy transfer at the lowest vibrational frequency is related to the transition probability f_{10} by the equations,

$$1/\beta = f_{10} - f_{01},$$

$$f_{01} = f_{10} \exp(- h\nu / kT),$$

assuming that this mode behaves like a simple harmonic oscillator.

The results are given in Table 34, and these are compared with the experimental results in the graph of $\log_{10}(1/\beta)$ vs. absolute temperature T° K, in fig. 35.

Table 34.

Transition probabilities for methyl chloride.

$T^\circ K$	$N \times 10^{-19}$	$f_{10} \times 10^{-6}$	$f_{01} \times 10^{-6}$	$(f_{10}-f_{01}) \times 10^{-6}$	$\beta \times 10^{6}$ sec.	$\log_{10}(1/\beta)$
300	2.447	9.22	0.28	8.94	0.112	6.951
400	3.632	11.30	0.81	10.49	0.095	7.021
500	4.819	14.21	1.73	12.48	0.080	7.096

The results agree well with experiment in both absolute magnitude/

magnitude and temperature dependence. This shows that the experimental results for even quite complicated molecules can be fitted by the theory using plausible initial assumptions.

Tanczos also obtained good agreement in absolute magnitude with the mean experimental value of the relaxation time at a single temperature:

	β at 300° K
Experiment	0.087×10^{-6} sec.
Tanczos	0.173×10^{-6} sec.
Present work	0.112×10^{-6} sec.

REFERENCES.

Alleman (1939) Phys. Rev. 55, 87.

Amme and Legvold (1959) J. chem. Phys. 30, 163.

Andrade and Lewer (1929) Nature 124, 724.

Arnold, McCoubrey and Usselohde (1957) Proc. Roy. Soc. A248, 445.

Beattie, Barriault and Brierley (1951) J. chem. Phys. 19, 1219.

Beattie, Brierley and Barriault (1952) J. chem. Phys. 20, 1615.

Bell (1950) Proc. Phys. Soc., Lond. B63, 958.

Bell (1953) J. Acoust. Soc. Amer. 25, 96.

Blythe, Cottrell and Read (1961) Trans. Faraday Soc. 57, 935.

Borgnis (1952) J. Acoust. Soc. Amer. 24, 19.

Boyer (1951) J. Acoust. Soc. Amer. 23, 176.

Carome and Witting (1961) J. Acoust. Soc. Amer. 33, 187.

Carome, Witting and Fleury (1961) J. Acoust. Soc. Amer. 33, 1417.

Cottrell and Mc Coubrey (1961) "Molecular Energy Transfer in Gases" Butterworths, Lond.

Cottrell and Ream (1955) Trans. Faraday Soc. 51, 159, 1453.

Devonshire (1936) Proc. Roy. Soc. A158, 269.

Dye (1926) Phys. Soc. Lond. 38, 399.

Dye (1932) Proc. Roy. Soc. A138, 834.

Edmonds and Lamb (1958) Proc. Phys. Soc. Lond. 72, 940.

Edwards (1959) B.Sc. Thesis, Oxford.

Ener, Garbrysh and Hubbard (1952) J. Acoust. Soc. Amer. 24, 474.

Fay (1931) J. Acoust. Soc. Amer. 3, 222.

Fricke (1940) J. Acoust. Soc. Amer. 12, 245.

Graham (1933) J. Acoust. Soc. Amer. 5, 1.

Graham (1953) J. Acoust. Soc. Amer. 25, 1124.

Gray, Matthews and MacRobert "A Treatise on Bessel Functions and their Application to Physics", 2nd Edn., Macmillan, London.

Greenspan (1950) J. Acoust. Soc. Amer. 22, 568.

Griffith (1950) J. Appl. Phys. 21, 1319.

Guptill/

Guptill (1953) Canad. J. Phys. 31, 393.
Hamann and Pearse (1952) 48, 101.
Hardy (1943) J. Acoust. Soc. Amer. 15, 91.
Hartig and Swanson (1938) Phys. Rev. 54, 618.
Hartig and Lambert (1950) J. Acoust. Soc. Amer. 22, 42.
Henry (1931) Proc. Phys. Soc. Lond. 43, 340.
Herzfeld (1938) Phys. Rev. 53, 899.
Herzfeld and Litovitz (1959) "Absorption and Dispersion of Ultrasonic Waves". Academic Press, New York.
Holborn and Otto (1925) Z Phys. 33, 1.
Johnston and Davies (1934) J. Amer. Chem. Soc. 56, 271.
Johnston and Walker (1933) J. Amer. Chem. Soc. 55, 172.
Kaye and Sherratt (1933) Proc. Roy. Soc. A141, 123.
Keenan and Kaye (1945) "Thermodynamics of Air". John Wiley and Sons, New York.
Kneser (1938) Ann. Phys. Lpz. 34, 665.
Krasnooshkin (1944) Phys. Rev. 65, 190.
Lambert (1953) J. Acoust. Soc. Amer. 25, 1068.
Landau and Teller (1936) Phys. Z. Sowjetunion 10, 34.
Lawley (1952) Proc. Phys. Soc. Lond. B65, 181.
Leonard (1940) J. Acoust. Soc. Amer. 12, 241.
Mott and Massey (1949) "The Theory of Atomic Collisions". 2nd edn. Oxford Univ. Press, Oxford.
Nielsen (1949) Trans. Don. Acad. Tech. Sc. No. 10.
Nixon and Williams (1950) J. Acoust. Soc. Amer. 22, 676.
Norton (1935) J. Acoust. Soc. Amer. 7, 16.
Pielemeier (1929) Phys. Rev. 34, 1184.
Pielemeier (1932) Phys. Rev. 41, 833.
Pielemeier (1935) J. Acoust. Soc. Amer. 7, 37.
Pielemeier (1939) J. Acoust. Soc. Amer. 10, 313.
Pierce (1925) Proc. Amer. Acad. 60, 271.
Redwood (1957) Proc. Phys. Soc. Lond. B70, 721.
Reid (1930) Phys. Rev. 35, 814.
Richards (1939) Rev. Mod. Phys. 11, 36.

Roberts/

Roberts (1951) "Heat and Thermodynamics".
Blackey, Lond.

Rowlinson (1949) Trans. Faraday Soc. 45, 974.

Seki, Granato and Truell (1956) J. Acoust. Soc. Amer. 28, 230.

Sette, Busala and Hubbard (1955) J. Chem. Phys. 23, 787.

Stewart and Stewart (1952) J. Acoust. Soc. Amer. 24, 23.

Suckling (1959) J. Acoust. Soc. Amer. 31, 678.

Takayanagi (1959) Sci. Rep. Saitama Univ. A3, No. 1.

Tanczos (1956) J. Chem. Phys. 25, 439.

Tilton (1934) J. Bur. Standards 13, 111.

van Dyke (1925) Phys. Rev. 25, 895 (abstract).

van Itterbeek and Verhagen (1951) Nature 167, 478.

Vigoureux (1952) "Ultrasonics".
Chapman and Hall, Lond.

von Grossmann (1934) Phys. Z. 35, 83.

Weston (1953) Proc. Phys. Soc. Lond. B66, 695.

Whytlaw-Gray, Reeves and Bottomley (1958) Nature 181, 1004.

Widom and Bauer (1953) J. Chem. Phys. 21, 1670.

Zartmann (1949) J. Acoust. Soc. Amer. 21, 171.

Zuhlke (1934) Ann. Phys. Lpz. 21, 667.

APPENDIX.

Numerical values used in calculations:

R = 8.3144×10^{7} ergs./deg./mole.

k = 1.3807×10^{-16} ergs./deg./mol.

N = 6.023×10^{23}

h = 6.626×10^{-27} erg. sec.

c = 2.99796×10^{10} cm./sec.

$0^{\circ}C.$ = $273.16^{\circ}K.$

π = 3.1416

log e = 0.43429

$m(O^{16})$ = $16 \times 1.660 \times 10^{-24}$ gm.

1 in. = 2.5399 cm.

V_m = 22.415 l/mole.

SYNOPSIS.

With a view to studying translational-vibrational relaxation times in gaseous systems such as CO_2/Ar mixtures, an accurate ultrasonic interferometer was built. With this apparatus sound velocities may be determined at 83 kc./sec. in the ranges 0 - 2 atm. and 20-200°C. The wavelength is measured with the aid of an optical Moiré fringe device accurate to 10^{-5} cm.

Preliminary experiments with CO_2-free, dry air indicated that diffraction and wave-guide effects would have to be taken into account. These effects were examined using pure inert gases (He, Ne, Ar, Kr) whose free-space, plane-wave velocities were calculated from available thermodynamic and virial data. A straight line was obtained when the relative increase of observed wavelength above the calculated free-space, plane-wave wavelength, $(\lambda_{exp} - \lambda_{calc}) / \lambda_{calc}$, was plotted against λ^2_{calc}. Using this as a calibration curve for the interferometer, absolute velocities may be estimated reliably to 1 part in 2,000, or better, in gases with molecular weights greater than 30. Further investigations were made in two gases with very low velocities: $CClF_3$ and $\underline{n}$ - C_4H_{10}.

A simple model of the interferometer has been treated theoretically using the method of normal modes of a tubular wave-guide. Numerical results, calculated on a computer (Deuce), give good agreement with experiment only when it is assumed that the appropriate boundary conditions at the sides of the interferometer tube are of the "free-wall" rather than "rigid-wall" type.

Additional theoretical work was done on the temperature dependence of the translational-vibrational energy transfer. Previous calculations have in general given unsatisfactory agreement/

agreement with experiment; in these calculations the authors have only introduced the effect of attractive forces between the molecules in an indirect way. In low-energy encounters of polar molecules the attractive forces may be important and it was therefore decided to investigate the effect of including them directly. Numerical results have been calculated for methyl chloride; the temperature dependence of the relaxation time and second virial coefficient are well established for this gas. It was found that both the semi-classical and fully quantum mechanical methods gave the same result, which agrees well with experiment in both absolute magnitude and temperature dependence.

Offprinted from the *Transactions of The Faraday Society*,
No. 462, Vol. 57, Part 6, June, 1961

TRANSITION PROBABILITY IN MOLECULAR ENCOUNTERS

PART 4.—TEMPERATURE DEPENDENCE OF RELAXATION TIME IN METHYL CHLORIDE AND NITROGEN

By A. R. Blythe, T. L. Cottrell and A. W. Read
Dept. of Chemistry, University of Edinburgh

Received 23*rd November*, 1960

The translational-vibrational relaxation times for methyl chloride and nitrogen have been calculated over a range of temperatures, taking explicit account of the attractive part of the intermolecular potential. The results for methyl chloride agree well with experiment, as do those for nitrogen above 1500°K. The calculated results for nitrogen at lower temperatures have a steeper temperature dependence than that observed.

Previous theoretical calculations of the probability of vibrational-translational energy transfer in molecular encounters have, in general, given unsatisfactory agreement with experiment in that the calculated temperature dependences are rather too steep in the important practical region, 300-1000°K.[1] Most authors have used an exponential repulsive intermolecular potential function, following the original work of Landau and Teller,[2] and only introduced the effect of an attractive term in an indirect way. In low-energy collisions the attractive term may be important and it was therefore decided to investigate the effect of including it directly. The methods are based on those of Cottrell and Ream [3] who showed in principle how to take account of attractive forces, but did not do so in their numerical calculations. Some investigation of the effect of the attractive term has been made by Takayanagi,[4] but he did not examine the temperature dependence of the results.

We have investigated both a polar and a non-polar molecule, in the expectation that the attractive term would be more important for the former. The choice of examples was limited by the experimental results, since there are few gases where the relaxation times are known over a wide temperature range and where the virial data are well established. The molecules chosen were methyl chloride and nitrogen.

METHYL CHLORIDE

The attractive term can be included explicitly and the results for head-on collisions calculated analytically, assuming a Morse potential function,

$$V(r) = D \exp\left[-2\alpha(r-r_e)\right] - 2D \exp\left[-\alpha(r-r_e)\right]. \qquad (1.1)$$

The constants in this potential for methyl chloride were evaluated by fitting it to a Krieger potential function,

$$V(r) = 4u[(r_0/r)^{12} - (r_0/r)^6] - 2d^2/r^3, \qquad (1.2)$$

where the angle-dependent contribution of the Stockmayer potential has been replaced by the expression for the interaction of two point-dipoles, which are aligned so as to exert a maximum mutual attraction. The parameters of the Stockmayer potential were obtained from the second virial coefficient data [5, 6] by the method of Rowlinson.[7] The electric dipole moment of a methyl chloride molecule was taken as $d = 1{\cdot}86$ D. Hence:

$$u/k = 380°\text{K}, \qquad r_0 = 3{\cdot}43 \text{ Å}.$$

The method of fitting (1) to (2) was to arrange a common potential minimum $(r_e, -D)$ and to set

$$\alpha = 6/2^{\frac{1}{6}}r_z,$$

where the Krieger potential crosses the r-axis at $(r_z, 0)$. Hence

$$D = 18{\cdot}9\times 10^{-14}\text{ ergs}, \qquad r_e = 3{\cdot}61\text{ Å}, \qquad \alpha = 1{\cdot}69\times 10^{8}\text{ cm}^{-1}.$$

An alternative fit is one where the two curves have the two common points $(r_e, -D)$, $(r_z, 0)$ when

$$\alpha = \ln 2/(r_e - r_z).$$

However, this does not give such good agreement with the slope in the repulsive region of the Krieger potential. The double exponential function used by Cottrell and Ream,[3]

$$V(r) = \lambda \exp(-2\alpha r) - \mu \exp(-\alpha r),$$

was obtained from the Morse function through the equations,

$$\lambda = D \exp(2\alpha r_e), \quad \mu = 2D \exp(\alpha r_e).$$

Substitution was now made in the formula for the probability, p_{10}, of the transition $1\rightarrow 0$ in the lowest vibrational mode of an excited molecule in a head-on collision with another molecule of relative velocity v:

$$p_{10} = \frac{16\pi^2}{h^2} X_{10}^2 I^2. \tag{1.3}$$

The lowest vibrational frequency of methyl chloride belongs to the C—Cl stretching mode, $\nu = 732\text{ cm}^{-1}$. If we assume this to be a simple harmonic oscillator, we obtain for the matrix element of co-ordinates between the first excited state and the ground state,

$$X_{10} = \left(\frac{h}{8\pi^2 M\nu}\right)^{\frac{1}{2}}, \tag{1.4}$$

where M is the " effective " mass of the system; the maximum value of M, shown by Arnold, McCoubrey and Ubbelohde [1] to be one-half the reduced mass m of the colliding system, was used here. Since $\pi^2 v/\alpha v > 3$, we can use the approximation,

$$I = \frac{2\pi^2 m v}{\alpha} \exp -\frac{\pi v(\pi - 2\phi)}{\alpha v}, \tag{1.5}$$

where

$$\tan^2\phi = \mu^2/2mv^2\lambda,$$

for the perturbation integral.

The curve obtained, fig. 1, for $\log_{10} p_{10}$ as a function of the relative kinetic energy E of a collision was arbitrarily cut off at $\log_{10}(1/2)$. The rise of the probability above unity is physically unreasonable and is due to the failure of normalization for large perturbations.

The results were confirmed by a fully quantum-mechanical treatment using the Morse potential. The formula is

$$p_{10} = \frac{1}{k_1 k_0}\left(\frac{32\pi^2\alpha D m}{h^2}\right)^2 X_{10}^2 R_{10}^2, \tag{1.6}$$

where

$$R_{10}^2 = \frac{\pi^2\nu^2\boldsymbol{h}^2}{16\alpha^2 D^2}\frac{\sinh 2\pi\mu_1 \sinh 2\pi\mu_0}{(\cosh 2\pi\mu_1 - \cosh 2\pi\mu_0)^2}\frac{(A\mu_1 + A\mu_0)^2}{A\mu_1 A\mu_0},$$

$$A\mu_1 = \left|\,\Gamma(-\eta + i\mu_1 + \tfrac{1}{2})\,\right|^2, \quad A\mu_0 = \left|\,\Gamma(-\eta + i\mu_0 + \tfrac{1}{2})\,\right|^2,$$

$$\eta = 2\pi(2mD)^{\frac{1}{2}}/\alpha\boldsymbol{h}, \quad \mu_1 = 2\pi(2mE_1)^{\frac{1}{2}}/\alpha\boldsymbol{h}, \quad \mu_0 = 2\pi(2mE_0)^{\frac{1}{2}}/\alpha\boldsymbol{h},$$

$$k_1 = \alpha\mu_1, \quad k_0 = \alpha\mu_0.$$

E_1 is the relative kinetic energy of the two molecules before collision, and

$$E_0 = E_1 + \boldsymbol{h}\nu.$$

In deriving the formula for R_{10}, the perturbation transition matrix element in the co-ordinates of the centres of mass of the two molecules, use was made of the integration worked out by Devonshire [8] in his paper on the interaction of atoms with solid surfaces.

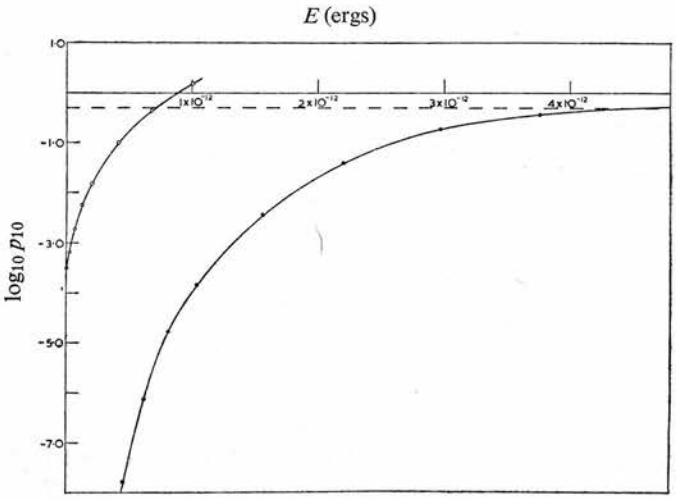

FIG. 1.—$\text{Log}_{10}\,p_{10}$ against relative kinetic energy: ○ methyl chloride; ● nitrogen.

In this calculation, the values of μ_1, μ_0 are sufficiently large for the approximation,

$$\frac{\sinh 2\pi\mu_1 \sinh 2\pi\mu_0}{(\cosh 2\pi\mu_1 - \cosh 2\pi\mu_0)^2} = \exp 2\pi(\mu_1 - \mu_0), \tag{1.7}$$

to be satisfactory, and also for the gamma functions to be calculated from the first four terms of Stirling's expansion,

$$\ln \Gamma(z) = (z - \tfrac{1}{2}) \ln z - z + \tfrac{1}{2} \ln (2\pi) + 1/12z - \ . \ . \ .$$

In order to weight the probability over all collisions, the approximation,

$$p_{10}(E, b) = p_{10}(r_c),$$

is made, where b is the "impact" parameter (statistically independent of E) and r_c is the distance of closest approach. Then the $1 \to 0$ transition probability, i.e.,

the probability that an excited molecule will lose one quantum of vibrational energy in 1 sec, is given by

$$f_{10} = \frac{4c}{s}\left(\frac{\pi}{2mkT}\right)^{\frac{1}{2}}\int_0^\infty r_c^2 p(V)\exp(-V/kT)\mathrm{d}V,$$

where c is the number of molecules per cm^3 and s is a symmetry number, equal to 2 for identical molecules. The value of r_c varies slowly over the region where the integrand is significant, and so was taken as a constant, $r_c = 3{\cdot}16$ Å. Corresponding to a particular value of V, $p(V)$ was read from the $\log_{10}p_{10}$ $(E, 0)$ curve, fig. 1, at $E = \bar{E}$, where $\bar{E}$ is the symmetrized relative kinetic energy of a collision of initial relative kinetic energy V, i.e.,

$$\bar{E} = V + \tfrac{1}{2}h\nu.$$

The integral was evaluated by applying Simpson's rule.

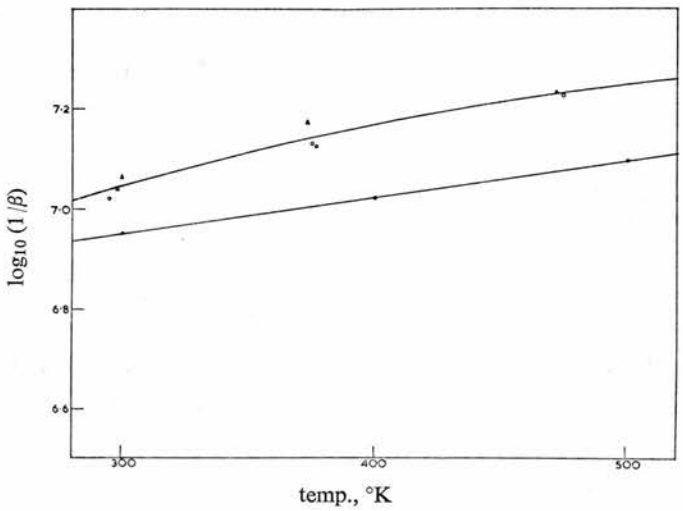

FIG. 2.—Temperature dependence of relaxation time in methyl chloride: △ Edmonds and Lamb,[9] ○ Edwards and Lambert,[10] ▲ Amme and Legvold,[11] ● theory.

The relaxation time β for energy transfer at the lowest vibrational frequency is related to the transition probability f_{10} by the equations,

$$1/\beta = f_{10} - f_{01}, \tag{1.8}$$

$$f_{01} = f_{10}\exp(-h\nu/kT), \tag{1.9}$$

assuming that this mode behaves like a simple harmonic oscillator.

The theoretical results are given in table 1, and these are compared with the experimental results in the graph of $\log_{10}(1/\beta)$ against absolute temperature T°K, in fig. 2.

TABLE 1.—TRANSITION PROBABILITIES FOR METHYL CHLORIDE

T,°K	$c\times10^{-19}$	$f_{10}\times10^{-6}$	$f_{01}\times10^{-6}$	$(f_{10}-f_{01})\times10^{-6}$	$\beta\times10^{6}$ sec	$\log_{10}(1/\beta)$
300	2·447	9·22	0·28	8·94	0·112	6·951
400	3·632	11·30	0·81	10·49	0·095	7·021
500	4·819	14·21	1·73	12·48	0·080	7·096

Tanczos [12] used the Krieger potential,

$$V(r) = 4u[(r_0/r)^{12} - (r_0/r)^6 - \delta(r_0/r)^3],$$

as a basis for his calculation of transition probabilities in methyl chloride. However, he used the Krieger parameters consistent with viscosity and thermal conductivity data. These parameters differ from ours, which only relate to perfectly aligned molecules. Introducing the attractive component of the potential in an indirect way, Tanczos obtained good agreement with the mean experimental value, $\beta = 0{\cdot}093 \times 10^{-6}$ sec, at 300°K. He did not calculate for any other temperature.

TABLE 2

	u/k, °K	r_0, Å	δ	β, sec at 300°K
Tanczos	244	4·332	0·761	$0{\cdot}173 \times 10^{-6}$
present paper	383	3·43	0·816	$0{\cdot}112 \times 10^{-6}$

NITROGEN

For nitrogen a Lennard-Jones potential, the constants of which are well established, was used in place of the Morse function in the perturbation integral. Although the integral may not be evaluated analytically there is a numerical method available [3] allowing the form of the Lennard-Jones potential to be taken into account explicitly. In contrast, Herzfeld and his school [13-15] have fitted an exponential function to the Lennard-Jones, taking the most accurate method of fitting to be that giving the best agreement between theoretical and experimental results,[15] and including the attractive term indirectly.

The 12 : 6 Lennard-Jones function may be expressed in the form

$$V(r) = V_0\{(\rho)^{-12} - 2(\rho)^{-6}\} \tag{2.1}$$

where

$$\rho = r/a.$$

Corner [16] gives, for nitrogen, $V_0/k = 95$°K and $a = 3{\cdot}78$ Å. The perturbation integral I is given by

$$I = \int_0^\infty F(t) \cos 2\pi\nu t \mathrm{d}t. \tag{2.2}$$

It is more convenient to work in terms of the dimensionless variables, τ and ω, defined by

$$\tau = t\left(\frac{2V_0}{ma^2}\right)^{\frac{1}{2}}, \quad \omega = \frac{2\pi\nu t}{\tau}.$$

Defining

$$f(\rho) = (\rho^{-13} - \rho^{-7}),$$

then

$$F(\tau) = (12V_0/a)f(\tau)$$

and

$$I = 6(2mV_0)^{\frac{1}{2}}\int_0^\infty f(\tau) \cos \omega\tau \mathrm{d}\tau = 6(2mV_0)^{\frac{1}{2}}J. \tag{2.3}$$

The problem of calculating I reduces to that of calculating J. Numerically this may not be done directly for the reason given by Cottrell and Ream.[3] Numerical

integration is possible, however, if $f(\tau)$ is replaced by one of its derivatives. Integrating by parts, (2.3) becomes

$$J = (-)^k \int_0^\infty f^{2k}(\tau) \cos \frac{\omega\tau}{\omega^{2k}} d\tau, \tag{2.4}$$

where $2k$ is the number of the derivative of $f(\tau)$, k being an integer. J is now in a form suitable for numerical integration if the derivatives of $f(\tau)$ are known. The second, fourth and sixth derivatives were calculated by Cottrell and Ream, the eighth was evaluated in the course of this work and is given in the appendix.

The derivatives, as given, are not in the most convenient form since they are power series in ρ, whereas J is expressed in terms of τ. ρ and τ are not simply connected and a " linking " variable ε must be introduced. This is defined by

$$\rho = \rho_0(1+\varepsilon), \tag{2.5}$$

where

$$\rho_0 = r_0/a.$$

From the equations of motion for a collision

$$\tau = 2\rho_0 \int_0^{\sqrt{\varepsilon}} \frac{\sqrt{\varepsilon} d\sqrt{\varepsilon}}{(\sigma + 2\rho^{-6} - \rho^{-12})^{\frac{1}{2}}},$$

where

$$\sigma = mv^2/2V_0.$$

Using the limitation

$$\sigma = \rho_0^{-6}(\rho_0^{-6} - 2),$$

the above equation simplifies to a form more amenable to numerical work, i.e.

$$\tau = 2\rho_0^{+4} \int_0^{\sqrt{\varepsilon}} \frac{\sqrt{\varepsilon} d\sqrt{\varepsilon}}{\{\rho_0^{-6}(1-(1+\varepsilon)^{-12}) - 2(1-(1+\varepsilon)^{-6})\}^{\frac{1}{2}}}. \tag{2.6}$$

Values of τ, for a range of values of $\sqrt{\varepsilon}$, were obtained from this equation by the use of Simpson's rule for several values and numerical interpolation for the rest. The constants used in the evaluation of J are shown in table 3.

TABLE 3

σ	ρ_0^{-6}	k
288	18	1
224	16	1
168	14	1
120	12	2
80	10	2
63	9	2
48	8	3
35	7	3

From the values of I, the probability p_{10} was calculated as for methyl chloride, assuming the effective mass to be half the reduced mass and the vibrational frequency to be 2331 cm^{-1}. The values obtained for p_{10} are plotted in fig. 1. The higher probability for methyl chloride is due to the large attractive term in its intermolecular potential, compared to that in the non-polar nitrogen potential.

The calculation of f^{10} was carried out using the method described above for methyl chloride. The distance of closest approach was taken as 3 Å and values of f_{10} were calculated for the temperature range 300-6000°K. The theoretical results are given in table 4.

TABLE 4.—TRANSITION PROBABILITIES FOR NITROGEN

T, °K	c	f_{10}	f_{01}	$\log_{10}(1/\beta)$
300	$2{\cdot}448\times10^{19}$	$1{\cdot}414\times10^{1}$	0	0·150
500	$1{\cdot}468\times10^{19}$	$4{\cdot}118\times10^{1}$	$\cdot049\times10^{0}$	1·610
750	$9{\cdot}790\times10^{18}$	$5{\cdot}871\times10^{2}$	$\cdot065\times10^{2}$	2·764
1000	$7{\cdot}342\times10^{18}$	$3{\cdot}534\times10^{3}$	$\cdot121\times10^{3}$	3·533
1500	$4{\cdot}894\times10^{18}$	$3{\cdot}826\times10^{4}$	$\cdot403\times10^{4}$	4·534
2000	$3{\cdot}672\times10^{18}$	$1{\cdot}797\times10^{5}$	$\cdot332\times10^{5}$	5·165
3000	$2{\cdot}446\times10^{18}$	$1{\cdot}192\times10^{6}$	$\cdot387\times10^{6}$	5·906
4000	$1{\cdot}836\times10^{18}$	$3{\cdot}556\times10^{6}$	$1{\cdot}529\times10^{6}$	6·307
5000	$1{\cdot}468\times10^{18}$	$7{\cdot}147\times10^{6}$	$3{\cdot}639\times10^{6}$	6·545
6000	$1{\cdot}224\times10^{18}$	$1{\cdot}154\times10^{7}$	$\cdot657\times10^{7}$	6·696

The absolute value of $1/\beta$, in the temperature range 2000-6000°K, is high, by approximately one power of ten, when compared with the experimental results of Blackman.[17] However, the above treatment is based upon the assumption that all collisions are direct; thus it will predict, for a linear molecule, results which are too high. The theoretical results, therefore, were fitted to the experimental data in the temperature range 5000-6000°K. The modified results are plotted in fig. 3, for comparison with the experimental data and also the theoretical results of Hertzfeld and Litovitz.[15]

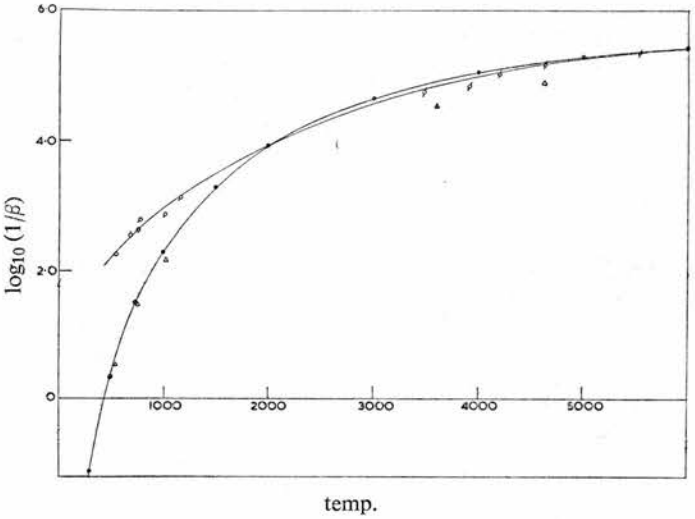

FIG. 3.—Temperature dependence of relaxation time in nitrogen: ○ Huber and Kantrowitz,[18] ⌕ Lukasik and Young,[19] ⌓ Blackman,[17] △ Herzfeld and Litovitz [15] (theoretical), ● theory.

CONCLUSION

The results for methyl chloride agree well with experiment in both absolute magnitude and temperature dependence. This shows that the experimental results for even quite complicated molecules can be fitted by the theory using plausible initial assumptions. The results for nitrogen are in agreement with experiment down to 1500°K, while below that value the temperature dependence is steeper than that found experimentally. However, the experimental results are less reliable in this region because of the presence of impurities [18] and the theory may be correct over the whole range. The close agreement of the results with

those of Herzfeld and Litovitz indicates that their method of fitting an exponential function to the 12 : 6 Lennard-Jones is theoretically justified.

It is noteworthy that the same theory can deal adequately with the very slight temperature dependence of transition probability in methyl chloride and the much greater temperature dependence for nitrogen. This is good evidence that the present theoretical picture is basically correct.

1 Arnold, McCoubrey and Ubbelohde, *Trans. Faraday Soc.*, 1957, **53**, 738.
2 Landau and Teller, *Physik. Z. Sowjetunion*, 1936, **10**, 34.
3 Cottrell and Ream, *Trans. Faraday Soc.*, 1955, **51**, 159, 1453.
4 Takayanagi, *Sci. Rep. Saitama University*, series A, **3**, no. 1.
5 Hamann and Pearse, *Trans. Faraday Soc.*, 1952, **48**, 101.
6 Whytlaw-Gray, Reeves and Bottomley, *Nature*, 1958, **181**, 1004.
7 Rowlinson, *Trans. Faraday Soc.*, 1949, **45**, 974.
8 Devonshire, *Proc. Roy. Soc. A*, 1936, **158**, 269.
9 Edmonds and Lamb, *Proc. Physic. Soc.*, 1958, **72**, 940.
10 Edwards, *Thesis* (Oxford), 1959.
11 Amme and Legvold, *J. Chem. Physics*, 1959, **30**, 163.
12 Tanczos, *J Chem. Physics*, 1956, **25**, 439.
13 Herzfeld, Schwartz and Slawsky, *J. Chem. Physics*, 1952, **20**, 1591.
14 Herzfeld and Schwartz, *J. Chem. Physics*, 1954, **22**, 767.
15 Herzfeld and Litovitz, *Absorption and Dispersion of Ultrasonic Waves* (Academic Press, 1959).
16 Corner, *Proc. Roy. Soc. A*, 1948, **192**, 275.
17 Blackman, *Vibrational Relaxation in* O_2 *and* N_2, *Tech. Rept.* II-20, N. 6, ori-105 II (Princeton University, Princeton, New Jersey), May, 1955.
18 Huber and Kantrowitz, *J. Chem. Physics*, 1947, **15**, 275.
19 Lukasik and Young, *J. Chem. Physics*, 1957, **27**, 1149.

APPENDIX

(12 : 6 Lennard-Jones function)

$$
\begin{aligned}
f^{\mathrm{VIII}}(\tau) = 432\,\rho^{-15}\{&-280{,}280\,\sigma^4+(11{,}757{,}200\,\sigma^4-15{,}619{,}240\,\sigma^3)\rho^{-6}\\
&+(375{,}935{,}560\,\sigma^3-161{,}048{,}888\,\sigma^2)\,\rho^{-12}-(568{,}877{,}400\,\sigma^3\\
&-3{,}108{,}382{,}368\,\sigma^2+532{,}965{,}160\,\sigma)\,\rho^{-18}-(7{,}136{,}755{,}395\sigma^2\\
&-9{,}258{,}200{,}490\,\sigma-547{,}63\,/{,}475)\,\rho^{-24}+(3{,}630{,}802{,}175\,\sigma^2\\
&-26{,}431{,}775{,}370\,\sigma+9{,}027{,}593{,}575)\,\rho^{-30}+(23{,}987{,}555{,}900\,\sigma\\
&-29{,}947{,}417{,}500)\,\rho^{-36}-(6{,}727{,}821{,}100\,\sigma-37{,}331{,}132{,}300)\,\rho^{-42}\\
&-19{,}679{,}655{,}600\,\rho^{-48}+3{,}707{,}761{,}200\,\rho^{-54}\}.
\end{aligned}
$$

Erratum—

In $f^{\mathrm{VI}}(\tau)$ quoted in Cottrell and Ream, part 1, $+3{,}080\,\sigma^3$ should be $-3{,}080\sigma^3$.

PRINTED IN GREAT BRITAIN AT
THE UNIVERSITY PRESS
ABERDEEN